Summer 8-15-2015

Structural and Functional Analysis of the Reaction Center Complexes from the Photosynthetic Green Sulfur Bacteria

Guannan He
Washington University in St. Louis

WASHINGTON UNIVERSITY IN ST. LOUIS

Department of Chemistry

Dissertation Examination Committee:
Robert E. Blankenship, Chair
Michael L. Gross
Dewey Holten
Joseph Jez
Liviu Mirica
Timothy Wencewicz

Structural and Functional Analysis of the Reaction Center Complexes from the Photosynthetic Green Sulfur Bacteria

by

Guannan He

A dissertation presented to the
Graduate School of Arts & Sciences
of Washington University in
partial fulfillment of the
requirements for the degree
of Doctor of Philosophy

August 2015
St. Louis, Missouri

Table of Contents

List of Figures

List of Tables

Acknowledgments

I would like to thank my advisor, Professor Blankenship. First of all, thank you so much for bringing me into the magic world of photosynthesis. Secondly, thank you for being a wonderful advisor. Whenever I met an obstacle during research, you always directed me to the right way. You have great knowledge and wisdom. Finally, thank you for being so supportive all the time. You felt happy for me at every milestone in my life and inspired my career development. I deeply appreciate all your help and encouragement.

I would like to thank Dr. Hao Zhang, Dr. Dariusz M. Niedzwiedzki, Mr. Jeremy D. King, Dr. Gregory S. Orf, Dr. Haijun Liu and Dr. Jing Jiang. Thank you for teaching me the techniques, helping me with different aspects of the experiments and great discussions. My thanks are extended to other former or current group members: Ms. Yue Lu, Dr. Erica W. Majumder, Ms. Junqing Zhang, Mr. Nathan Port, Dr. Rafael Saer, Mr. Chris Sherman, Mr. Nathan Wolf, Mr. Ben Wolf, Dr. Chelsea McIntosh, Ms. Carrie Goodson, Dr. Jianzhong Wen, Dr. Connie Kang, Dr. Hai Yue and Ms. Mindy Prado. Thank you for your help with my experiments and being my friends. I also want to thank all my other friends. All of you have made my life during graduate school so colorful.

I would like to thank my committee members Professor Michael Gross and Professor Dewey Holten for your insightful advice and great discussions during my annual committee meeting. I also would like to thank other dissertation examination committee members Professor Timothy Wencewicz, Professor Liviu Mirica and Professor Joseph Jez.

Finally, I want to give my deep thanks to my family. I want to thank my parents and my parents-in-law. Thank you for your support, encouragement, comfort and patience. I want to thank my

husband Chengjie Wu and my daughter Ellie Y. Wu. Thank you for being my sunshine and brightening my day.

Guannan He

Washington University in St. Louis

August 2015

ABSTRACT OF THE DISSERTATION

Structural and Functional Analysis of the Reaction Center Complexes from the Photosynthetic Green Sulfur Bacteria

by

Guannan He

Doctor of Philosophy in Chemistry

Washington University in St. Louis, 2015

Robert E. Blankenship, Chair

The reaction center (RC) complex of the green sulfur bacterium *Chlorobaculum tepidum* is composed of the Fenna-Matthews-Olson (FMO) antenna protein and the reaction center core (RCC) complex. The RCC complex has four subunits: PscA, PscB, PscC, and PscD. The structure of the intact and functional FMO-RCC complex was studied by chemically cross-linking the purified sample followed by biochemical and spectroscopic analysis. The interaction sites of the cross-linked complex were also studied using LC-MS/MS. A structural model is proposed based on those results. In addition, the RCC complexes were purified, both the PscA-PscC complex from the *Chlorobaculum tepidum* and the PscA-PscB complex from *Prosthecochloris aestuarii*. The intact FMO-RCC complex and the RCC complexes were further studied comparatively by steady-state and time-resolved fluorescence and femtosecond time-resolved transient absorption spectroscopies to elucidate the pathway of FMO-to-RCC inter-protein energy transfer as well as RCC intra-protein energy and electron transfer.

Chapter 1: Introduction to the Structure and Energy Transfer Mechanism of the Reaction Center Complexes from the Green Sulfur Bacteria

Photosynthesis is a biological process that converts the light energy into stable chemical energy. The energy produced by photosynthesis provides the major food and fuel for the life on earth.[1] Photosynthetic species appeared billions of years ago and initially lived in an anaerobic environment. Oxygen-evolving photosynthesis didn't appear until approximately 2.4 billion years ago.[2] Phototrophic prokaryotes can be divided into six distinct major groups including the purple bacteria, the green sulfur bacteria, the green non-sulfur bacteria, the heliobacteria, the chloroacidobacteria and the cyanobacteria.[1, 3, 4] All of them are anoxygenic phototrophic organisms except cyanobacteria. The chloroplasts of phototrophic eukaryotic organisms were derived via endosymbiosis of cyanobacteria.[1]

1.1 Antenna complexes in the green sulfur bacteria

Pigments are a critical component for photosynthesis because they not only absorb the light from the sun but also serve as energy converter when associated with protein complexes. Various groups of pigments are developed to absorb almost the entire solar spectrum. The major groups of pigments are (bacterio)chlolorophylls, bilins and carotenoids. Chlolorophylls and derivatives are porphyrin-based pigments. There are chlorophylls *a*-*d* and *f*, and the bacteriochlorophylls *a*-*g*, named based on the order of discovery.[1] Chlorophyll *a* (Chl *a*) is found in all known

photosynthetic eukaryotic organisms. It is also found in prokaryotes such as cyanobacteria.[1] There is only a limited amount of Chl *a* in some anaerobic photosynthetic bacteria such as the green sulfur bacteria and heliobacteria, but it plays a critical role in the electron transfer when associated with protein complexes.

Bacteriochlorophylls *a* (BChl *a*) is the major chlorophyll-based pigment in the anoxygenic photosynthetic bacteria. The structure of BChl *a* is very similar to Chl *a*, except the acetyl group at the C-3 position and the single bond in ring B between C-7 and C-8, instead of the double bond found in Chl *a* (Figure 1.1). Bilins are linear, open-chain tetrapyrrole pigments, including phycocyanobilin and phycoerythrobilin as two major groups (Figure 1.2). They are found in one of the most well-known antenna complexes called phycobilisomes. Carotenoids are molecules with a delocalized π electron system, and there are hundreds of different carotenoids. The structure of β–carotene is shown in Figure 1.3. Carotenoids play some important roles in photosynthetic organisms including light absorption, photo-protection and regulation of energy transfer in antenna through the xanthophyll cycle.

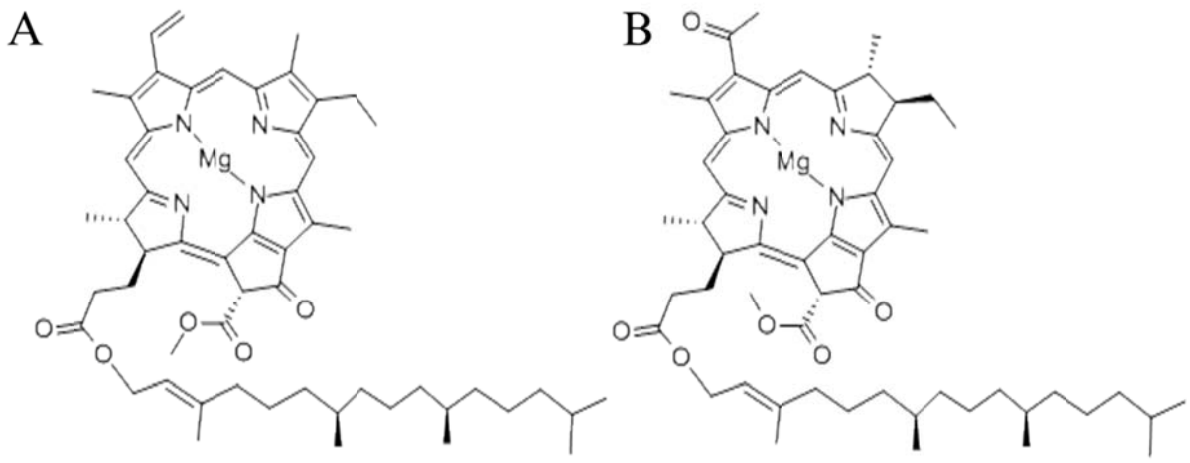

Figure 1.1 Structures of chlorophyll *a* (A) and bacteriachlorophyll *a* (B)

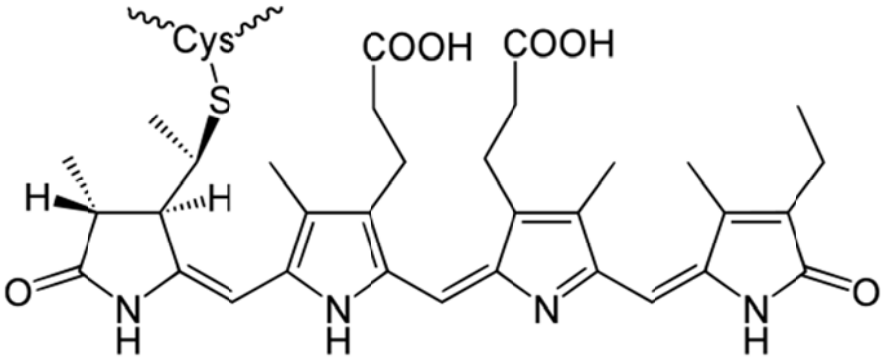

Figure 1.2 Structure of phycocyanobilin

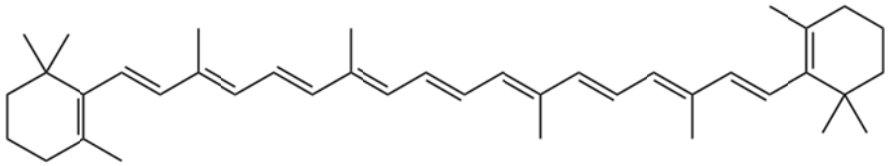

Figure 1.3 Structure of β–carotene

Those pigments are oriented in light-harvesting antenna complexes to efficiently transfer absorbed energy to the reaction center complexes. There are a number of groups of antenna complexes, and almost every group of photosynthetic species has unique antenna ones. Almost all antenna complexes organize their pigments through pigment-protein interactions except the chlorosome antenna complex from the green photosynthetic bacteria, which contains self-assembled bacteriochlorophyll (BChl) *c*, *d*, *e*, or *f* pigments.[5] The green sulfur bacteria, the chloroacidobacteria and the filamentous anoxygenic phototrophs all have chlorosomes, but only the first two have the peripheral antenna FMO protein (Figure 1.4). In organisms that do not have

the FMO protein, the energy is transferred directly from the chlorosomes to the reaction center complex, which is a "Type II" reaction center. FMO protein is associated with the "Type I" reaction center, which has iron-sulfur clusters to reduce ferredoxin protein.

The BChls in the chlorosomes are self-assembled through pigment-pigment interactions to make large supermolecular structures that are enclosed by a lipid monolayer.[5] Besides those BChls, carotenoids and quinones are also enclosed in the lipid monolayer. These cofactors play an important role in light absorption and photo-protection.[6] There are over 11 proteins surrounding the self-assembled pigments on the lipid monolayer as characterized from *Chlorobi*, including CsmA, CsmB, CsmC, CsmD, CsmE, CsmF, CsmH, CsmI, CsmJ, CsmK, and CsmX.[5, 7] CsmA is the only highly conserved component in all the chlorosome-containing bacteria. The CsmA protein is associated with BChl *a* and only locates on the bottom side of the chlorosomes. A repeating dimer unit of the CsmA-BChl *a* complex forms a two-dimensional paracrystalline structure that is called the baseplate.[8-13] The long-range excitonic coupling in the chlorosomes allows rapid energy transfer to the baseplate with high quantum yield.[5] In the green sulfur bacteria, the energy is transferred to the FMO protein through the baseplate.[14] Cross-linking data using zero-length 1-Ethyl-3-(3-dimethylaminopropyl)carbodiimide (EDC) suggests that the FMO protein directly interacts with the CsmA protein, facilitating energy transfer.[15]

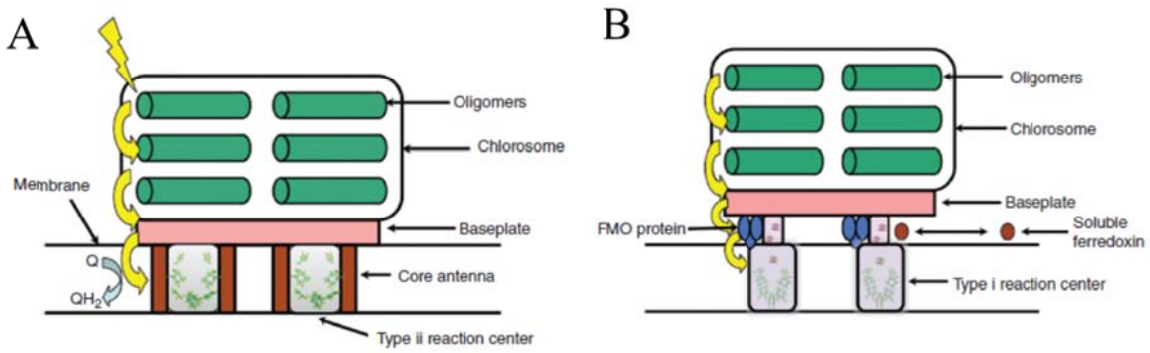

Figure 1.4 Schematic models of chlorosomes from (A) filamentous anoxygenic phototrophs and (B) green sulfur bacteria. The green tubes represent the pigment oligomers. The salmon layer is the baseplate complex. Blue ovals are FMO trimers. Brown ovals are soluble ferredoxins. The energy transfer sequence is shown by yellow arrows. (Figure adapted from ref. 1, Fig. 5.19)[1]

The water-soluble peripheral antenna FMO protein was the first pigment-containing complex with its atomic structure determined via X-ray crystallography.[16] The FMO protein is a homotrimer embracing 24 BChl *a* pigments (Figure 1.5).[17] Direct mass spectrometry measurement of the molecular weight of the intact FMO protein complex indicates that the eighth pigment is easily lost during purification.[18] The closely interacting BChl *a* in FMO facilitates exciton coupling.[19, 20] Owing to excitonic interactions, the collective BChl *a* Q_y absorption bands appear between 790 and 830 nm.[17, 21, 22] Energy transfer between individual pigments/excitons in the FMO protein reveals wave-like quantum coherence.[23, 24] The energy is further transferred to the reaction center complex through the FMO protein. Our lab, in collaboration with the Michael Gross group, revealed the orientation of FMO protein between the baseplate and the reaction center.[25, 26] We found that the side of FMO containing BChl *a* #3 contacts the cytoplasmic membrane using glycine ethyl ester (GEE) labeling.[26]

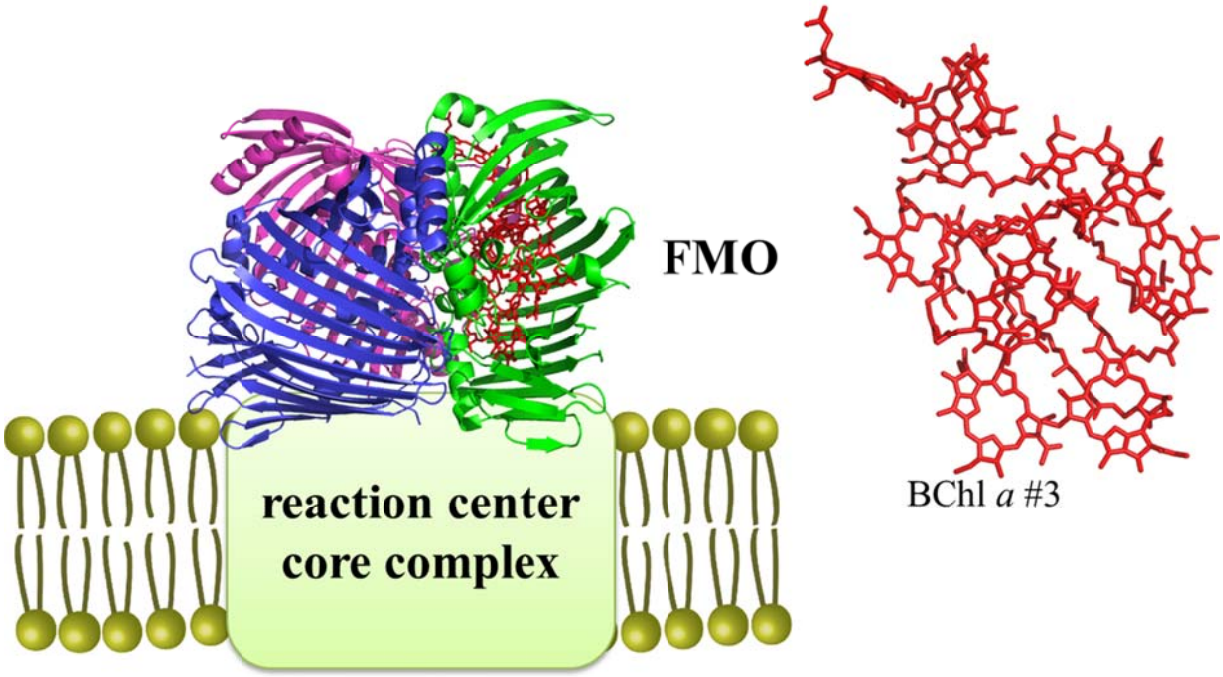

Figure 1.5 Orientation of the trimeric FMO protein associated with the reaction center core complex. The right side is the enlarged view showing the orientation of the BChls from a monomeric FMO. The BChl *a* #3 contacts the cytoplasmic membrane.

1.2 The reaction center complexes from green sulfur bacteria

The reaction center complex in *Chlorobaculum tepidum* is composed of the abovementioned FMO complex and the reaction center core (RCC) complex. The energy is transferred from the FMO protein complex to the RCC complex, which is an FeS-type (type I) reaction center, generally similar to photosystem I (PSI) in oxygenic photosynthetic organisms. Unlike the heterodimeric core PsaA-PsaB of PSI, the reaction center in *Chlorobaculum tepidum* exhibits a homodimeric core structure formed by two 82 kDa PscA proteins. The other three gene products in the RCC are the 24 kDa PscB Fe-S protein, a 23 kDa cytochrome c_{551} (PscC) protein and a 17

kDa PscD protein. [27] The PscA protein carries the primary donor P840 (a special pair of BChl *a*), the primary electron acceptor A_0 (Chl *a* 670), a possible secondary electron acceptor A_1 (menaquinone) and FeS-center X (F_x). [27-30] The PscA homodimer contains 16 BChls *a* revealing Q_y bands between 780 and 840 nm, four Chl *a* molecules and two carotenoid molecules.[31, 32] The four Chl *a*-molecules are esterified to 2, 6-phytadienol.[29] The PscB protein binds two 4Fe4S-centers called F_A and F_B as the terminal electron acceptors. The PscC protein, which mediates electron transfer from the menaquinol/cytochrome *c* oxidoreductase to P840, has three membrane-spanning regions at the N terminal end and a soluble domain that binds a single heme group at the C terminal end on the periplasmic side of the membrane.[33] The PscD subunit of RCC shows some similarities in the amino acid sequences with PsaD in the PSI of plants and cyanobacteria.[34] PscD is loosely bound to the RCC and is not essential for photosynthetic growth.[34] In addition, the lack of the PscD subunit does not induce any serious defect in the kinetics of electron transfer reactions.[34, 35]

The intact FMO-RCC complex and subunits of the RCC complex can be purified through detergent treatment of the photosynthetic membranes.[27, 32, 36-39] The PscA-PscB complex was purified previously from the green sulfur bacterium *Prosthecochloris aestuarii* using a hydroxyapatite column after detergent treatment.[27, 40, 41] The PscA-PscC complex was purified from *Chlorobaculum tepidum* and *Chlorobium limicola*.[32, 38, 40, 42] Two biochemical preparations can be made of the *Chlorobaculum tepidum* reaction center consisting of FMO and RCC (FMO-RCC) or a minimal complex containing only PscA and PscC. These two preparations have been commonly used for spectroscopic and biochemical analysis, but their use for successful structural studies has been limited.[37, 42-45] Both complexes have been studied by scanning transmission electron microscopy (STEM). STEM predicts 1-2 FMO copies per RCC for FMO-

RCC with a predicted mass of 454 kDa (Figure 1.6).[37] In the STEM images containing a single FMO, there is an apparent place for a second FMO, suggesting that either some FMO is lost during preparation or there may be two distinct populations of FMO-RCC. A small knob protrudes from the RCC that is likely PscB and PscD (Figure 1.7). For PscA-PscC, STEM analysis suggests two copies of the PscA subunit and at least one copy of the PscC subunit with a mass of 248 kDa (Figure 1.8).[42]

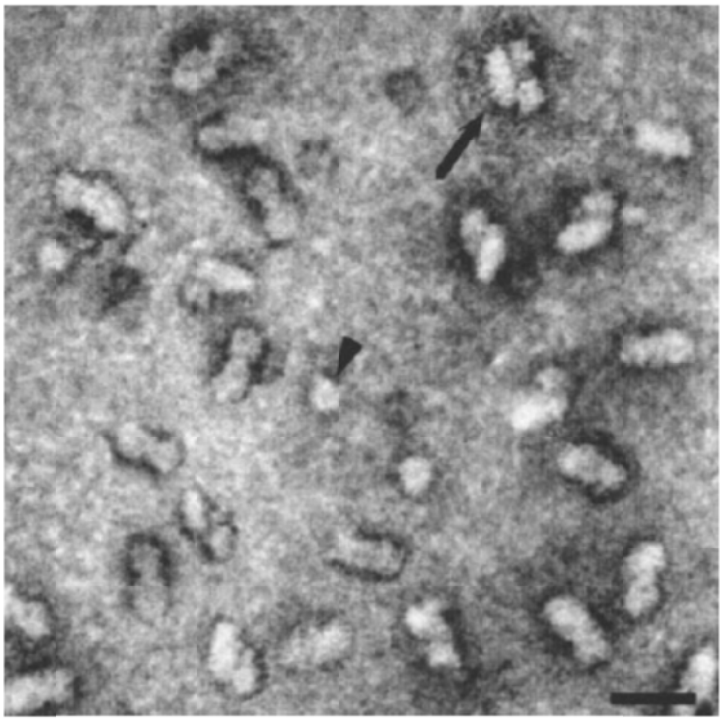

Figure 1.6 STEM dark field image of *Chlorobium tepidum* RC complexes. The arrowhead indicates the small particles identified as FMO proteins, while the arrow indicates RC complexes with two associated FMO trimers. The scale bar represents 20 nm. (Figure adapted from ref. 37, Fig. 3, Copyright (1999), with permission from Elsevier)[37]

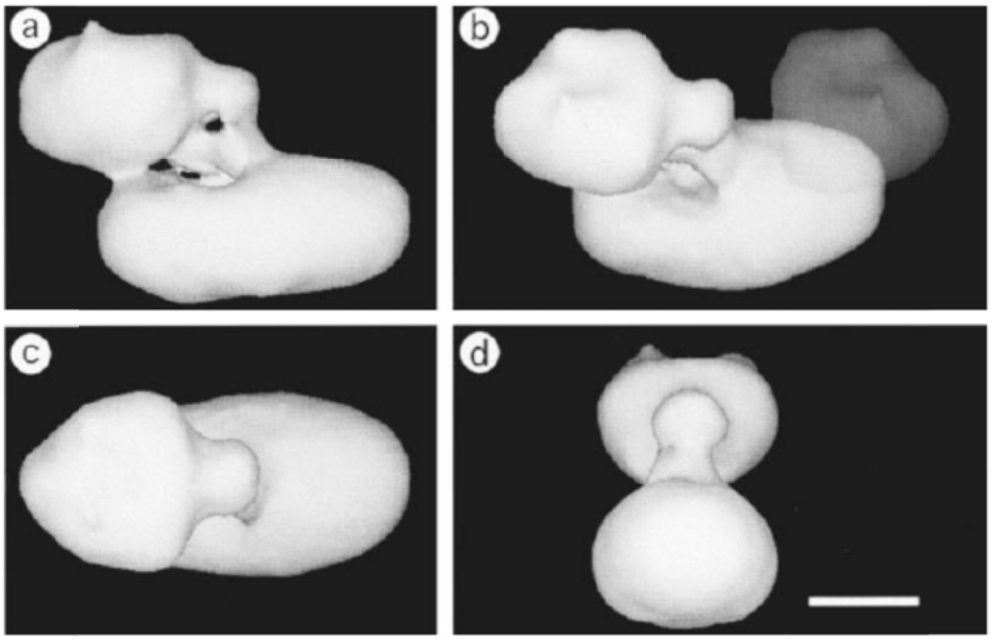

Figure 1.7 The 3D reconstruction of the RC complex. A total of 2741 images were used from the total data set of 4094. (b) The additional copy of an FMO trimer was placed to indicate its hypothetical location. The scale bar represents 5 nm. (Figure adapted from ref. 37, Fig. 6, Copyright (1999), with permission from Elsevier)[37]

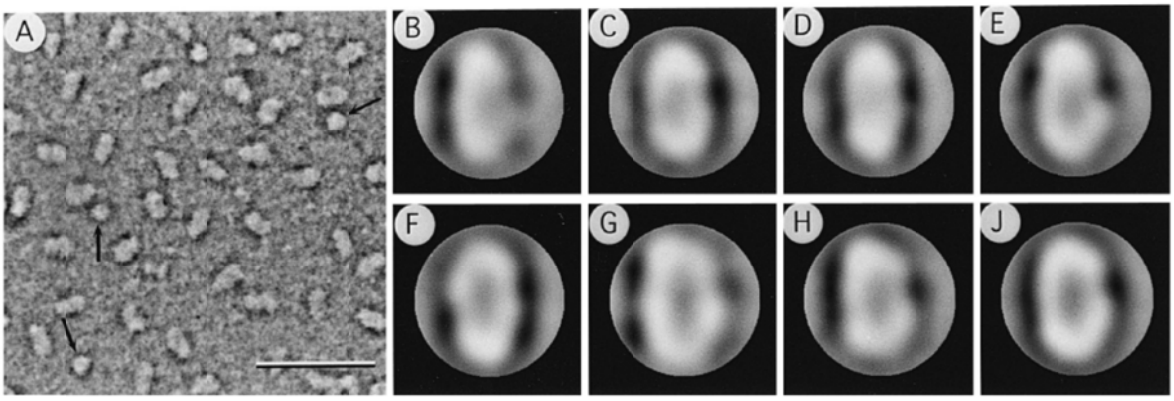

Figure 1.8 Electron microscopy and classification of negatively stained PscA-PscC complexes. (A) STEM dark field electron micrographs of *Chlorobium tepidum* PscA-PscC complexes. The contrast has been adapted to show the protein in light shades. Arrows mark the small particles identified as FMO proteins. The scale bar represents 50 nm. (B–J). Classification of 1690 projections, which were aligned and treated with multivariate statistical analysis. (Figure adapted from ref. 42, Fig. 4, Copyright (1997), with permission from Elsevier)[42]

High-resolution crystal structures are only available for FMO and the soluble heme-containing domain of PscC (Figure 1.5 and Figure 1.9). [33, 46] The lack of FMO-RCC crystal structure and the low resolution nature of STEM leave significant gaps in our understanding of the subunit organization of the FMO-RCC complex.

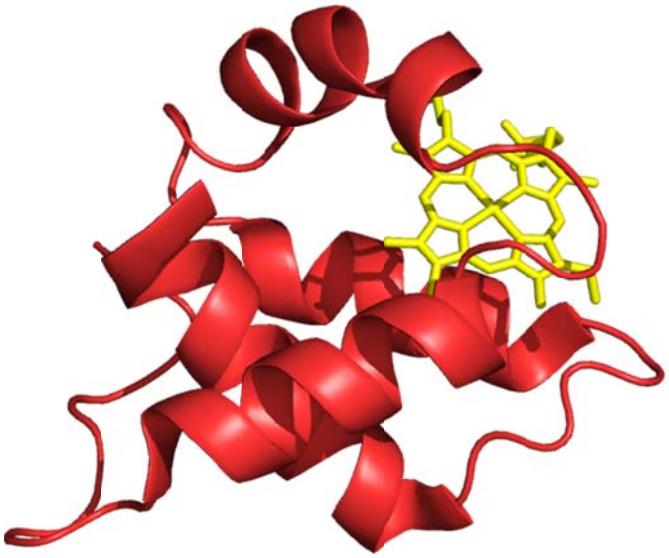

Figure 1.9 Crystal structure of PscC soluble domain. (Figure generated by Pymol from PDB file 3A9F)

1.3 Energy and electron transfer mechanisms

The photosynthetic apparatus of the anoxygenic photosynthetic green sulfur bacteria consists of the reaction center core (RCC) complex, the FMO peripheral antenna protein, and chlorosome antenna complexes plus the menaquinol/cytochrome *c* oxidoreductase (cytochrome *bc* complex).[30] The light energy collected by the chlorosomes is transferred to the reaction center

core (RCC) complex through the chlorosome baseplate and the FMO protein.[30-32, 47-52] The chlorosomes dominate the absorption spectrum of intact cells in the region of 720-750 nm. The FMO trimer contains 24 molecules of bacteriochlorophyll *a* (BChl *a*) with Q_y absorption bands in the region of 790-830 nm.[17, 21, 22] The reaction center of the green sulfur bacteria is a P840-reaction center. Functional intact reaction center is composed of a 120 kDa FMO trimer, an 82 kDa homodimer PscA protein, a 24 kDa PscB, a 23 kDa cytochrome c_{551} (PscC) protein and a 17 kDa PscD protein.[30, 41] The primary electron donor P840 (a special pair of BChl *a* with a Q_y band appearing at cryogenic temperature at ~838 nm), the primary electron acceptor A_0 (Chl *a*-derivative), a secondary electron acceptor A_1 (menaquinone) and iron-sulfur cluster F_x are all located in the PscA.[28-30] The PscB contains iron-sulfur clusters F_A and F_B that are analogous to the terminal electron acceptors of the PsaC in Photosystem I (PSI).[53] All the three iron-sulfur clusters are 4Fe-4S clusters.[30] The PscD subunit is analogous to the PsaD in PSI.[34]

The dynamics of excitation energy and electron transfer in the reaction center complex from the green sulfur bacteria have been studied for many years.[27-29, 39-41, 44, 45, 48, 50, 51, 54-64] The electron transport chain and the time for each step are summarized in Figure 1.10.[30] The redox potential of the P840 is found to be 240 mV.[65, 66] The PscC subunit has three transmembrane complexes and a heme domain. There are two copies of PscC associated with each RCC.[50] The redox potential of the cytochrome *c* is approximately 53 mV more negative than that of P840.[62] The cytochrome *c* donates electrons to the $P840^+$ with a time of 7 μs in whole cells and 100 μs in isolated reaction center complexes.[30, 62] The time also depends on the viscosity of the medium.[67] The excited P840 reacts with A_0 to form $P840^+A_0^-$. The step is called primary charge separation and the time is 10-30 ps.[27, 40, 45, 48, 56, 62] The time of the charge recombination between $P840^+$ and A_0^- to the triplet state of P840 is about 20-35 ns and the decay of the triplet P840 is 90 μs.[56, 68]

The electron is transferred forward from A_0^- to F_x and the transfer time is approximately 600 ps.[56] F_x further transfers the electron to the terminal electron acceptor F_A and F_B in the PscB subunit. The F_A and F_B reduce ferredoxin at high rates.[69]

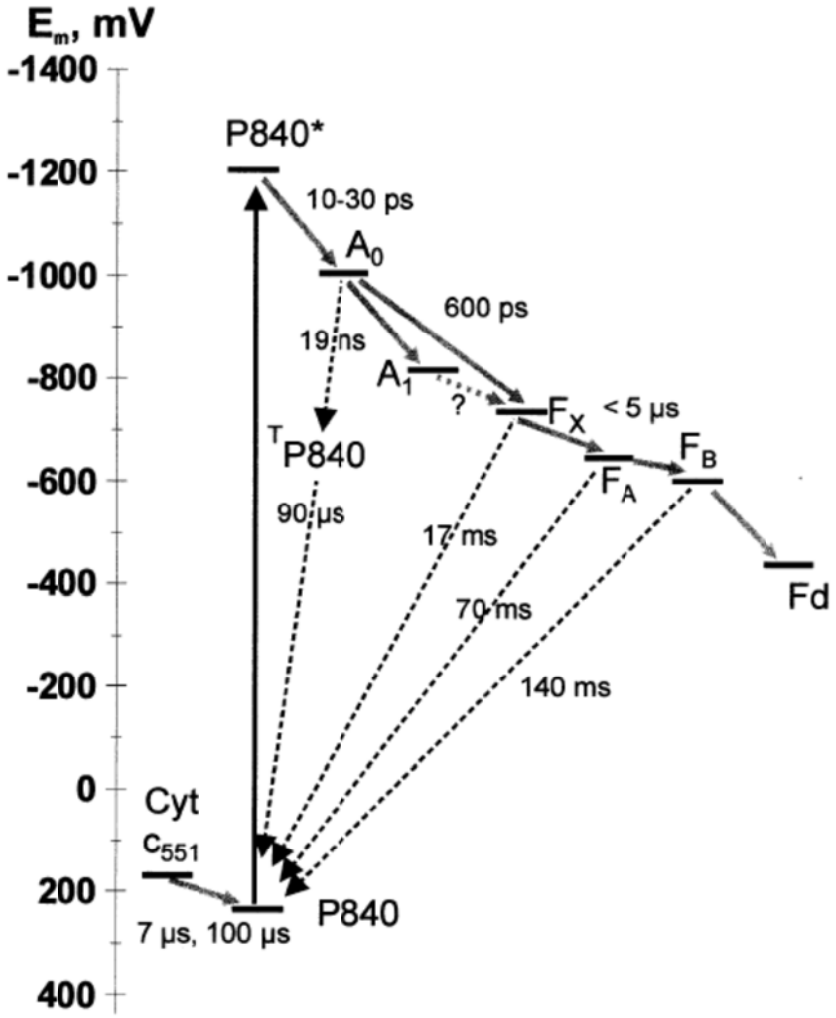

Figure 1.10 Redox potentials and time of electron transfer in the P840-reaction center. (Figure reprinted from ref. 30, Fig. 7, Copyright (2001), with permission from Elsevier)[30]

Transient absorption (TA) studies performed on the RCC complex show that energy transfer to BChl *a*-837 in the electronically coupled system is approximately 2 ps, and the subsequent

charge separation is about 25 ps.[39] It also shows that the Chl *a* can transfer energy to the BChl *a* and P840. The rate determination step remains unclear, however, as shown in Figure 1.11. The process can be either limited by the charge separation (Figure 1.11A) or by the energy transfer rate from BChl *a* 837 to P840 (Figure 1.11B).[30]

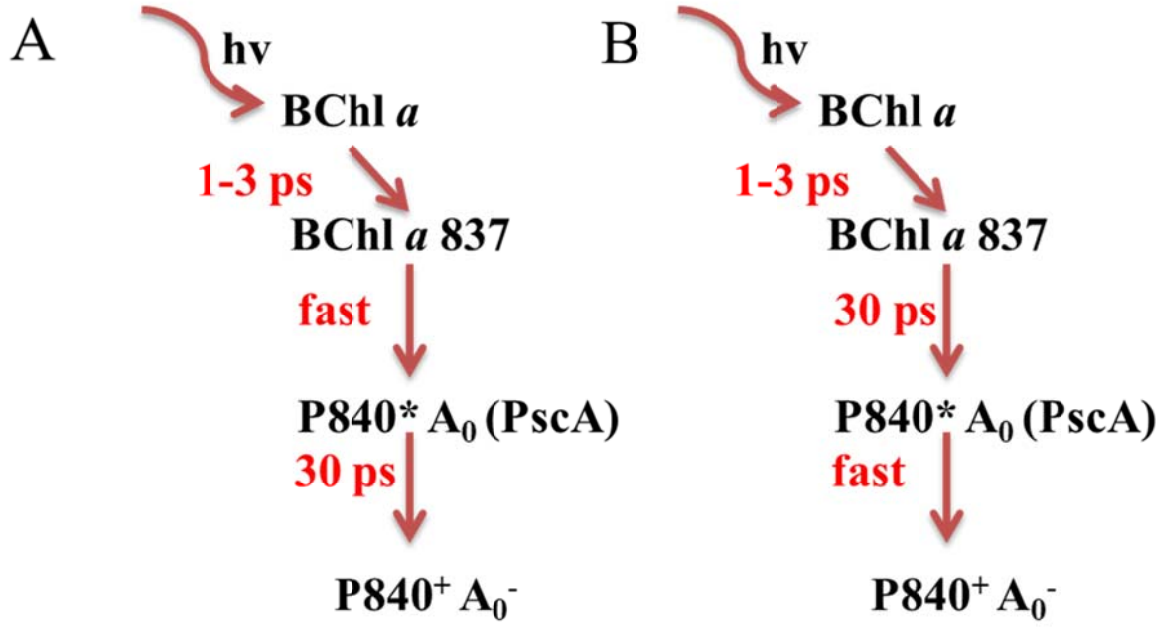

Figure 1.11 Two models for energy transfer and charge separation in the reaction center: the trap-limited model (A) and the diffusion limited model (B)

The energy transfer efficiency from the FMO complex to the RCC were studied by TA and fluorescence, and all the studies showed relatively low efficiency. TA studies performed in the sub-nanosecond time scale on the FMO-RCC complex showed similar spectral and dynamic features as the isolated FMO complex when excited at BChl *a* Q_x or Q_y bands (~590 and 790 nm, respectively), indicating that the energy transfer efficiency from the FMO complex to the RCC is low.[44, 45] The energy transfer efficiency from the FMO protein to the RCC complex was reported

to be 35% or lower based on the fluorescence analysis.[51] The reason for the low efficiency is not clear.

1.4 Thesis statement

The crystal structure of the reaction center complex from the green sulfur bacteria is not available yet, and high resolution crystal structures are only available for FMO and the soluble heme-containing domain of PscC. The lack of the crystal structure of the intact reaction center complex leaves significant gaps in our understanding of the subunit organization. In addition, the energy transfer mechanism from FMO to RCC is not well understood. Studies on the kinetics of the energy/electron transfer in the RCC (PscA-PscC) complex are also relatively limited. To understand the spatial interaction between FMO and RCC, we studied the intact reaction center complex (FMO-RCC) by chemically cross-linking the purified sample and subsequent LC-MS/MS. We proposed a structural model of the intact reaction center complex based on those results. Besides, we have made detailed comparisons of the reaction center complex of green sulfur bacteria both with (FMO-RCC complex) and without (RCC complex) the FMO antenna complex to elucidate an anticipated FMO-to-RCC inter-protein energy transfer as well as RCC intra-protein energy and electron transfer.

References

(1) Blankenship, R. E. Molecular mechanisms of photosynthesis, 2nd Edition. *Wiley-Blackwell* **2014**.

(2) Bekker, A.; Holland, H. D.; Wang, P. L.; Rumble, D.; Stein, H. J.; Hannah, J. L.; Coetzee, L. L.; Beukes, N. J. Dating the rise of atmospheric oxygen. *Nature* **2004**, *427*, 117-120.

(3) Boone, D. R.; Garrity, G. M.; Castenholz, R. W. (eds) Bergey's Manual of systematic bacteriology: volume one: The archaea and the deeply branching and phototrophic bacteria, 2nd Edn. *Dordrecht: Springer* **2001**.

(4) Dworkin, M.; Falkow, S.; Rosenberg, E.; Schleifer KH; Stackebrandt E. (eds) The Prokaryotes, 3rd Edn. *Berlin: Springer* **2006**.

(5) Orf, G. S.; Blankenship, R. E. Chlorosome antenna complexes from green photosynthetic bacteria *Photosynthesis Research* **2013**, *116*, 315-331.

(6) Robert E. Blankenship; John M. Olson; Miller, M. Advances in photosynthesis and respiration: volume two: Antenna complexes from green photosynthetic bacteria. *Springer* **1995**.

(7) Li, H.; Bryant, D. A. Envelope proteins of the CsmB/CsmF and CsmC/CsmD motif families influence the size, shape, and composition of chlorosomes in *Chlorobaculum tepidum*. *Journal of Bacteriology* **2009**, *191*, 7109-7120.

(8) Betti, J. A.; Blankenship, R. E.; Natarajan, L. V.; Dickinson, L. C.; Fuller, R. C. Antenna organization and evidence for the function of a new antenna pigment species in the green photosynthetic bacterium *Chloroflexus aurantiacus*. *Biochimica Et Biophysica Acta* **1982**, *680*, 194-201.

(9) Bryant, D. A.; Vassilieva, E. V.; Frigaard, N. U.; Li, H. Selective protein extraction from *Chlorobium tepidum* chlorosomes using detergents. Evidence that CsmA forms multimers and binds bacteriochlorophyll *a*. *Biochemistry* **2002**, *41*, 14403-14411.

(10) Gerola, P. D.; Olson, J. M. A new bacteriochlorophyll *a*-protein complex associated with chlorosomes of green sulfur bacteria. *Biochimica Et Biophysica Acta* **1986**, *848*, 69-76.

(11) Montano, G. A.; Wu, H. M.; Lin, S.; Brune, D. C.; Blankenship, R. E. Isolation and characterization of the B798 light-harvesting baseplate from the chlorosomes of *Chloroflexus aurantiacus*. *Biochemistry* **2003**, *42*, 10246-10251.

(12) Sakuragi, Y.; Frigaard, N. U.; Shimada, K.; Matsuura, K. Association of bacteriochlorophyll *a* with the CsmA protein in chlorosomes of the photosynthetic green filamentous bacterium *Chloroflexus aurantiacus*. *Biochimica Et Biophysica Acta-Bioenergetics* **1999**, *1413*, 172-180.

(13) Pedersen, M. O.; Borch, J.; Hojrup, P.; Cox, R. P.; Miller, M. The light-harvesting antenna of *Chlorobium tepidum*: Interactions between the FMO protein and the major chlorosome protein CsmA studied by surface plasmon resonance. *Photosynthesis Research* **2006**, *89*, 63-69.

(14) Olson, J. M. The FMO protein. *Photosynthesis Research* **2004**, *80*, 181-187.

(15) Li, H.; Frigaard, N. U.; Bryant, D. A. Molecular contacts for chlorosome envelope proteins revealed by cross-linking studies with chlorosomes from *Chlorobium tepidum*. *Biochemistry* **2006**, *45*, 9095-9103.

(16) Li, Y. F.; Zhou, W. L.; Blankenship, R. E.; Allen, J. P. Crystal structure of the bacteriochlorophyll *a* protein from *Chlorobium tepidum*. *Journal of Molecular Biology* **1997**, *271*, 456-471.

(17) Busch, M. S. A.; Mueh, F.; Madjet, M. E.-A.; Renger, T. The eighth bacteriochlorophyll completes the excitation energy funnel in the FMO protein. *Journal of Physical Chemistry Letters* **2011**, *2*, 93-98.
(18) Wen, J. Z.; Zhang, H.; Gross, M. L.; Blankenship, R. E. Native electrospray mass spectrometry reveals the nature and stoichiometry of pigments in the FMO photosynthetic antenna protein. *Biochemistry* **2011**, *50*, 3502-3511.
(19) Freiberg, A.; Lin, S.; Timpmann, K.; Blankenship, R. E. Exciton dynamics in FMO bacteriochlorophyll protein at low temperatures. *Journal of Physical Chemistry B* **1997**, *101*, 7211-7220.
(20) Fidler, A. F.; Caram, J. R.; Hayes, D.; Engel, G. S. Towards a coherent picture of excitonic coherence in the Fenna-Matthews-Olson complex. *Journal of Physics B-Atomic Molecular and Optical Physics* **2012**, *45*, 154013- 154022.
(21) Wen, J.; Zhang, H.; Gross, M. L.; Blankenship, R. E. Native electrospray mass spectrometry reveals the nature and stoichiometry of pigments in the FMO photosynthetic antenna protein. *Biochemistry* **2011**, *50*, 3502-3511.
(22) Tronrud, D. E.; Wen, J.; Gay, L.; Blankenship, R. E. The structural basis for the difference in absorbance spectra for the FMO antenna protein from various green sulfur bacteria. *Photosynthesis Research* **2009**, *100*, 79-87.
(23) Engel, G. S.; Calhoun, T. R.; Read, E. L.; Ahn, T. K.; Mancal, T.; Cheng, Y. C.; Blankenship, R. E.; Fleming, G. R. Evidence for wavelike energy transfer through quantum coherence in photosynthetic systems. *Nature* **2007**, *446*, 782-786.
(24) Panitchayangkoon, G.; Hayes, D.; Fransted, K. A.; Caram, J. R.; Harel, E.; Wen, J.; Blankenship, R. E.; Engel, G. S. Long-lived quantum coherence in photosynthetic complexes at physiological temperature. *Proceedings of the National Academy of Sciences* **2010**, *107*, 12766-12770.
(25) Huang, R. Y. C.; Wen, J.; Blankenship, R. E.; Gross, M. L. Hydrogen-deuterium exchange mass spectrometry reveals the interaction of Fenna-Matthews-Olson protein and chlorosome CsmA protein. *Biochemistry* **2012**, *51*, 187-193.
(26) Wen, J.; Zhang, H.; Gross, M. L.; Blankenship, R. E. Membrane orientation of the FMO antenna protein from *Chlorobaculum tepidum* as determined by mass spectrometry-based footprinting. *Proceedings of the National Academy of Sciences* **2009**, *106*, 6134-6139.
(27) Permentier, H. P.; Schmidt, K. A.; Kobayashi, M.; Akiyama, M.; Hager-Braun, C.; Neerken, S.; Miller, M.; Amesz, J. Composition and optical properties of reaction centre core complexes from the green sulfur bacteria *Prosthecochloris aestuarii* and *Chlorobium tepidum*. *Photosynthesis Research* **2000**, *64*, 27-39.
(28) Kjaer, B.; Frigaard, N. U.; Yang, F.; Zybailov, B.; Miller, M.; Golbeck, J. H.; Scheller, H. V. Menaquinone-7 in the reaction center complex of the green sulfur bacterium *Chlorobium vibrioforme* functions as the electron acceptor A_1. *Biochemistry* **1998**, *37*, 3237-3242.
(29) Kobayashi, M.; Oh-oka, H.; Akutsu, S.; Akiyama, M.; Tominaga, K.; Kise, H.; Nishida, F.; Watanabe, T.; Amesz, J.; Koizumi, M.; Ishida, N.; Kano, H. The primary electron acceptor of green sulfur bacteria, bacteriochlorophyll 663, is chlorophyll *a* esterified with Delta 2,6-phytadienol. *Photosynthesis Research* **2000**, *63*, 269-280.
(30) Hauska, G.; Schoedl, T.; Remigy, H.; Tsiotis, G. The reaction center of green sulfur bacteria. *Biochimica Et Biophysica Acta-Bioenergetics* **2001**, *1507*, 260-277.

(31) Remigy, H. W.; Hauska, G.; Muller, S. A.; Tsiotis, G. The reaction centre from green sulphur bacteria: progress towards structural elucidation. *Photosynthesis Research* **2002**, *71*, 91-98.
(32) Griesbeck, C.; Hager-Braun, C.; Rogl, H.; Hauska, G. Quantitation of P840 reaction center preparations from *Chlorobium tepidum*: chlorophylls and FMO-protein. *Biochimica Et Biophysica Acta-Bioenergetics* **1998**, *1365*, 285-293.
(33) Hirano, Y.; Higuchi, M.; Azai, C.; Oh-oka, H.; Miki, K.; Wang, Z.-Y. Crystal structure of the electron carrier domain of the reaction center cytochrome *c(z)* subunit from green photosynthetic bacterium *Chlorobium tepidum*. *Journal of Molecular Biology* **2010**, *397*, 1175-1187.
(34) Tsukatani, Y.; Miyamoto, R.; Itoh, S.; Oh-oka, H. Function of a PscD subunit in a homodimeric reaction center complex of the photosynthetic green sulfur bacterium *Chlorobium tepidum* studied by insertional gene inactivation - Regulation of energy transfer and ferredoxin-mediated $NADP^+$ reduction on the cytoplasmic side. *Journal of Biological Chemistry* **2004**, *279*, 51122-51130.
(35) Azai, C.; Kim, K.; Kondo, T.; Harada, J.; Itoh, S.; Oh-oka, H. A heterogeneous tag-attachment to the homodimeric type 1 photosynthetic reaction center core protein in the green sulfur bacterium *Chlorobaculum tepidum*. *Biochimica Et Biophysica Acta-Bioenergetics* **2011**, *1807*, 803-812.
(36) Hagerbraun, C.; Xie, D. L.; Jarosch, U.; Herold, E.; Buttner, M.; Zimmermann, R.; Deutzmann, R.; Hauska, G.; Nelson, N. Stable photobleaching of P840 in chlorobium reaction-center preparations - Presence of the 42-kDa bacteriochlorophyll *a*-protein and a 17-kDa polypeptide. *Biochemistry* **1995**, *34*, 9617-9624.
(37) Remigy, H. W.; Stahlberg, H.; Fotiadis, D.; Muller, S. A.; Wolpensinger, B.; Engel, A.; Hauska, G.; Tsiotis, G. The reaction center complex from the green sulfur bacterium *Chlorobium tepidum*: A structural analysis by scanning transmission electron microscopy. *Journal of Molecular Biology* **1999**, *290*, 851-858.
(38) Oh-oka, H.; Kakutani, S.; Kamei, S.; Matsubara, H.; Iwaki, M.; Itoh, S. Highly purified photosynthetic reaction-center (Psca/cytochrome $c_{551})_2$ complex of the green sulfur bacterium *Chlorobium limicola*. *Biochemistry* **1995**, *34*, 13091-13097.
(39) Neerken, S.; Schmidt, K. A.; Aartsma, T. J.; Amesz, J. Dynamics of energy conversion in reaction center core complexes of the green sulfur bacterium *Prosthecochloris aestuarii* at low temperature. *Biochemistry* **1999**, *38*, 13216-13222.
(40) Schmidt, K. A.; Neerken, S.; Permentier, H. P.; Hager-Braun, C.; Amesz, J. Electron transfer in reaction center core complexes from the green sulfur bacteria *Prosthecochloris aestuarii* and *Chlorobium tepidum*. *Biochemistry* **2000**, *39*, 7212-7220.
(41) Francke, C.; Permentier, H. P.; Franken, E. M.; Neerken, S.; Amesz, J. Isolation and properties of photochemically active reaction center complexes from the green sulfur bacterium *Prosthecochloris aestuarii*. *Biochemistry* **1997**, *36*, 14167-14172.
(42) Tsiotis, G.; Hager-Braun, C.; Wolpensinger, B.; Engel, A.; Hauska, G. Structural analysis of the photosynthetic reaction center from the green sulfur bacterium *Chlorobium tepidum*. *Biochimica Et Biophysica Acta-Bioenergetics* **1997**, *1322*, 163-172.
(43) Oh-oka, H.; Kakutani, S.; Matsubara, H.; Malkin, R.; Itoh, S. Isolation of the photoactive reaction center complex that contains 3 types of Fe-S centers and a cytochrome-c subunit from the green sulfur bacterium *chlorobium limicola f. thiosulfatophilum*, Strain Larsen. *Plant and Cell Physiology* **1993**, *34*, 93-101.

(44) Neerken, S.; Permentier, H. P.; Francke, C.; Aartsma, T. J.; Amesz, J. Excited states and trapping in reaction center complexes of the green sulfur bacterium *Prosthecochloris aestuarii*. *Biochemistry* **1998**, *37*, 10792-10797.
(45) Oh-Oka, H.; Kamei, S.; Matsubara, H.; Lin, S.; van Noort, P. I.; Blankenship, R. E. Transient absorption spectroscopy of energy-transfer and trapping processes in the reaction center complex of *Chlorobium tepidum*. *Journal of Physical Chemistry B* **1998**, *102*, 8190-8195.
(46) Camara-Artigas, A.; Blankenship, R. E.; Allen, J. P. The structure of the FMO protein from *Chlorobium tepidum* at 2.2 angstrom resolution. *Photosynthesis Research* **2003**, *75*, 49-55.
(47) Swarthoff, T.; Amesz, J. Photochemically active pigment-protein complexes from the green photosynthetic bacterium *Prosthecochloris-aestuarii*. *Biochimica et biophysica acta* **1979**, *548*, 427-432.
(48) Swarthoff, T.; Vanderveekhorsley, K. M.; Amesz, J. The primary charge separation, cytochrome oxidation and triplet formation in preparations from the green photosynthetic bacterium *Prosthecochloris aestuarii*. *Biochimica et biophysica acta* **1981**, *635*, 1-12.
(49) Feiler, U.; Nitschke, W.; Michel, H. Characterization of an improved reaction center preparation from the photosynthetic green sulfur bacterium *Chlorobium* containing the FeS centers F_a and F_b and a bound cytochrome subunit. *Biochemistry* **1992**, *31*, 2608-2614.
(50) Oh-oka, H.; Kamei, S.; Matsubara, H.; Iwaki, M.; Itoh, S. 2 molecules of cytochrome c function as the electron-donors to P840 in the reaction center complex isolated from a green sulfur bacterium, *Chlorobium tepidum*. *FEBS Letters* **1995**, *365*, 30-34.
(51) Francke, C.; Otte, S. C. M.; Miller, M.; Amesz, J.; Olson, J. M. Energy transfer from carotenoid and FMO protein in subcellular preparations from green sulfur bacteria. Spectroscopic characterization of an FMO-reaction center core complex at low temperature. *Photosynthesis Research* **1996**, *50*, 71-77.
(52) Itoh, M.; Seo, D.; Sakurai, H.; Setif, P. Kinetics of electron transfer between soluble cytochrome c-554 and purified reaction center complex from the green sulfur bacterium *Chlorobium tepidum*. *Photosynthesis Research* **2002**, *71*, 125-135.
(53) Figueras, J. B.; Cox, R. P.; Hojrup, P.; Permentier, H. P.; Miller, M. Phylogeny of the PscB reaction center protein from green sulfur bacteria. *Photosynthesis Research* **2002**, *71*, 155-164.
(54) Neerken, S.; Ma, Y. Z.; Aschenbrucker, J.; Schmidt, K. A.; Nowak, F. R.; Permentier, H. P.; Aartsma, T. J.; Gillbro, T.; Amesz, J. Kinetics of absorbance and anisotropy upon excited state relaxation in the reaction center core complex of a green sulfur bacterium. *Photosynthesis Research* **2000**, *65*, 261-268.
(55) Vassiliev, I. R.; Kjaer, B.; Schorner, G. L.; Scheller, H. V.; Golbeck, J. H. Photoinduced transient absorbance spectra of P840/$P840^+$ and the FMO protein in reaction centers of *Chlorobium vibrioforme*. *Biophysical Journal* **2001**, *81*, 382-393.
(56) Nuijs, A. M.; Vasmel, H.; Joppe, H. L. P.; Duysens, L. N. M.; Amesz, J. Excited states and primary charge separation in the pigment system of the green photosynthetic bacterium *Prosthecochloris aestuarii* as studied by picosecond absorbance difference spectroscopy. *Biochimica et Biophysica Acta* **1985**, *807*, 24-34.
(57) Miller, M.; Liu, X. M.; Snyder, S. W.; Thurnauer, M. C.; Biggins, J. Photosynthetic electron-transfer reactions in the green sulfur bacterium *Chlorobium vibrioforme* - Evidence for the functional involvement of iron-sulfur redox centers on the acceptor side of the reaction center. *Biochemistry* **1992**, *31*, 4354-4363.

(58) Dimagno, L.; Chan, C. K.; Jia, Y. W.; Lang, M. J.; Newman, J. R.; Mets, L.; Fleming, G. R.; Haselkorn, R. Energy transfer and trapping in photosystem I reaction centers from cyanobacteria. *Proceedings of the National Academy of Sciences* **1995**, *92*, 2715-2719.
(59) Kusumoto, N.; Inoue, K.; Sakurai, H. Spectroscopic studies of bound cytochrome c and an iron-sulfur center in a purified reaction center complex from the green sulfur bacterium *Chlorobium tepidum*. *Photosynthesis Research* **1995**, *43*, 107-112.
(60) Frankenberg, N.; HagerBraun, C.; Feiler, U.; Fuhrmann, M.; Rogl, H.; Schneebauer, N.; Nelson, N.; Hauska, G. P840-reaction centers from *Chlorobium tepidum* - Quinone analysis and functional reconstitution into lipid vesicles. *Photochemistry and Photobiology* **1996**, *64*, 14-19.
(61) Oh-Oka, H.; Iwaki, M.; Itoh, S. Membrane-bound cytochrome *c(z)* couples quinol oxidoreductase to the P840 reaction center complex in isolated membranes of the green sulfur bacterium *Chlorobium tepidum*. *Biochemistry* **1998**, *37*, 12293-12300.
(62) Kusumoto, N.; Setif, P.; Brettel, K.; Seo, D.; Sakurai, H. Electron transfer kinetics in purified reaction centers from the green sulfur bacterium *Chlorobium tepidum* studied by multiple-flash excitation. *Biochemistry* **1999**, *38*, 12124-12137.
(63) Seo, D.; Itou, M.; Sakurai, H.; Setif, P. Studies on electron transfer reactions linked to the reaction center complex from the green sulfur bacterium *Chlorobium tepidum*. *Plant and Cell Physiology* **2002**, *43*, S29-S29.
(64) Azai, C.; Tsukatani, Y.; Itoh, S.; Oh-oka, H. C-type cytochromes in the photosynthetic electron transfer pathways in green sulfur bacteria and heliobacteria. *Photosynthesis Research* **2010**, *104*, 189-199.
(65) Prince R. C., Olson J. M. Some thermodynamic and kinetic properties of the primary photochemical reactants in a complex from a green photosynthetic bacterium. *Biochimica et Biophysica Acta* **1976**, *423*, 357-362.
(66) Fowler C. F.; Nugent N. A.; Fuller, R. C. The Isolation and Characterization of a Photochemically Active Complex from *Chloropseudomonas ethylica*. *Proceedings of the National Academy of Sciences* **1971**, *68*, 2278-2282.
(67) Oh-Oka, H.; Iwaki, M.; Itoh, S. Viscosity dependence of the electron transfer rate from bound cytochrome c to P840 in the photosynthetic reaction center of the green sulfur bacterium *Chlorobium tepidum*. *Biochemistry* **1997**, *36*, 9267-9272.
(68) Shuvalov, V. A.; Amesz, J.; Duysens, L. N. M. Picosecond spectroscopy of isolated membranes of the photosynthetic green sulfur bacterium *Prosthecochloris aestuarii* upon selective excitation of the primary electron donor. *Biochimica et Biophysica Acta* **1986**, *851*, 1-5.
(69) Kjaer, B.; Jung, Y. S.; Yu, L. A.; Golbeck, J. H.; Scheller, H. V. Iron-sulfur centers in the photosynthetic reaction center complex from *Chlorobium vibrioforme* - Differences from and similarities to the iron-sulfur centers in photosystem I. *Photosynthesis Research* **1994**, *41*, 105-114.

Chapter 2: Structural Analysis of the Homodimeric Reaction Center Complex from the Photosynthetic Green Sulfur Bacterium *Chlorobaculum tepidum*

This chapter is based on a recent publication:
He, G.; Zhang, H.; King, J. D.; Blankenship, R. E. Structural Analysis of the Homodimeric Reaction Center Complex from the Photosynthetic Green Sulfur Bacterium *Chlorobaculum tepidum*. *Biochemistry* **2014**, *53*, 4924-4930.

Abstract

The reaction center (RC) complex of the green sulfur bacterium *Chlorobaculum tepidum* is composed of the Fenna-Matthews-Olson (FMO) antenna protein and the reaction center core (RCC) complex. The RCC complex has four subunits: PscA, PscB, PscC, and PscD. We studied the FMO-RCC complex by chemically cross-linking the purified sample followed by biochemical and spectroscopic analysis. Blue-native gels showed that there were two types of FMO-RCC complexes, which are consistent with complexes with one copy of FMO per RCC and two FMO per RCC. SDS-PAGE analysis of the samples after cross-linking showed that all the five subunits of the RC can be linked by three different cross-linkers: Bissulfosuccinimidyl suberate (BS^3), Disuccinimidyl suberate (DSS) and 3,3-Dithiobis-sulfosuccinimidyl propionate (DTSSP). The interaction sites of the cross-linked complex were also studied using LC-MS/MS. The results indicated that FMO, PscB, PscD and part of PscA are exposed on the cytoplasmic side of the membrane. PscD helps stabilize FMO to the reaction center and may facilitate the electron transfer from RC to ferredoxin (Fd). The soluble domain of the heme-containing cytochrome subunit PscC and part of the core subunit PscA are located on the periplasmic side of

the membrane. There is a close relationship between the periplasmic portions of PscA and PscC, which is needed for efficient electron transfer between PscC and P840.

2.1 Introduction

The photosynthetic apparatus of the anoxygenic photosynthetic green sulfur bacterium *Chlorobaculum tepidum* consists of the reaction center core (RCC) complex, the FMO antenna protein and chlorosome antenna complexes plus the menaquinol/cytochrome *c* oxidoreductase (cytochrome *bc* complex).[1] The light energy collected by the chlorosome is transferred to the reaction center core (RCC) complex through the chlorosome baseplate and the FMO protein. [1] The chlorosomes dominate the absorption spectrum of intact cells in the region of 720-750 nm. The FMO trimer contains 24 molecules of bacteriochlorophyll *a* (BChl *a*) with Q_y absorption bands in the region of 790-830 nm.[2-4] The RCC complex, which is embedded in the cytoplasmic membrane, contains 16 BChl *a*, 4 chlorophyll *a* (Chl *a*) and 2 carotenoids.[1, 5, 6] The RCC complex in *Chlorobaculum tepidum* is an FeS-type (type I) reaction center with a homodimeric core structure formed by two 82 kDa PscA proteins. The other three gene products in the RCC are the 24 kDa PscB Fe-S protein, a 23 kDa cytochrome c_{551} (PscC) protein, and a 17 kDa PscD protein (Figure 2.1). [5] The PscA protein carries the primary donor P840 (a special pair of BChl *a*), the primary electron acceptor A_0 (Chl *a* 670), a possible secondary electron acceptor A_1 (menaquinone) and FeS-center X (F_x). [1, 5, 7, 8] The PscB protein binds two 4Fe4S-centers called F_A and F_B as the terminal electron acceptors. The PscC protein, which mediates electron transfer from the menaquinol/cytochrome *c* oxidoreductase to P840, has three membrane-spanning regions at the N terminus and a soluble domain that binds a single heme group at the C terminal end on the periplasmic side of the membrane. [9] The PscD subunit of RCC shows some

similarities in the amino acid sequences with that of PsaD in the PSI of plants and cyanobacteria.[10] PscD is loosely bound to the RCC and is not essential for photosynthetic growth.[10] In addition, the lack of the PscD subunit does not induce any serious defect in the kinetics of electron transfer reactions. [10, 11] A structural model of the RC complex is shown in Figure 2.1.

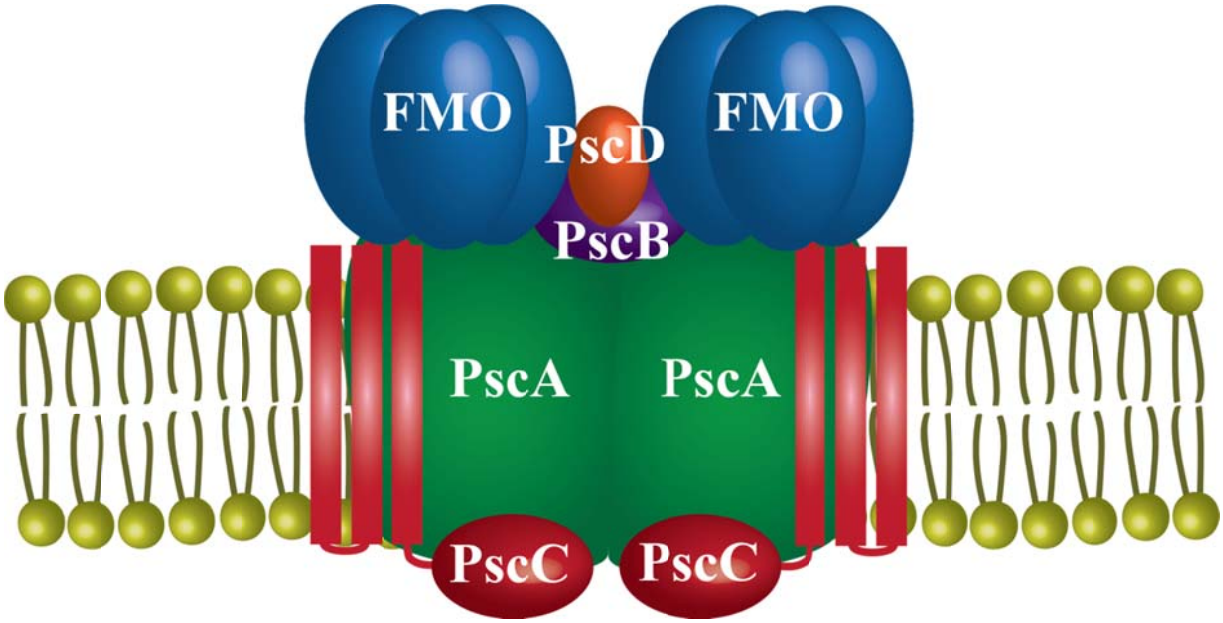

Figure 2.1 A structural model of the FMO-RCC complex

Both FMO-RCC complex and the RCC complex (a minimal complex containing PscA-PscC) can be made of the *Chlorobaculum tepidum* reaction center. The two complexes have been studied by scanning transmission electron microscopy (STEM). STEM predicts 1-2 FMO copies per RCC for FMO-RCC with a predicted mass of 454 kDa.[12] A small knob protrudes from the RCC, which is likely PscB and PscD. For PscA-PscC, STEM analysis suggests two copies of the PscA subunit and at least one copy of the PscC subunit with a mass of 248 kDa.[13] High resolution crystal structures are only available for FMO and the soluble heme-containing domain of PscC. [9,

[14] The lack of FMO-RCC crystal structure and the low resolution nature of STEM limit our understanding of the subunit organization of the FMO-RCC complex.

Structural mass spectrometry provides useful tools for characterizing protein organization.[15-17] Previously, our lab, working with the Michael Gross lab, revealed the orientation of FMO protein between the baseplate and the RCC.[18, 19] We found, using glycine ethyl ester (GEE) labeling, that the side of FMO containing Bchl *a* #3 contacts the cytoplasmic membrane.[19] Additional cross-linking data using zero-length 1-Ethyl-3-(3-dimethylaminopropyl)carbodiimide (EDC) suggests that the FMO protein directly interacts with the CsmA protein, which is located in the chlorosome baseplate.[20] The combination of protein cross-linking and mass spectrometry in studies of native proteins and protein complexes has become a popular tool in structural mass spectrometry.[21-25] Previous studies have demonstrated the application of protein cross-linking in studies of protein complexes in photosynthetic systems [26, 27]

In this chapter, we report the study of purified intact FMO-RCC complex by chemically cross-linking the purified sample with three different cross-linkers: BS^3, DSS and DTSSP. The interaction sites of the cross-linked reaction center were revealed by LC-MS/MS. The results indicate that FMO, PscB, PscD and part of PscA are exposed on the cytoplasmic side of the membrane. The close distance of the soluble heme domain of PscC and PscA facilitates the electron transfer between PscC and P840.

2.2 Materials and methods

2.2.1 FMO-RCC complex purification

Green sulfur bacterium *Chlorobaculum tepidum* strain TLS was grown anaerobically at 45 °C for 2 days. The cells were harvested by centrifugation at 8000 *g* for 15 min. The FMO-RCC

complex was purified by a method reported previously with minor modifications. [28] The cells were resuspended in 20 mM Tris-HCl buffer (pH = 8.0) and broken by sonication. The supernatant was collected after low-speed centrifugation and then ultracentrifuged at 150,000 *g* for 1 h to pellet the membranes. After washing in 20 mM Tris-HCl buffer containing 150 mM NaCl plus 1 mM EDTA, the pellet was resuspended in 20 mM Tris-HCl buffer to an OD_{810} of 6 cm^{-1}. 10% DDM was added to the suspension to a final concentration of 2% DDM and the mixture was left at 4 °C for 1.5 h in dark. The solution was loaded onto step sucrose density gradients from 10 to 50% sucrose and ultracentrifuged at 160,000 *g* for 13 h. The dark green band from the sucrose gradient was then loaded onto a DEAE-cellulose column of about 50 mL bed volume, which was equilibrated with 20 mM Tris-HCl buffer (pH = 8.0) and 0.05% DDM. The sample was eluted using a linear gradient from 0 to 1 M NaCl in the same buffer. Fractions containing both FMO and the RCC complex determined from the shoulder at 807 nm and 835 nm were collected and concentrated for future use.

2.2.2 Chemically cross-linked FMO-RCC complex

The purified FMO-RCC complex as described above was washed with 20 mM phosphate buffer and cross-linked by BS^3 (11.4 Å), DSS (11.4 Å) and DTSSP (12.0 Å). The mixture was incubated for 30 min at room temperature and then loaded onto the desalting column (Zeba™ Spin Desalting Columns, 7K MWCO, Thermo Fisher Scientific Inc). For BS^3 and DSS, both isotopic (1:1 mixture of deuterated (d12) and non-deuterated (d0), Creative Molecules Inc) and non-isotopic linkers are used. SDS-PAGE and Blue-native (BN) gel were performed as described before.[29, 30]

2.2.3 LC-MS/MS and Data Analysis

The stained bands of SDS-PAGE were excised and digested with trypsin. The samples were analyzed by LC-MS/MS using both a Waters Synapt G2 Q-IM-TOF and a Thermo LTQ Orbitrap (Thermo-Scientific, San Jose, CA) as described in the published protocol. [31] The data from Waters Synapt G2 Q-IM-TOF were submitted to the ProteinLynx Global Server (V2.5, Waters Inc., Milford, MA) to identify the peptide sequence. The data for cross-linked peptide identification obtained from a Thermo LTQ Orbitrap were analyzed by *xQuest*. [31, 32] The cross-linked peptides identified by *xQuest* were further manually validated.

2.3 Results and discussion

2.3.1 Purification and identification of FMO-RCC complex

The purified FMO-RCC complex exhibits a BChl *a* absorption band at 809 nm with a slight shoulder at 835 nm, which is consistent with previous work, as shown in Figure 2.2A. [28] The Q_x band of the BChl *a* at 600 nm and Q_y band of Chl *a* at 670 nm are also observed. [12] Five bands on the SDS-PAGE at 60 kDa, 40 kDa, 30 kDa, 19 kDa and 16 kDa were identified to be PscA, FMO, PscB, PscC and PscD, respectively, by in-gel digestion and subsequent LC-MS/MS analysis (Figure 2.2B).

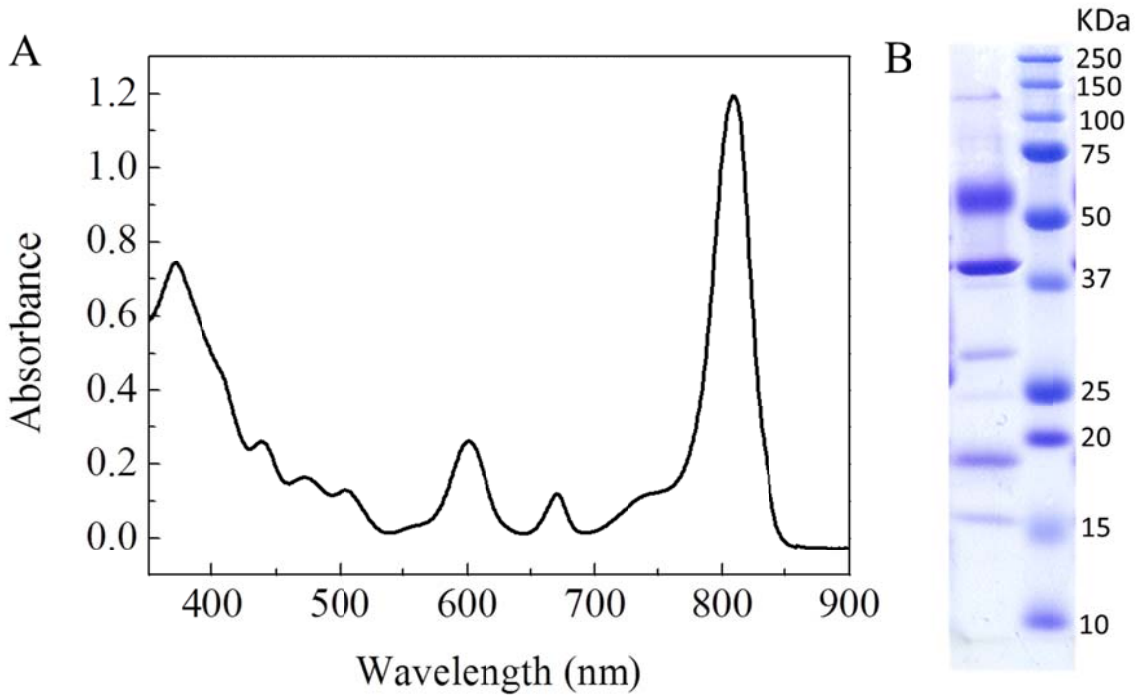

Figure 2.2 Absorption spectrum (A) and SDS-PAGE (B) of the FMO-RCC complex

2.3.2 Cross-linking by BS^3, DSS and DTSSP

The purified FMO-RCC complex was cross-linked with BS^3 at different concentrations as shown in Figure 2.3A. After cross-linked by BS^3, the complex could not be denatured by SDS buffer, which resulted in a bright band on top of the separating gel with a mass of more than 250 kDa. With lower concentrations of cross-linker, some FMO-RCC complexes were not fully cross-linked, resulting in faint bands of the five subunits. The cross-linked complex was further evaluated by BN gels (Figure 2.3B). The faint band at 145 kDa could be assigned to some free FMO trimers in the sample. The higher mass region showed two bands, corresponding to 450 kDa and 600 kDa. The mass difference is similar to that of an FMO trimer. The data suggest that there are two types of FMO-RCC complex in the sample, which is consistent with the STEM

data reported before.[12] The band corresponding to a mass of approximately 600 kDa can be explained by a complex with composition of $2(FMO)_3(PscA)_2(PscB)(PscC)_2(PscD)$ plus 48 BChl *a* in FMO, 16 BChl *a* and 4 Chl *a* in RCC.[1] The predicted mass is ~ 560 kDa, which is close to the 600 kDa as shown in blue-native gels.

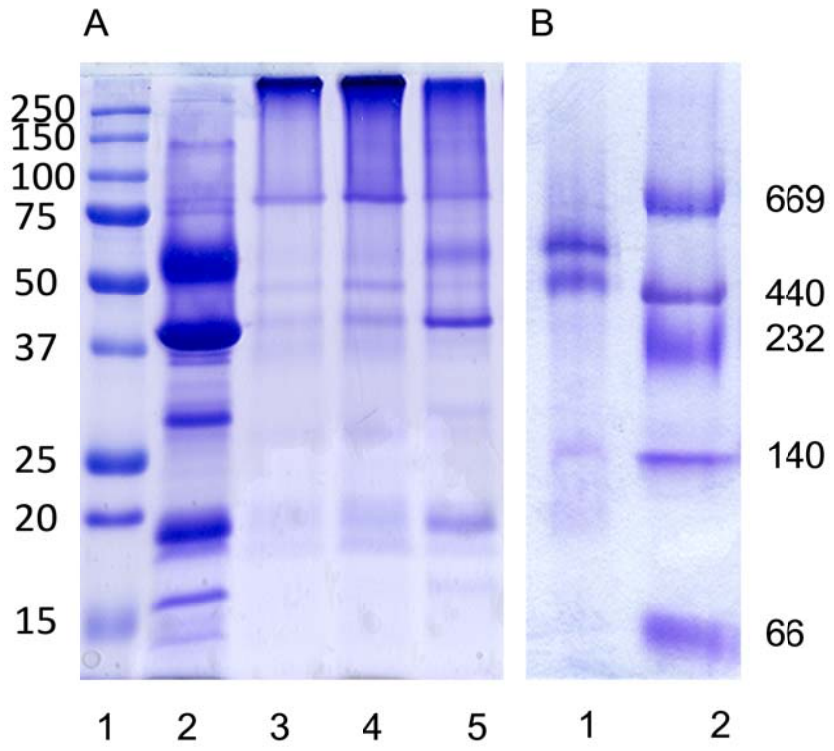

Figure 2.3 (A) SDS-PAGE of FMO-RCC complex: Marker (Lane 1); non-crosslinked control sample (Lane 2); cross-linked FMO-RCC complex by different concentrations of BS^3 at room temperature (Lanes 3-5: 10 mM, 5mM, 0.5 mM). (B) BN gel of crosslinked FMO-RCC complex by 10 mM BS^3 (Lane 1) and marker (Lane 2).

The purified complex was then cross-linked with three different cross-linkers, including DTSSP, DSS and BS^3. The disulfide (S-S) bonds in DTSSP can be broken by reducing agents such as β-mercaptoethanol. DSS is a hydrophobic cross-linker whereas BS^3 is hydrophilic, but they have the same linking length. Figure 2.4A and B show the results of the cross-linking experiments. All

three cross-linkers resulted in a bright band on the top of the separating gel; that band was identified to be the cross-linked FMO-RCC complex. In Figure 2.4B, very faint FMO bands are visible in Lane 7 and 8 for DSS cross-linked samples; these bands are absent in Lane 3 and 4 for BS^3 cross-linked samples, indicating the hydrophilic cross-linker BS^3 works slightly better for this experiment. Lane 5 indicates the FMO-RCC complex cross-linked with BS^3 on ice, a faint FMO band is observed as those with DSS. In Figure 2.4A, β-mercaptoethanol was added to DTSSP cross-linked samples to break S-S bonds in DTSSP, giving a similar band pattern as the control sample. The presence of β-mercaptoethanol had no effect on BS^3 and DSS linked samples. The appearance of a bright band on top of the separating gel and the reversibility of DTSSP cross-linking (lane 1 in Figure 2.4A) clearly indicate that all five subunits of FMO-RCC complex can be successfully cross-linked.

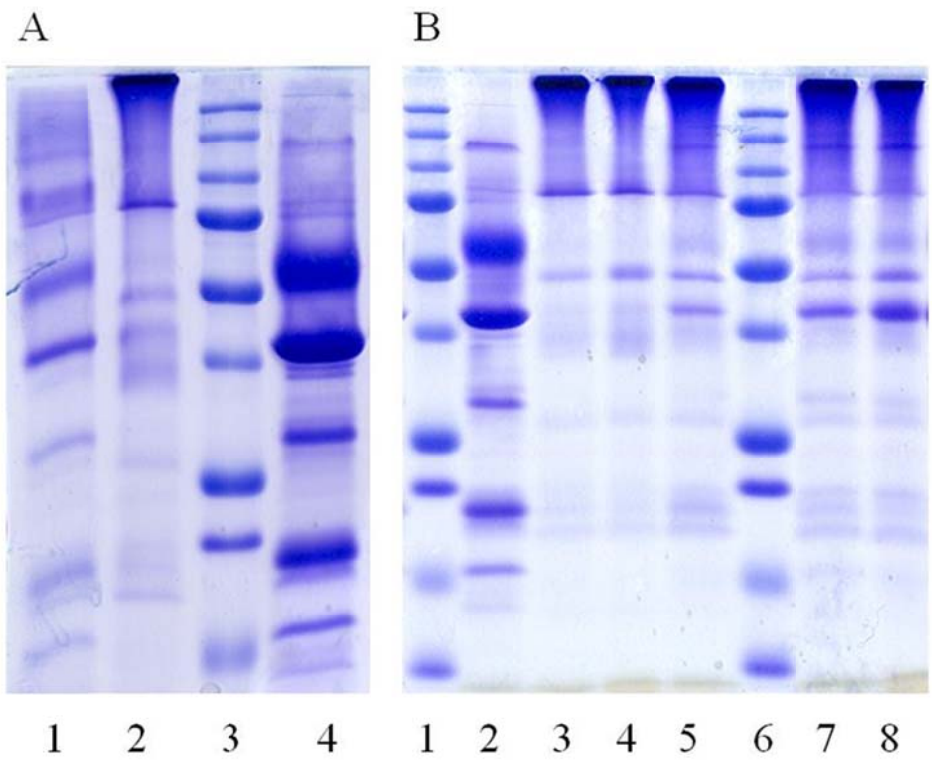

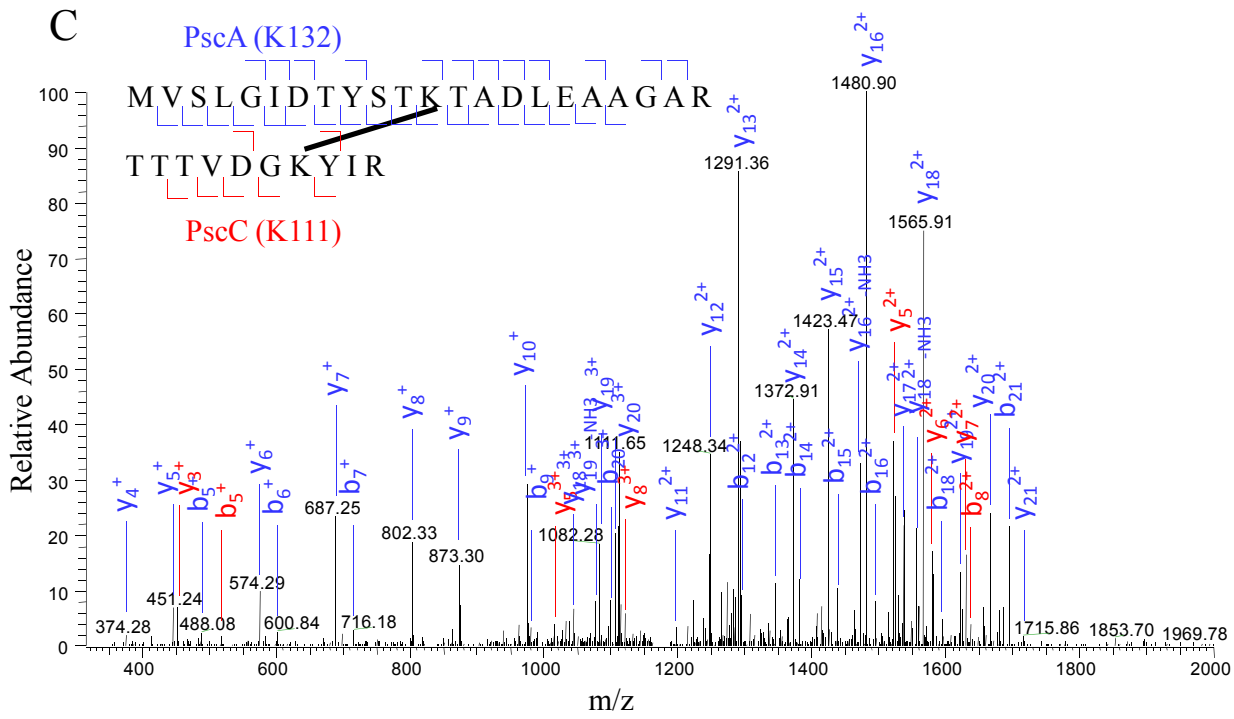

Figure 2.4 Chemical cross-linking of FMO-RCC complex by 10 mM different cross-linkers and identification of subunit interactions by LC-MS/MS: (A) DTSSP (cross-linked sample treated with (Lane 1) and without (Lane 2) reducing agent, markers (Lane 3) and non-crosslinked control sample (Lane 4); (B) BS^3 (cross-linked sample treated with (Lane 3) and without (Lane 4) reducing agent, Lane 5 is the sample cross-linked on ice and treated without reducing agent)and DSS (cross-linked sample treated with (Lane 7) and without (Lane 8) reducing agent), markers (Lane1 and Lane 6), non-crosslinked control sample (Lane 2); (C) The MS/MS spectrum of the inter-linked peptide between PscA and PscC induced by BS^3.

2.3.3 Structural analysis by chemical cross-linking and LC-MS/MS

The results from LC-MS/MS were grouped into mono-linked peptides, intra-linked peptides and inter-linked peptides.[24] The product-ion (MS/MS) spectrum in Figure 2.4C shows the inter-link between PscA and PscC by BS^3. As the cross-linker targets solvent accessible lysine side chains, all those linked peptides should be located on the solvent accessible surfaces. The number of

mono-linked peptides exceeds the number of intra- or inter-linked peptides as mono-linked peptides indicate the lysines available for cross-linking, but only a subset of the available lysines that are spatially close enough can form intra- or inter-links. The mono-linked lysines of soluble domain of PscC is shown in Figure 2.5. As is shown in Figure 2.6, the distance between the intra-linked lysines ^{93}K and ^{247}K is 18.8 Å in the crystal structure of the FMO trimer, and they may be even closer because ^{93}K is located on the loop.

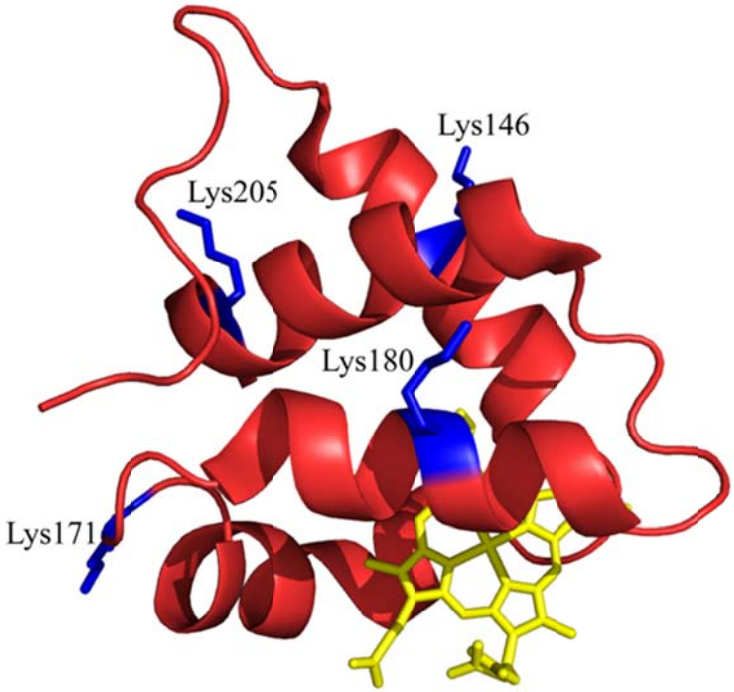

Figure 2.5 The mono-linked lysines of soluble domain of PscC

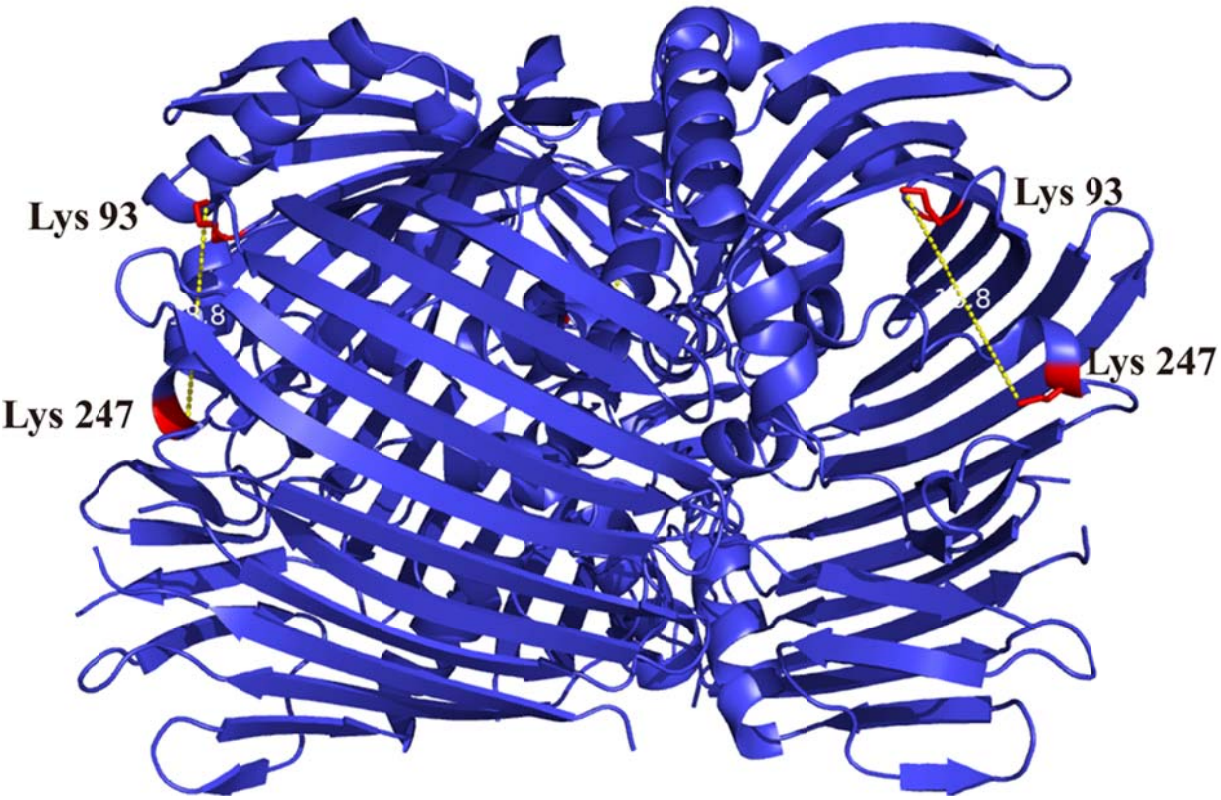

Figure 2.6 The intra-linked lysines of FMO

Figure 2.7A summarizes the inter-links between the subunits of FMO-RCC complex. The inter-links were classified into two groups, confirmed and likely cross-links, based on the quality of the product-ion spectra (i.e., the identifications of the peaks in the spectra and the sequence ion coverage of the peptide (Figure 2.8 and Figure 2.9)). For both of them, almost all the major peaks in the product-ion spectra can be assigned. The cross-linked products with high quality of product-ion spectra that meet the criteria that sequence ions covers over 70% sequence of the peptide, are classified as confirmed cross-links. And the confirmed cross-links were used as major constraints in establishing the structural model of FMO-RCC complex. The cross-links with relative lower quality product-ion spectra (e.g., ones that have sequence ions covering

~50% sequence of the peptide) are listed as likely cross-links to support our model. ^{79}K of FMO in the middle of the FMO trimer is found to be linked with ^{107}K of PscD and possibly ^{45}K of PscA, ^{36}K and ^{60}K of PscB. Because FMO is cytoplasmic, PscB, PscD and ^{45}K of PscA should also be cytoplasmic. As reported previously, ^{93}K and ^{215}K are located on the upper exterior loops near the chlorosome.[19] Our results show that ^{215}K of FMO is linked to ^{46}K of PscD and ^{93}K of FMO is likely to be linked to ^{30}K of PscD. Therefore, the C and N terminal lysines of PscD bind to both the top and middle side of the FMO trimer allowing for the proper binding of FMO to the RCC complex. This result is consistent with previous report that in the PscD deletion strain, the ratio of BChl *a*/P840 in FMO-RCC is lower, suggesting that some of the FMO proteins were partially detached from the RCC without PscD.[10]

Our results are also informative about electron transfer within the FMO-RCC complex on both the donor and acceptor sides. ^{111}K of PscD is a conserved lysine residue thought to be similar to lysine 106 in PsaD from PSI, which is involved in the direct interaction of Fd with the iron-sulfur protein PsaC.[10] Our results indicate that the ^{107}K of PscD is linked to ^{79}K of FMO whereas ^{36}K and ^{60}Kof PscB are probably linked to the same lysine of FMO. At the same time, ^{107}K of PscD is linked to the conserved lysine ^{111}K of PscD (Figure 2.10). Thus, those lysines should be fairly close, and it is very likely that the conserved lysine ^{111}K of PscD is close to PscB to facilitate the electron transfer from RC to Fd, similar to the role of PsaD in PSI.[10]

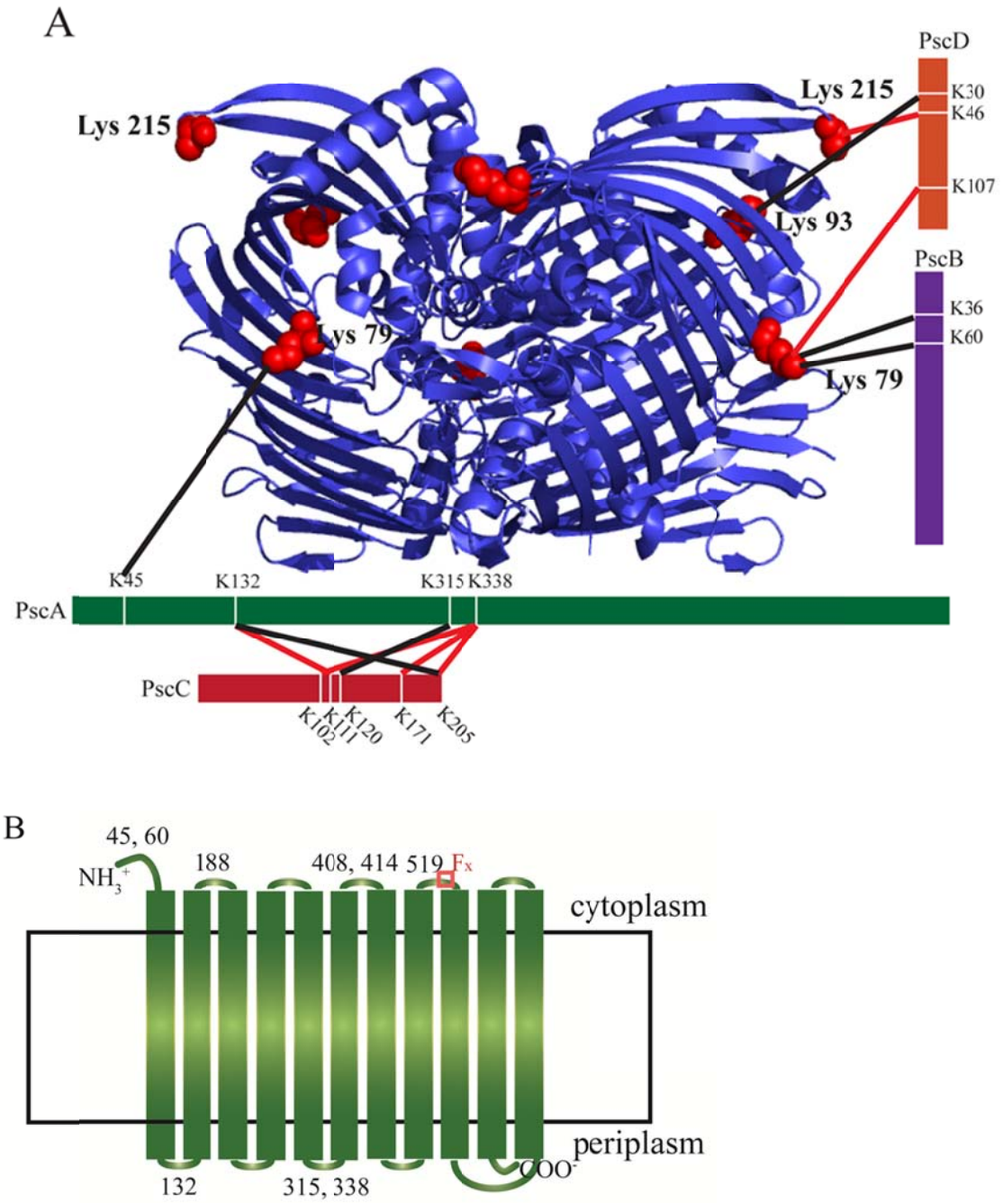

Figure 2.7 (A) Identification of the inter-links between the subunits of FMO-RCC complex (red: confirmed; black: likely); The structure of the FMO complex is shown with the linkages to the other subunits indicated; (B) Membrane topological model of PscA with mono-linked or cross-linked lysines indicated. The region of sequence that binds the F_x iron-sulfur center is indicated with a red box.

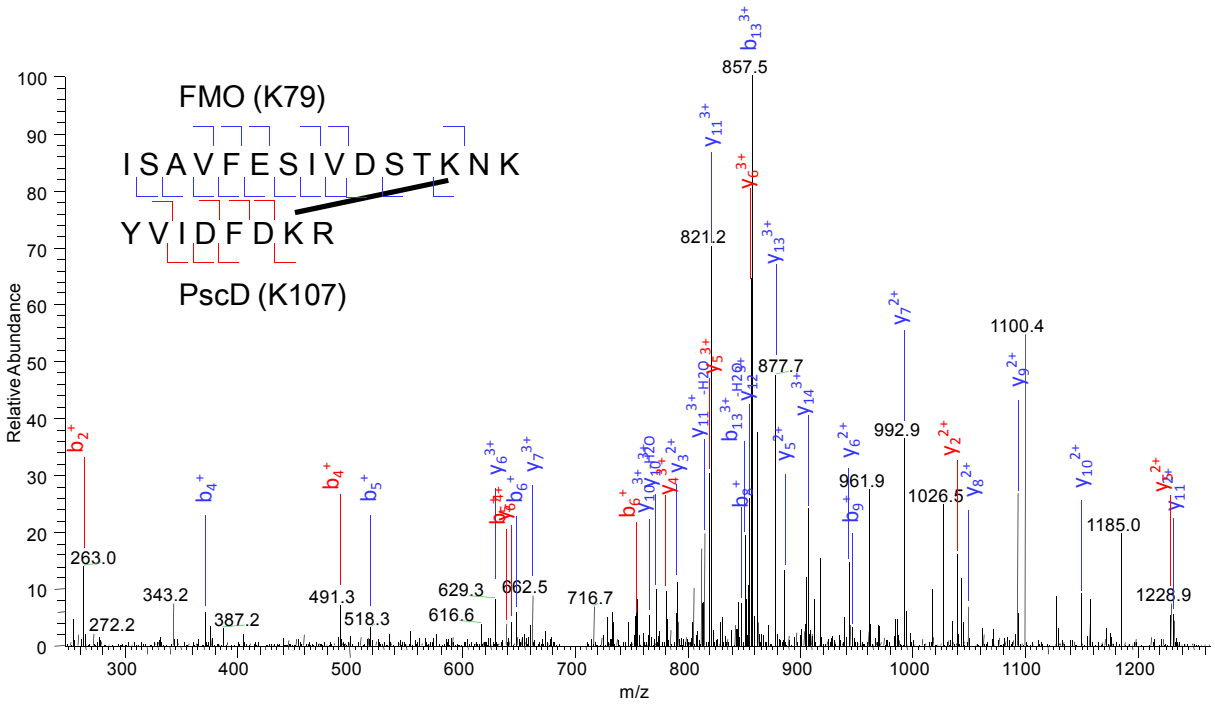
FMO (K79)
I S A V F E S I V D S T K N K
Y V I D F D K R
PscD (K107)
Relative Abundance
m/z

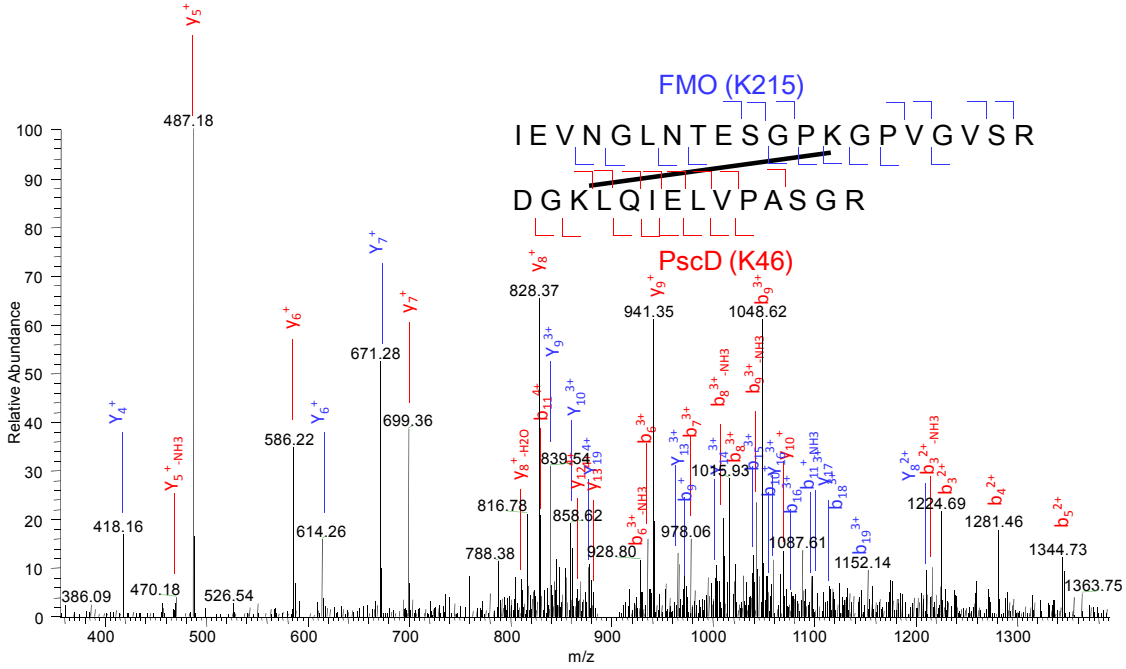
FMO (K215)
I E V N G L N T E S G P K G P V G V S R
D G K L Q I E L V P A S G R
PscD (K46)
Relative Abundance
m/z

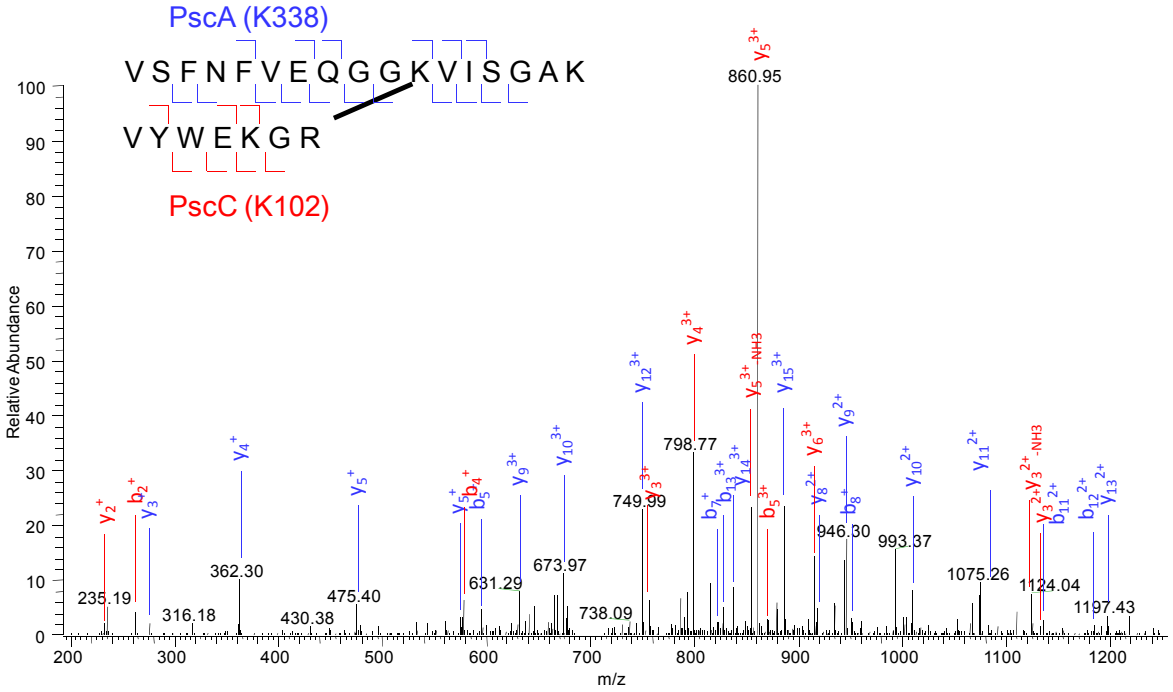
PscA (K338)
VSFNFVEQGGKVISGAK
VYWEKGR
PscC (K102)
Relative Abundance
m/z
860.95
798.77
749.99
946.30
993.37
673.97
631.29
362.30
475.40
430.38
316.18
235.19
738.09
1075.26
1124.04
1197.43

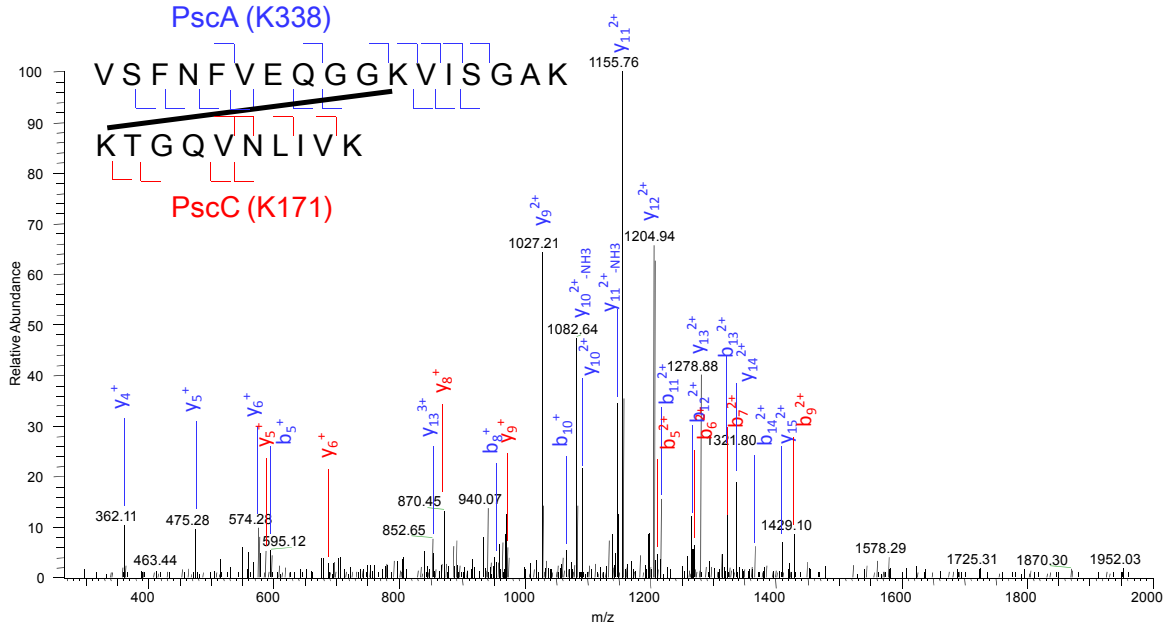
PscA (K338)
VSFNFVEQGGKVISGAK
KTGQVNLIVK
PscC (K171)
Relative Abundance
m/z
1155.76
1027.21
1204.94
1082.64
1278.88
1321.80
870.45
940.07
852.65
362.11
475.28
574.28
595.12
463.44
1429.10
1578.29
1725.31
1870.30
1952.03

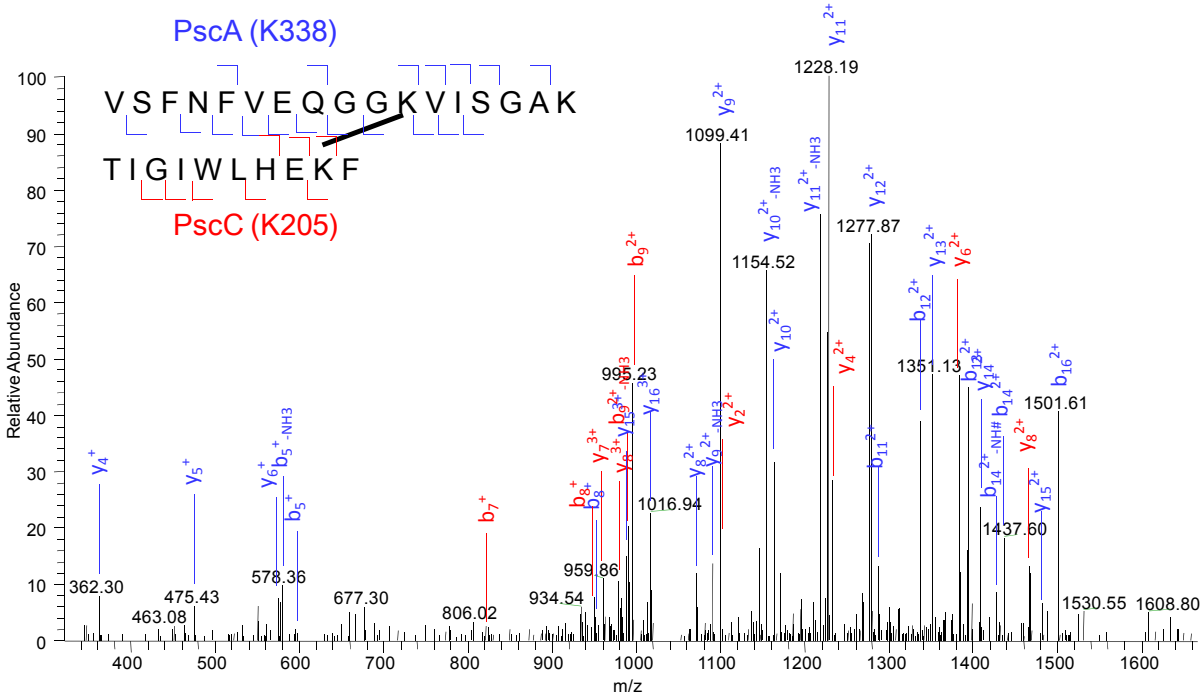

Figure 2.8 The MS/MS spectra of the confirmed cross-linked peptides

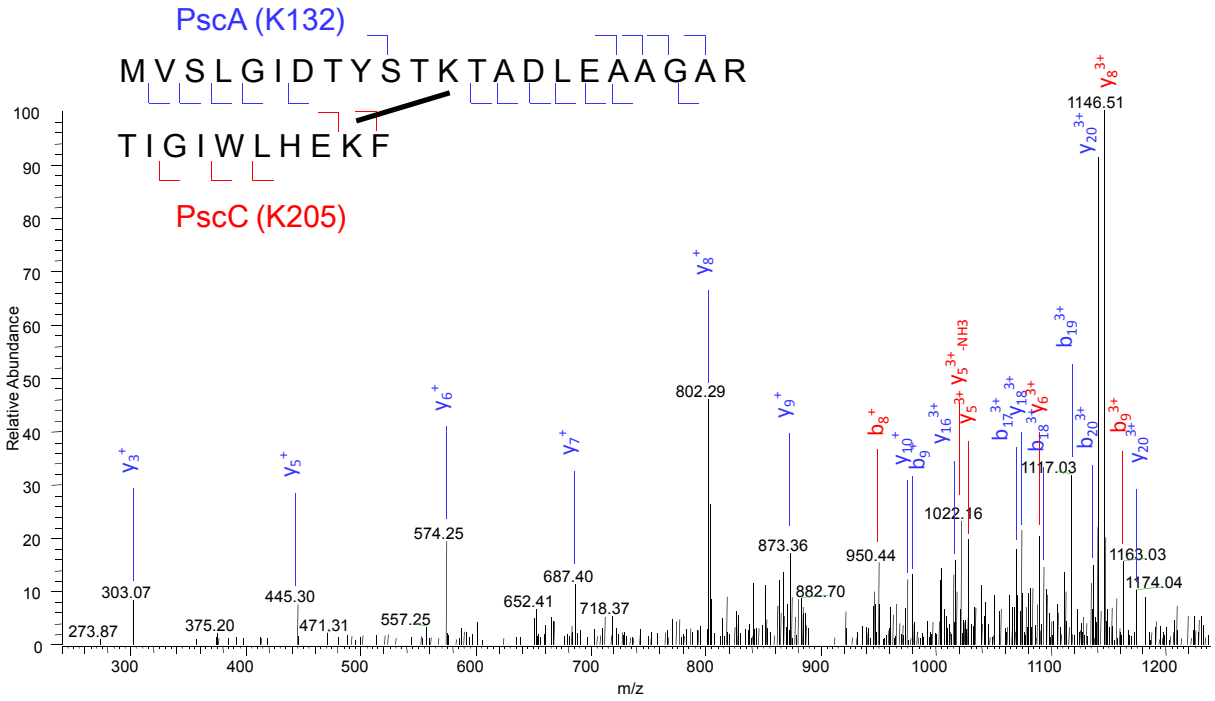

Figure 2.9 The MS/MS spectrum of the likely cross-linked peptides

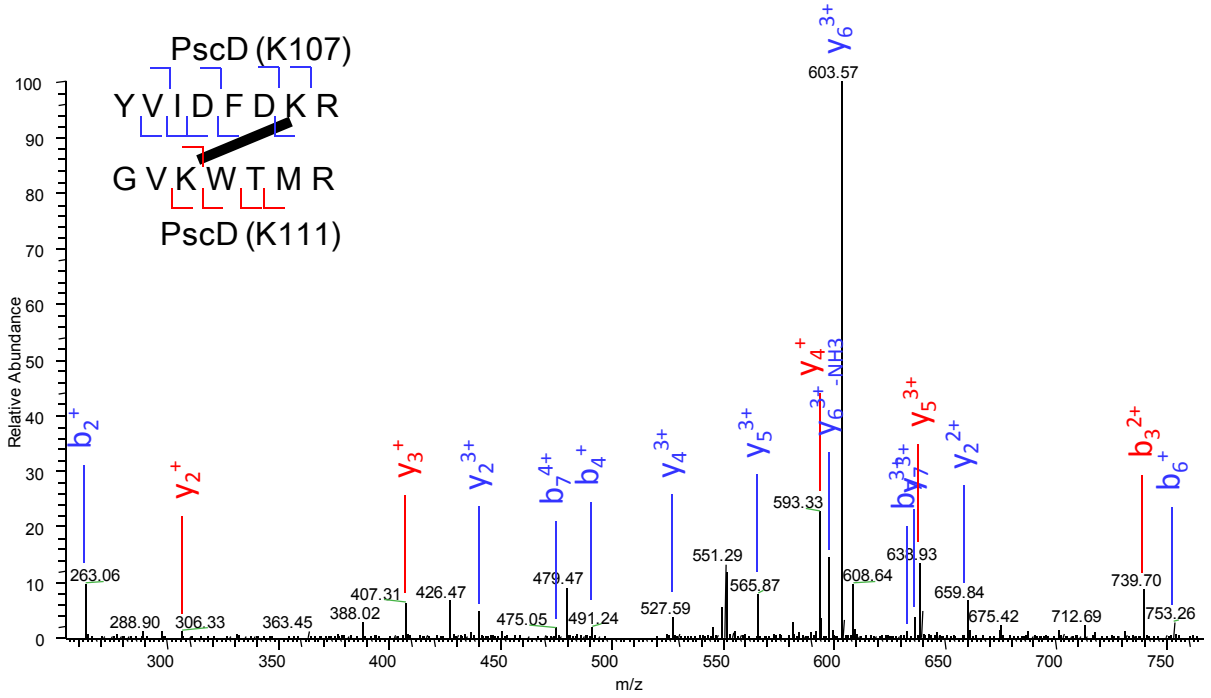

Figure 2.10 The MS/MS spectra of the intra-linked peptide between PscD K107 and K111

On the periplasmic side of the complex, we found several cross-links between PscA and PscC. The N-terminal domain of PscC contains three-transmembrane helices, and the C-terminal, soluble heme domain is located on the periplasmic side of the membrane.[9, 33] ^{132}K and ^{338}K of PscA are linked to several lysines in the soluble domain of PscC. Therefore, ^{132}K and ^{338}K of PscA should also be located on the periplasmic side and the soluble domain of PscC should be close to PscA. ^{315}K of PscA is probably linked to PscC and thus is also likely to be on the periplasmic side of the membrane. The cross-link between PscA and the soluble heme-binding domain of PscC is consistent with the efficient electron transfer from PscC to P840.[9, 33-35]

Hydropathy plot is commonly used for the prediction of the transmembrane helixes based on the hydrophobicity of the amino acids. A hydropathy plot prediction of possible transmembrane

helices of PscA and PscC was constructed by ExPASy ProtScale (Figure 2.11). Mono-links can provide further structural information based on the hydropathy plot. As shown in Table 2.1, 9 mono-links were found from the top to bottom sides of the FMO protein because it is a water-soluble protein. Six mono-links from the soluble domain of PscC were found, and four of them are shown in the crystal structure.

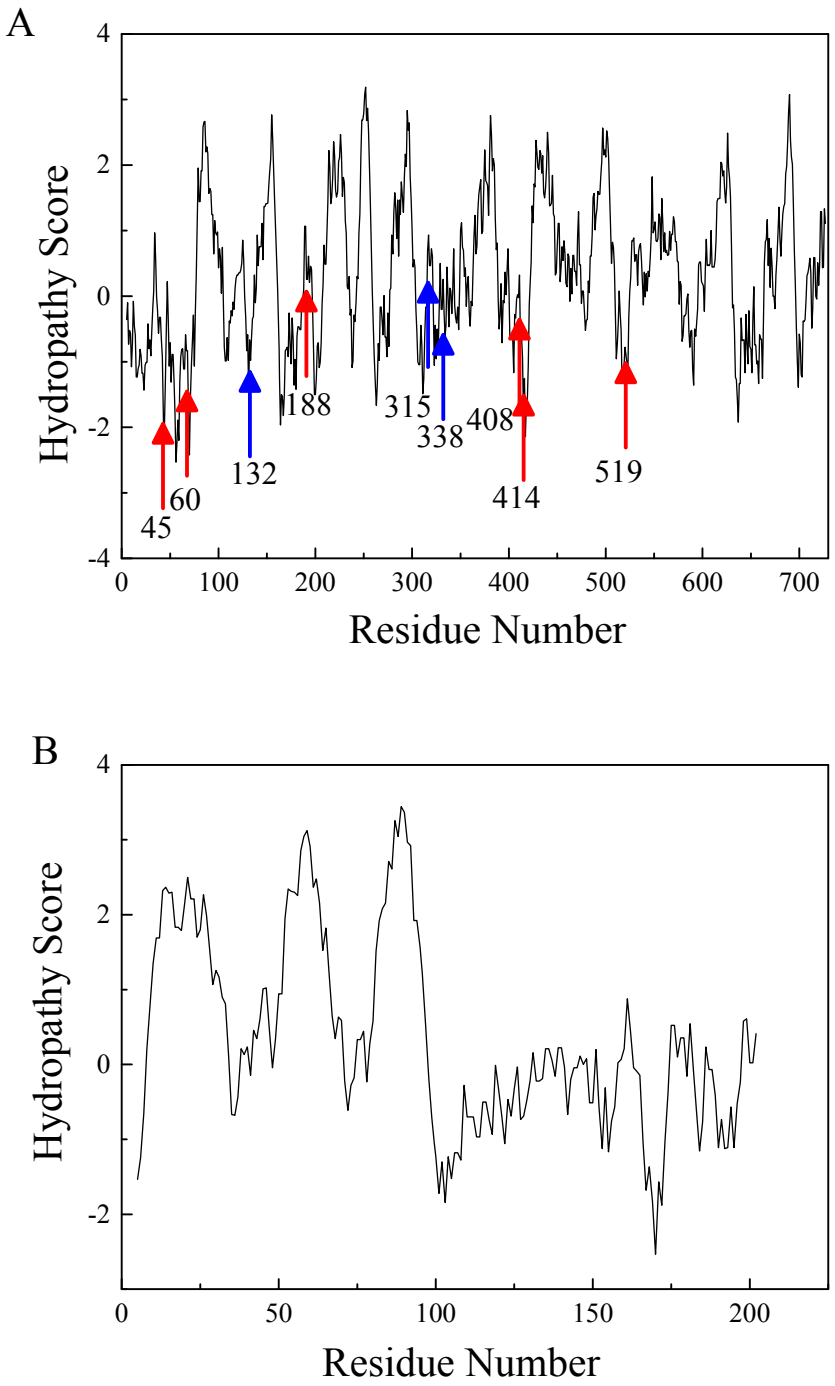

Figure 2.11 Hydropathy plots of (A) PscA and (B) PscC (Red arrows: cytoplasmic membrane side; blue arrows: periplasmic membrane side)

Table 2.1 Summary of the mono-linked lysines

Subunits	Mono-linked lysine numbers
FMO	56, 62, 81, 93, 151, 215, 247, 268, 319
PscA	60, 132 (P), 188, 315(P), 338(P), 408, 414, 519
PscB	160
PscC	102 (P), 120 (P), 146 (P), 171 (P), 180 (P), 205 (P)
PscD	40, 46, 107, 111

"P" indicates periplasmic side of the membrane

Figure 2.7B shows a membrane topological model of PscA. As mentioned above, ^{45}K of PscA was likely cross-linked to FMO. Mono-linked ^{60}K of PscA was found, and there should not be any transmembrane helix between the two lysines based on the hydropathy plot; thus, residues 45-60 of PscA should all be located on the cytoplasmic side of the membrane. In addition, ^{132}K of PscA was cross-linked with the soluble domain of PscC on the periplasmic side. At the same time, ^{188}K of PscA mono-link was observed and there should be one transmembrane helix between the two lysines based on the hydropathy plot. Thus, ^{188}K of PscA should be located on the cytoplasmic domain. Residues 315-338 of PscA should be located on the periplasmic domain as they were both linked to the soluble domain of PscC. Mono-links of ^{408}K and ^{414}K indicate that residues 408-414 should all be located on the same side of the membrane. Meanwhile, residues 315-338 are in the periplasmic domain, and there is one transmembrane helix between those two domains based on the hydropathy plot. Thus, residue 408-414 should be on the cytoplasmic domain. As there are two transmembrane helices between ^{408}K and the mono-linked ^{519}K of PscA, the latter lysine should also be on the cytoplasmic domain. Furthermore, based on

the hydropathy plot, the region containing residues 525-536, which contains the F_x binding motif FPCxGPxxGGTC, should also be on the cytoplasmic side of the membrane.[36] In analogy with Photosystem I, it is anticipated that F_x, F_A and F_B are all in the cytoplamic side to facilitate electron transfer. Several mono-links were found on the PscD protein at ^{40}K, ^{46}K, ^{107}K and ^{111}K, some of which were linked to FMO as mentioned above. It is not surprising to see that ^{160}K of PscB was mono-linked and is thus deemed to be water accessible as it is close to the iron-sulfur cluster binding peptide containing the CxxCxxCxxxCP motif (residues 140-151), as shown in Figure 2.12.

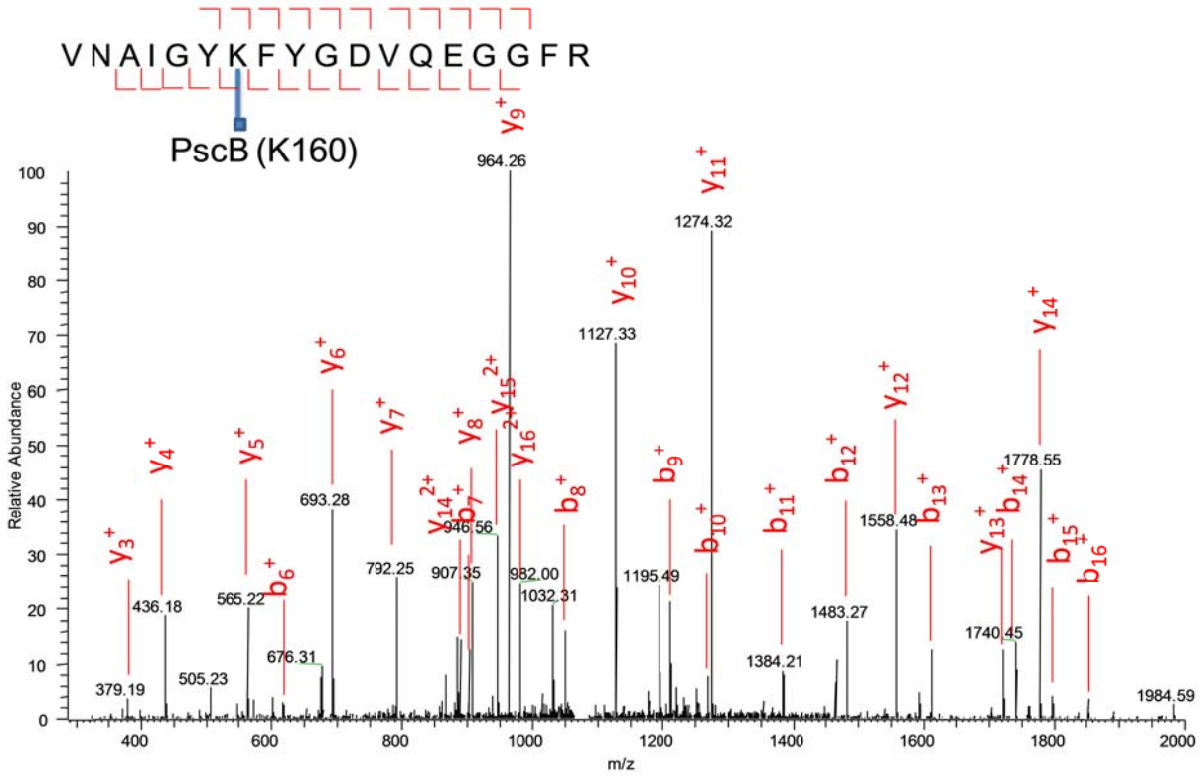

Figure 2.12 The MS/MS spectra of the mono-linked peptide of PscB (K160)

We propose a structural model of the FMO-RCC complex as shown in Figure 2.13. The crystal structure of FMO from PDB file 3ENI and PscC soluble domain from PDB file 3A9F were used. The inter-links between the FMO trimer and the PscD protein indicate that both are located on the cytoplasmic domain. Mono-links of PscA and the inter-links between PscA and the soluble domain of PscC showed that PscA is a membrane protein composed of transmembrane helices (probably 11) and the periplasmic domain is very close to the soluble domain of PscC. The likely cross-linking between PscA and FMO indicated that the FMO protein is close to the cytoplasmic domain of the PscA. The likely cross-linkings of PscB and FMO means that PscB is spatially close to the FMO trimer, and thus FMO, PscB and PscD should all reside on PscA. The STEM dark field images reported previously showed a knob protruding from the RCC. [12] Our results suggest that PscB and PscD should be the knob sitting on PscA. In addition, the iron-sulfur cluster binding domain of PscB should be water-accessible, and PscD should be close to the chlorosomal side of the FMO trimer.

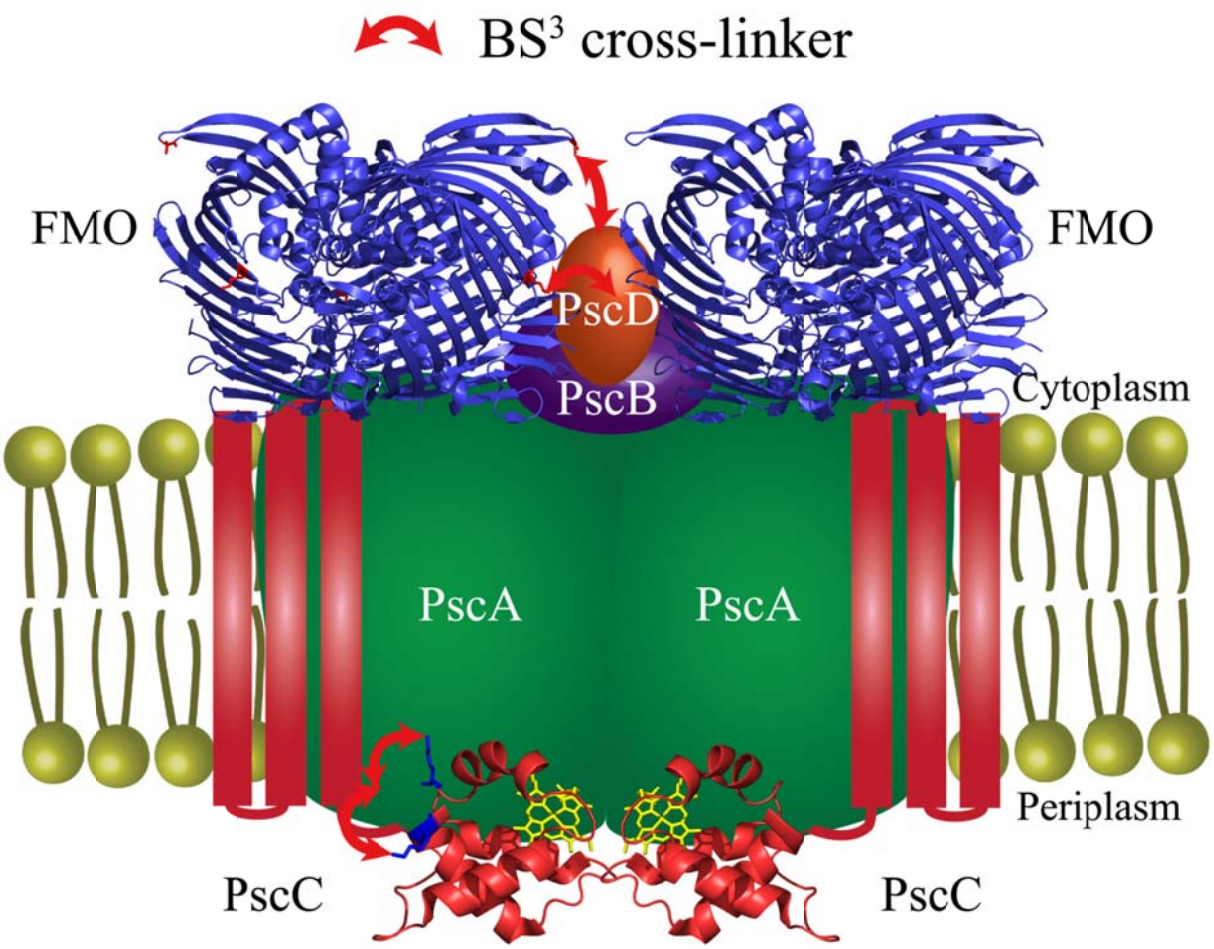

Figure 2.13 Proposed structural model of FMO-RCC complex, the red arrows indicate the cross-linker between the lysines.

2.4 Conclusions

The spatial interaction between FMO and RCC was studied by chemically cross-linking the purified FMO-RCC sample. All the subunits of RC can be linked together by BS^3, DSS and DTSSP. The interaction sites of the cross-linked complex were identified using LC-MS/MS. The results showed close spatial distance between FMO and RCC. The PscD subunit is thought to stabilize FMO to RCC complex and facilitate the electron transfer from RCC to Fd. The close distance of the soluble domain of PscC and PscA explains the efficient electron transfer between

PscC and P840. A structural model for the FMO-RCC complex is proposed consistent with these results.

References

(1) Hauska, G.; Schoedl, T.; Remigy, H.; Tsiotis, G. The reaction center of green sulfur bacteria. *Biochimica Et Biophysica Acta-Bioenergetics* **2001**, *1507*, 260-277.

(2) Busch, M. S. A.; Mueh, F.; Madjet, M. E.-A.; Renger, T. The eighth bacteriochlorophyll completes the excitation energy funnel in the FMO protein. *Journal of Physical Chemistry Letters* **2011**, *2*, 93-98.

(3) Wen, J.; Zhang, H.; Gross, M. L.; Blankenship, R. E. Native electrospray mass spectrometry reveals the nature and stoichiometry of pigments in the FMO photosynthetic antenna protein. *Biochemistry* **2011**, *50*, 3502-3511.

(4) Tronrud, D. E.; Wen, J.; Gay, L.; Blankenship, R. E. The structural basis for the difference in absorbance spectra for the FMO antenna protein from various green sulfur bacteria. *Photosynthesis Research* **2009**, *100*, 79-87.

(5) Permentier, H. P.; Schmidt, K. A.; Kobayashi, M.; Akiyama, M.; Hager-Braun, C.; Neerken, S.; Miller, M.; Amesz, J. Composition and optical properties of reaction centre core complexes from the green sulfur bacteria *Prosthecochloris aestuarii* and *Chlorobium tepidum*. *Photosynthesis Research* **2000**, *64*, 27-39.

(6) Griesbeck, C.; Hager-Braun, C.; Rogl, H.; Hauska, G. Quantitation of P840 reaction center preparations from *Chlorobium tepidum*: chlorophylls and FMO-protein. *Biochimica Et Biophysica Acta-Bioenergetics* **1998**, *1365*, 285-293.

(7) Kjaer, B.; Frigaard, N. U.; Yang, F.; Zybailov, B.; Miller, M.; Golbeck, J. H.; Scheller, H. V. Menaquinone-7 in the reaction center complex of the green sulfur bacterium *Chlorobium vibrioforme* functions as the electron acceptor A_1. *Biochemistry* **1998**, *37*, 3237-3242.

(8) Kobayashi, M.; Oh-oka, H.; Akutsu, S.; Akiyama, M.; Tominaga, K.; Kise, H.; Nishida, F.; Watanabe, T.; Amesz, J.; Koizumi, M.; Ishida, N.; Kano, H. The primary electron acceptor of green sulfur bacteria, bacteriochlorophyll 663, is chlorophyll *a* esterified with Delta 2,6-phytadienol. *Photosynthesis Research* **2000**, *63*, 269-280.

(9) Hirano, Y.; Higuchi, M.; Azai, C.; Oh-oka, H.; Miki, K.; Wang, Z.-Y. Crystal structure of the electron carrier domain of the reaction center cytochrome c(z) subunit from green photosynthetic bacterium *Chlorobium tepidum*. *Journal of Molecular Biology* **2010**, *397*, 1175-1187.

(10) Tsukatani, Y.; Miyamoto, R.; Itoh, S.; Oh-oka, H. Function of a PscD subunit in a homodimeric reaction center complex of the photosynthetic green sulfur bacterium Chlorobium tepidum studied by insertional gene inactivation - Regulation of energy transfer and ferredoxin-mediated $NADP^+$ reduction on the cytoplasmic side. *Journal of Biological Chemistry* **2004**, *279*, 51122-51130.

(11) Azai, C.; Kim, K.; Kondo, T.; Harada, J.; Itoh, S.; Oh-oka, H. A heterogeneous tag-attachment to the homodimeric type 1 photosynthetic reaction center core protein in the green sulfur bacterium *Chlorobaculum tepidum*. *Biochimica Et Biophysica Acta-Bioenergetics* **2011**, *1807*, 803-812.

(12) Remigy, H. W.; Stahlberg, H.; Fotiadis, D.; Muller, S. A.; Wolpensinger, B.; Engel, A.; Hauska, G.; Tsiotis, G. The reaction center complex from the green sulfur bacterium *Chlorobium tepidum*: A structural analysis by scanning transmission electron microscopy. *Journal of Molecular Biology* **1999**, *290*, 851-858.

(13) Tsiotis, G.; Hager-Braun, C.; Wolpensinger, B.; Engel, A.; Hauska, G. Structural analysis of the photosynthetic reaction center from the green sulfur bacterium *Chlorobium tepidum*. *Biochimica Et Biophysica Acta-Bioenergetics* **1997**, *1322*, 163-172.
(14) Camara-Artigas, A.; Blankenship, R. E.; Allen, J. P. The structure of the FMO protein from *Chlorobium tepidum* at 2.2 angstrom resolution. *Photosynthesis Research* **2003**, *75*, 49-55.
(15) Benesch, J. L. P.; Ruotolo, B. T. Mass Spectrometry: an approach come-of-age for structural and dynamical biology. *Current Opinion in Structural Biology* **2011**, *21*, 641-649.
(16) Walzthoeni, T.; Leitner, A.; Stengel, F.; Aebersold, R. Mass spectrometry supported determination of protein complex structure. *Current Opinion in Structural Biology* **2013**, *23*, 252-260.
(17) Politis, A.; Stengel, F.; Hall, Z.; Hernandez, H.; Leitner, A.; Walzthoeni, T.; Robinson, C. V.; Aebersold, R. A mass spectrometry-based hybrid method for structural modeling of protein complexes. *Nature Methods* **2014**, *11*, 403-406.
(18) Huang, R. Y. C.; Wen, J.; Blankenship, R. E.; Gross, M. L. Hydrogen-deuterium exchange mass spectrometry reveals the interaction of Fenna-Matthews-Olson protein and chlorosome CsmA Protein. *Biochemistry* **2012**, *51*, 187-193.
(19) Wen, J.; Zhang, H.; Gross, M. L.; Blankenship, R. E. Membrane orientation of the FMO antenna protein from *Chlorobaculum tepidum* as determined by mass spectrometry-based footprinting. *Proceedings of the National Academy of Sciences* **2009**, *106*, 6134-6139.
(20) Li, H.; Frigaard, N.-U.; Bryant, D. A. Molecular contacts for chlorosome envelope proteins revealed by cross-linking studies with chlorosomes from *Chlorobium tepidum*. *Biochemistry* **2006**, *45*, 9095-9103.
(21) Sinz, A. Chemical cross-linking and mass spectrometry to map three-dimensional protein structures and protein-protein interactions. *Mass Spectrometry Reviews* **2006**, *25*, 663-682.
(22) Lee, Y. J. Mass spectrometric analysis of cross-linking sites for the structure of proteins and protein complexes. *Molecular Biosystems* **2008**, *4*, 816-823.
(23) Tang, X.; Bruce, J. E. Chemical cross-linking for protein-protein interaction studies. *Methods in molecular biology* **2009**, *492*, 283-293.
(24) Leitner, A.; Walzthoeni, T.; Kahraman, A.; Herzog, F.; Rinner, O.; Beck, M.; Aebersold, R. Probing native protein structures by chemical cross-linking, mass spectrometry, and bioinformatics. *Molecular & Cellular Proteomics* **2010**, *9*, 1634-1649.
(25) Petrotchenko, E. V.; Borchers, C. H. Crosslinking combined with mass spectrometry for structural proteomics. *Mass Spectrometry Reviews* **2010**, *29*, 862-876.
(26) Liu, H.; Huang, R. Y. C.; Chen, J.; Gross, M. L.; Pakrasi, H. B. Psb27, a transiently associated protein, binds to the chlorophyll binding protein CP43 in photosystem II assembly intermediates. *Proceedings of the National Academy of Sciences* **2011**, *108*, 18536-18541.
(27) Liu, H.; Zhang, H.; Weisz, D. A.; Vidavsky, I.; Gross, M. L.; Pakrasi, H. B. MS-based cross-linking analysis reveals the location of the PsbQ protein in cyanobacterial photosystem II. *Proceedings of the National Academy of Sciences* **2014**, *111*, 4638-4643.
(28) Hagerbraun, C.; Xie, D. L.; Jarosch, U.; Herold, E.; Buttner, M.; Zimmermann, R.; Deutzmann, R.; Hauska, G.; Nelson, N. Stable photobleaching of P840 in chlorobium reaction-center preparations - Presence of the 42-kDa bacteriochlorophyll *a*-protein and a 17-kDa polypeptide. *Biochemistry* **1995**, *34*, 9617-9624.
(29) Schagger, H.; Vonjagow, G. Blue native electrophoresis for isolation of membrane-protein complexes in enzymatically active form. *Analytical Biochemistry* **1991**, *199*, 223-231.
(30) Schaegger, H. Tricine-SDS-PAGE. *Nature Protocols* **2006**, *1*, 16-22.

(31) Liu, H.; Zhang, H.; Niedzwiedzki, D. M.; Prado, M.; He, G.; Gross, M. L.; Blankenship, R. E. Phycobilisomes supply excitations to both photosystems in a megacomplex in cyanobacteria. *Science* **2013**, *342*, 1104-1107.
(32) Walzthoeni, T.; Claassen, M.; Leitner, A.; Herzog, F.; Bohn, S.; Forster, F.; Beck, M.; Aebersold, R. False discovery rate estimation for cross-linked peptides identified by mass spectrometry. *Nature Methods* **2012**, *9*, 901-903.
(33) Oh-Oka, H.; Iwaki, M.; Itoh, S. Viscosity dependence of the electron transfer rate from bound cytochrome c to P840 in the photosynthetic reaction center of the green sulfur bacterium *Chlorobium tepidum*. *Biochemistry* **1997**, *36*, 9267-9272.
(34) Oh-oka, H.; Kamei, S.; Matsubara, H.; Iwaki, M.; Itoh, S. 2 Molecules of cytochrome-c function as the electron-donors to P840 in the reaction-center complex isolated from a green sulfur bacterium, *Chlorobium tepidum*. *FEBS Letters* **1995**, *365*, 30-34.
(35) Tsukatani, Y.; Azai, C.; Kondo, T.; Itoh, S.; Oh-oka, H. Parallel electron donation pathways to cytochrome c(z) in the type I homodimeric photosynthetic reaction center complex of *Chlorobium tepidum*. *Biochimica Et Biophysica Acta-Bioenergetics* **2008**, *1777*, 1211-1217.
(36) Romberger, S. P.; Golbeck, J. H. The bound iron-sulfur clusters of Type-I homodimeric reaction centers. *Photosynthesis Research* **2010**, *104*, 333-346.

Chapter 3: Dynamics of Energy and Electron Transfer in the FMO-Reaction Center Core Complex from the Phototrophic Green Sulfur Bacterium *Chlorobaculum tepidum*

This chapter is based on a recent publication:
He, G.; Niedzwiedzki, D. M.; Orf G. S.; Zhang, H.; Blankenship, R. E. Dynamics of Energy and Electron Transfer in the FMO-Reaction Center Core Complex from the Phototrophic Green Sulfur Bacterium *Chlorobaculum tepidum*. *Journal of Physical Chemistry B* **2015**, *119*, 8321-8329.

Abstract

The reaction center core (RCC) complex and the RCC with associated Fenna-Matthews-Olson protein (FMO-RCC) complex from the green sulfur bacterium *Chlorobaculum tepidum* were studied comparatively by steady-state and time-resolved fluorescence (TRF) and femtosecond time-resolved transient absorption (TA) spectroscopies. The energy transfer efficiency from the FMO to the RCC complex was calculated to be ~40% based on the steady-state fluorescence. TRF showed that most of the FMO complexes (66%), regardless of the fact that they were physically attached to the RCC, were not able to transfer excitation energy to the reaction center. The TA spectra of the RCC complex showed a 30-38 ps lifetime component regardless of the excitation wavelengths, which is attributed to charge separation. Excitonic equilibration was shown in TA spectra of the RCC complex when excited into the BChl *a* Q_x band at 590 nm and the Chl *a* Q_y band at 670 nm, while excitation at 840 nm directly populated the low energy excited state and equilibration within the excitonic BChl *a* manifold was not observed. The TA spectra for the FMO-RCC complex excited into the BChl *a* Q_x band could be interpreted by a

combination of the excited FMO protein and RCC complex. The FMO-RCC complex showed an additional fast kinetic component compared with the FMO protein and the RCC complex, which may relate to FMO-to-RCC energy transfer.

3.1 Introduction

The reaction center complex of green sulfur bacteria is composed of the bacteriochlorophyll *a* (BChl *a*)-containing Fenna-Matthews-Olson (FMO) protein and the reaction center core complex (RCC). The water-soluble FMO protein was the first pigment-containing complex with its atomic structure determined via X-ray crystallography.[1] The FMO protein is a homotrimer embracing 24 BChl *a* pigments. The closely interacting BChl *a* in FMO facilitate exciton coupling.[2, 3] Due to excitonic interactions, the collective BChl *a* Q_y absorption band appears between 790 and 830 nm.[4-6] Energy transfer between individual pigments/excitons in the FMO protein reveals wave-like quantum coherence.[7, 8] The RCC complex consists of four subunits: an 82 kDa homodimer PscA protein, a 24 kDa PscB, a 23 kDa cytochrome c_{551} (PscC) protein and a 17 kDa PscD protein.[9, 10] The PscA homodimer contains 16 BChls *a* revealing Q_y bands between 780 and 840 nm, four Chl *a* molecules and two carotenoid molecules.[11, 12] The four Chl *a*-molecules are esterified to 2, 6-phytadienol.[13] The primary electron donor P840 (a special pair of BChl *a* with a Q_y band appearing at cryogenic temperature at ~838 nm), the primary electron acceptor A_0 (Chl *a*-derivative), a secondary electron acceptor A_1 (menaquinone) and iron-sulfur cluster F_x are all located in the PscA.[9, 13, 14] The PscB contains iron-sulfur clusters F_A and F_B, which are analogous to the terminal electron acceptors of the PsaC in Photosystem I (PSI).[15] The PscD subunit is analogous to the PsaD in PSI.[16] The lack of either PscC or PscD in a purified RCC does not induce any serious defect in the kinetics of electron transfer reactions.[16-19] Lack of

the PscB protein leads to fast recombination between the $P840^+$ and initial electron acceptors.[18, 20] The structure model of the intact FMO-RCC complex is proposed in the previous chapter and it is shown in Figure 3.1A.[21]

The intact FMO-RCC complex and subunits of the RCC complex can be purified through detergent treatment of the photosynthetic membranes.[12, 19, 22-25] The PscA-PscB complex was purified previously from the green sulfur bacterium *Prosthecochloris aestuarii* using a hydroxyapatite column after detergent treatment.[10, 18, 25] The PscA-PscC complex was purified from *Chlorobaculum tepidum* and *Chlorobium limicola*.[12, 18, 24, 26] The structural model of the PscA-PscC complex is shown in Figure 3.1B. The dynamics of the excitation energy and electron transfer in the FMO-RCC complex and PscA-PscB complex have been studied for many years.[18, 19, 27-31] Transient absorption (TA) studies performed in the sub-nanosecond time scale on the FMO-RCC complex showed similar spectral and dynamic features as isolated FMO complex excited at BChl *a* Q_x or Q_y bands (~590 and 790 nm, respectively).[27, 30] The FMO-RCC complex excited at 840 nm revealed a ~30 ps lifetime component, which was assumed to be attributed to charge separation in the RCC complex, and the PscA-PscB complex reveals similar kinetic components.[19, 27, 30] The excitation energy transfer efficiency from the FMO protein to the RCC complex was reported to be 35% or lower.[27, 30, 31] Studies on the kinetics of the energy/electron transfer in the PscA-PscC complex have been relatively limited.[18, 24] It was reported that the TA spectra of the PscA-PscC reveal two decay components with lifetimes in millisecond and second time scales (0.7 ms and 2 s, at room temperature). The faster component was presumably caused by a back reaction (recombination) of the $P840^+$ with the reduced electron acceptor F_x, in agreement with the loss of the terminal electron acceptors, F_A and F_B.[18]

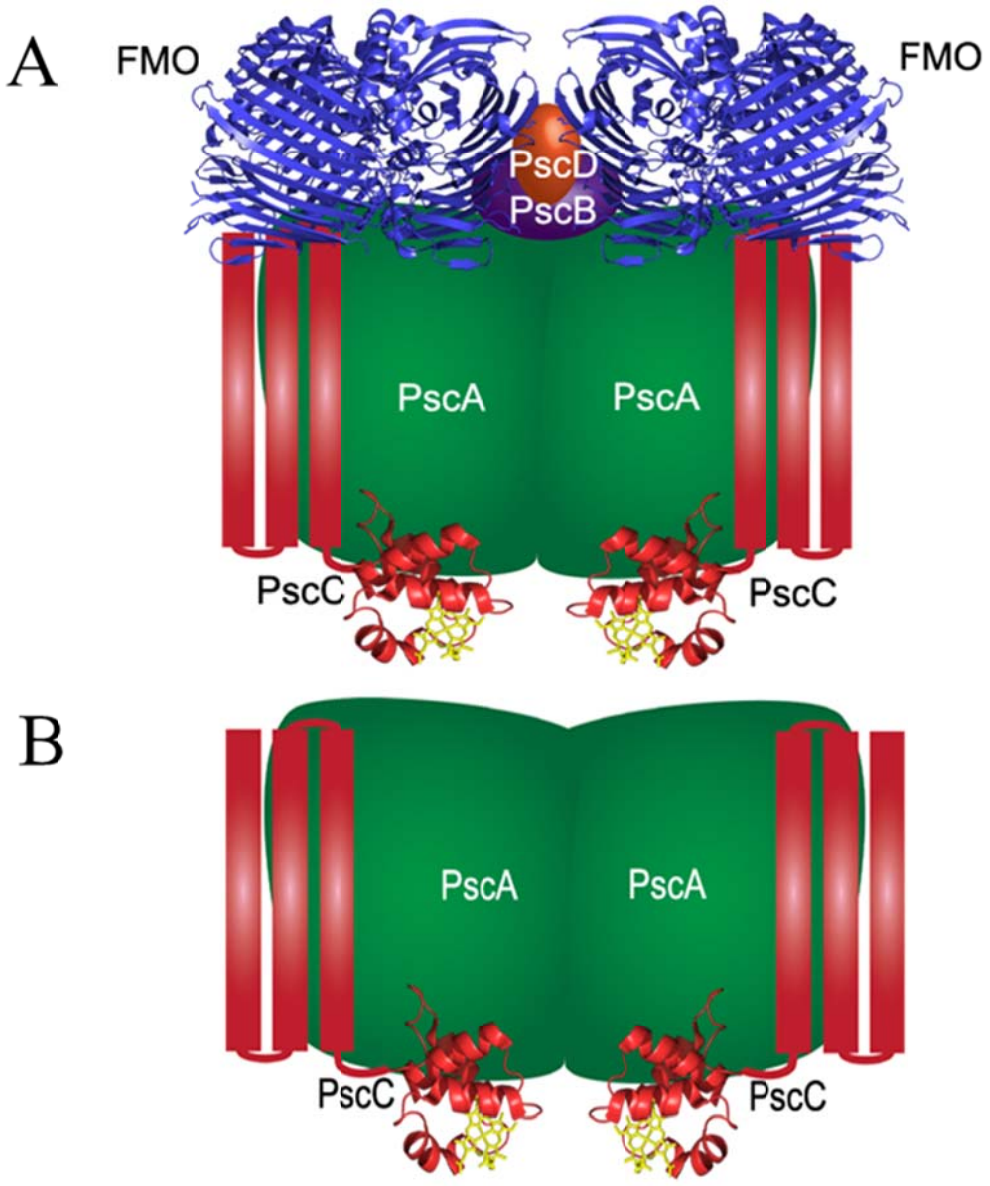

Figure 3.1 The structural model of FMO-RCC complex (A) and PscA-PscC complex (B)

This chapter presents application of a modified purification methodology in order to obtain the intact FMO-RCC and separate RCC (PscA-PscC) complexes from *Chlorobaculum tepidum*. These were further studied comparatively by steady-state and time-resolved fluorescence and

femtosecond time-resolved transient absorption spectroscopies to elucidate an anticipated FMO-to-RCC inter-protein energy transfer as well as RCC intra-protein energy and electron transfer.

3.2 Materials and methods

3.2.1 Protein purification and basic spectroscopic characterization

The FMO-RCC complex was purified from the green sulfur bacterium *Chlorobaculum tepidum* strain TLS as previously reported.[21] The RCC complex was purified by similar method with some modifications. Instead of loading onto a DEAE-cellulose column, the dark green band obtained from the centrifugation in the sucrose gradient was treated with 0.4 M Na_2CO_3 overnight and subsequently loaded onto a hydroxyapatite column of about 10 mL bed volume. The column was equilibrated with 5 mM potassium phosphate buffer (pH = 7.0) and 0.05% n-dodecyl β-D-maltoside (DDM). The sample was eluted with a linear gradient from 5 mM to 1 M potassium phosphate buffer (pH = 7.0) with 0.05% DDM. Fractions containing the RCC were collected. The FMO protein was purified as described previously.[1] Prior to spectroscopic experiments, sodium dithionite was added to 5 mM final concentration to all samples to keep them in a "reduced" state during measurements. Experiments at cryogenic temperature (77 K) were performed on samples diluted in 60% (v/v) glycerol/buffer mixture in either VNF-100, a liquid nitrogen cryostat from Janis (Janis Research Corp., Woburn, MA, USA) or in Optistat DN2, a liquid nitrogen cryostat from Oxford (Oxford Instruments, Oxfordshire, UK). The concentrations of the samples were adjusted to an absorbance of about 0.24 at 814 nm in a square 1 cm cuvette. Steady-state absorption spectra were taken using a UV-1800 UV/Vis spectrophotometer from Shimadzu (Shimadzu North America, Columbia, MD, USA). Steady-state fluorescence spectra were measured using a customized PTI fluorometer (Photon Technology International Inc., Birmingham, NJ, USA) as described in detail previously.[32] For

fluorescence emission measurements, both the FMO-RCC and RCC complexes were excited at 602 nm.

3.2.2 Time-resolved absorption and fluorescence spectroscopies

Transient absorption measurements were taken at 77 K using Helios, a TA spectrometer (UltrafastSystems LCC, Sarasota, FL, USA) coupled to a femtosecond laser system from Spectra-Physics described in detail previously.[33] The energy of the pump beam was unified for all excitation wavelengths and samples to 100 nJ in a circular spot size of 1 mm diameter corresponding to photon intensity of $4 - 5 \times 10^{13}$ photons cm^{-2} per pulse, unless stated otherwise. Previous studies done on the isolated FMO protein demonstrated that such laser intensity is low enough to substantially diminish excitation annihilation in the FMO exciton manifold.[34] The time-resolved fluorescence (TRF) experiments of FMO-RCC were carried out using a Hamamatsu universal streak camera setup described in details previously.[35] The full width at half maximum (FWHM) of the instrument response function (IRF) of the streak camera setup in the time window used for measurements is ~400 ps. The frequency of the excitation pulses produced by Inspire100, an ultrafast optical parametric oscillator (Spectra-Physics, CA, USA) pumped with 80 MHz ultrafast Mai-Tai, Ti:Sapphire laser (Spectra-Physics, CA, USA), was set at 1 MHz (1 μs between subsequent excitations) by a 3980 Pulse Selector from Spectra-Physics. The depolarized excitation beam set to 602 nm with power of ~30 μW was focused on the sample in a circular spot of ~1 mm diameter, corresponding to a photon intensity of $\sim 1 \times 10^{10}$ photons/cm^2 per pulse. The samples were adjusted to OD ~0.3 in the Q_y band in a 1 cm cuvette, however, the excitation beam focus point was adjusted to be very close to the cuvette wall that was used to measure emission (at right angle) and this procedure assured that emission filtering by self-absorption was practically negligible in all cases.

3.2.2 Spectroscopic datasets correction and analysis

The TA datasets were corrected for temporal dispersion using Surface Xplorer Pro 2.0 software from UltrafastSystems by building a dispersion correction curve from a set of initial times of transient signals obtained from single wavelength fits of representative kinetics. Global analysis of the TA datasets was performed using a modified version of ASUfit 3.0, program kindly provided by Dr. Evaldas Katilius at Arizona State University. The full width at half maximum (FWHM) of a Gaussian-like temporal response function was assumed to be in 120 – 150 fs range. Global analysis of TA datasets were done according to irreversible sequential decay path of the excitation decay or electron transfer, procedure that gives so-called evolution-associated difference spectra (EADS).[36] The fluorescence decay kinetics at specific wavelengths corresponding mostly to emission from the FMO protein were extracted from the TRF contours and fitted independently with an adequate sum of exponentially decaying components convoluted with the real IRF using DecayFit 1.3, fluorescence decay analysis software from FluorTools (www.fluortools.com). Global analysis of TRF was done according to parallel decay path that assumes that all kinetic components are populated simultaneously via excitation, decay independently and are convoluted by IRF. The results of this kind of fitting are commonly called decay associated spectra (DAS) [36] However, because in the literature the term DAS is generously used for fitting results of either TRF or TA, here it was modified to be FDAS (fluorescence decay associated spectra).

3.2.3 LC-MS/MS and Data Analysis

The stained bands of SDS-PAGE were excised and digested with trypsin by following a previously published protocol with minor changes.[37] Tryptic peptides from each gel band were analyzed by LC-MS/MS. The LC-MS/MS analysis followed the protocol adapted from previous

work with minor changes.[38] The samples were analyzed with LC-MS/MS using a Waters Synapt G2 Q-IM-TOF (Waters Inc., Milford, MA, USA) and Thermo LTQ Orbitrap (Thermo, San Jose, CA, USA). The data-dependent mode acquisition was used for the Orbitrap as previously described.[39] The MS^E mode acquisition was used in the LC-MS/MS experiment on the Synapt G2. Peptide ions were dissociated in the trap region by ramping the collision energy by gradually increasing voltage from 14 to 40 V. Tryptic digested sample was separated by reverse phase capillary column (0.075 mm × 150 mm), custom packed with C18 material (Magic C18, 5 um, 200 Å, Michrom Bioresources, Inc., Auburn, CA, USA). The flow from LC separation was directed to the mass spectrometer by a nanospray source. The raw data from the Orbitrap was analyzed by MassMatrix and data from the Synapt G2 was submitted to the ProteinLynx Global Server (V2.5, Waters Inc., Milford, MA, USA) to identify the peptide sequence.[40]

3.3 Results and discussion

3.3.1 Purification and identification of the FMO-RCC and RCC complexes

The steady-state absorption spectra of the FMO, FMO-RCC and RCC complexes recorded at 77 K are shown in Figure 3.2. The spectra reveal absorption bands associated with electronic transitions of (B)Chl *a* bound into the protein manifolds: Q_x band of BChl *a* at 602 nm (all samples), Q_y band of Chl *a* at 668 nm (RCC and FMO-RCC) and collective Q_y band of excitonically coupled BChls *a* appearing between 790 and 843 nm. Purity of the FMO-RCC complex was checked by taking an FMO-RCC minus RCC difference absorption spectrum as shown in Figure 3.3. It demonstrates a very good agreement with the absorption spectrum of separate FMO, thus the FMO-RCC sample is not compromised by any contaminations.

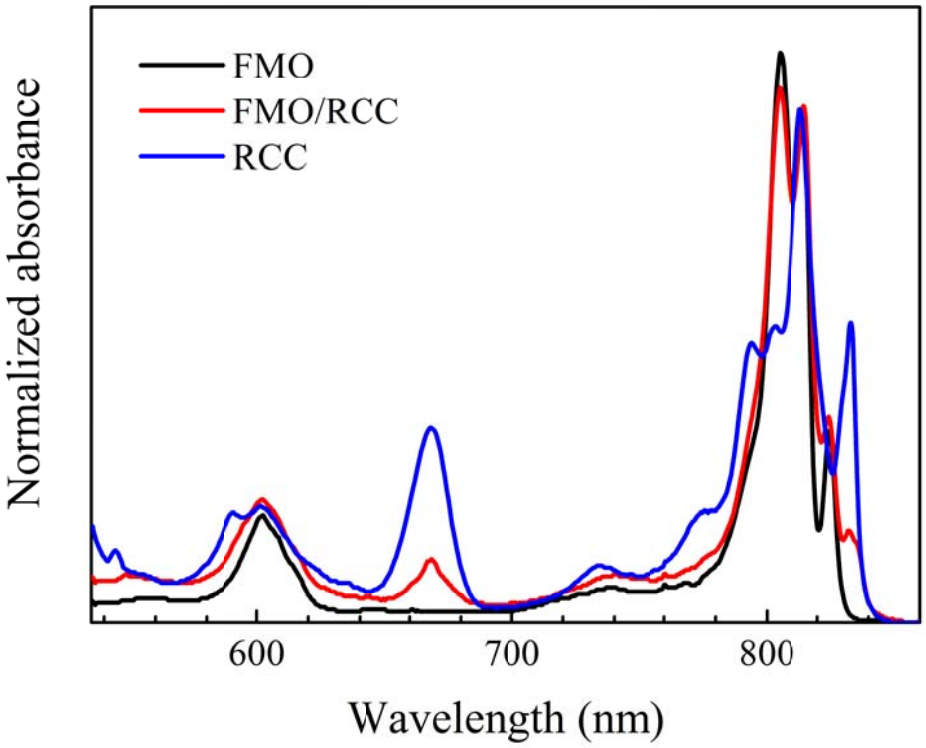

Figure 3.2 The steady-state absorption spectra of the FMO (black), FMO-RCC (red) and RCC (blue) complexes. For better comparability the spectra were normalized at 820 nm.

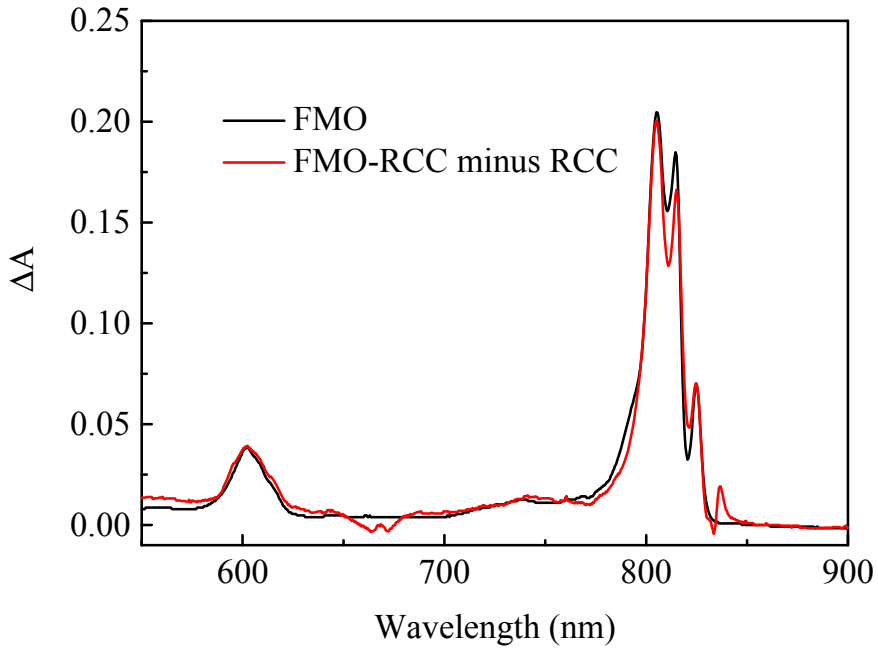

Figure 3.3 The FMO absorption spectrum and FMO-RCC minus RCC difference absorption spectrum, the spectra are normalized at 825 nm.

Good purity of the FMO-RCC sample was confirmed by the SDS-PAGE. The results for FMO-RCC and RCC complexes are shown Figure 3.4. Both complexes comprise a diffuse band ranging between 60 and 70 kDa that can be assigned to the PscA subunit. A second band around 19 kDa corresponds to the PscC subunit.[12, 24, 26] The FMO-RCC sample showed three additional bands at 16, 30 and 40 kDa which are identified to be PscD, PscB and FMO, respectively.[22, 23] The protein assignments were confirmed by in-gel digestion and subsequent mass spectrometry using LC-MS/MS (Figure 3.5). The RCC complex lacking FMO, PscB and PscD subunits was compared with the FMO-RCC complex.

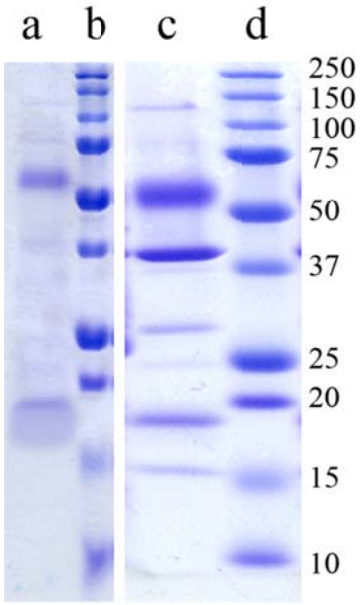

Figure 3.4 SDS-PAGE of (a) the RCC complex, (c) the FMO-RCC complex and (b, d) markers. Vertical scale is denominated in kDa.

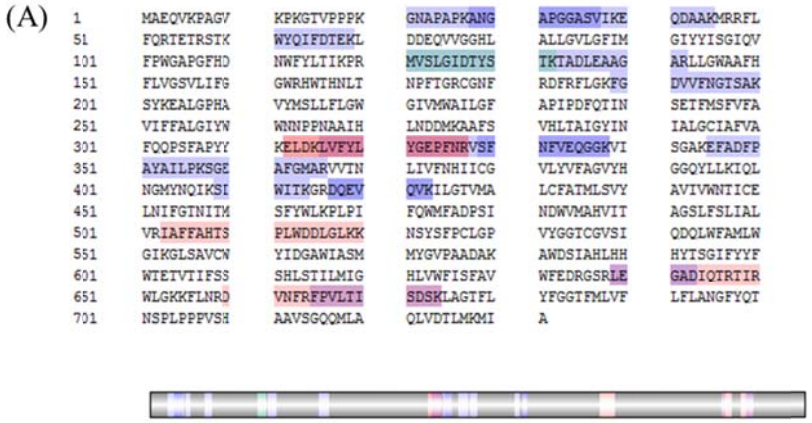

Figure 3.5 Peptide sequence coverage map of (A) PscA and (B) PscC (purple: matched to a peptide; red: matched to a partial peptide; green: matched to a modified peptide; yellow: matched to a partial modified peptide)

3.3.2 Steady-state and time-resolved fluorescence of FMO-RCC

The steady-state fluorescence emission spectra obtained after excitation of the FMO-RCC and RCC-only complexes at the BChl *a* Q_x band (602 nm) are given in Figure 3.6A. As shown, the emission spectrum of RCC can be fitted to that of the FMO-RCC complex and FMO-RCC – RCC difference spectrum can be obtained (blue). This spectrum mimics the emission spectrum of the pure FMO protein.[34] It shows that when the FMO-RCC complex was excited at 602 nm, 60% of the emission came from the RCC complex at 840 nm. An interesting aspect of these results is how much of the RCC emission is associated with direct excitation of BChl *a* in the RCC and how much actually originates from the FMO-RCC excitation energy transfer. As shown in Figure 3.7, the RCC complex showed much lower intensity of emission than the FMO-RCC complex at 840 nm if the emission spectra of the samples are normalized based on the same absorptance level at the Chl *a* 670 band in 1-T spectra (Figure 3.8). Therefore, a significant amount of the fluorescence emission of the FMO-RCC complex at 840 nm is due to the energy transfer from the FMO to RCC complex instead of directly exciting the RCC complex. The energy transfer efficiency from the FMO protein to the RCC complex is calculated based on $(F_C-A_C)/(A_{FC}-A_C)$ as reported before.[31] F_C is the contribution of the RCC complex in the height at 602 nm in the excitation spectrum of the FMO-RCC complex for emission at 840 nm (Figure 3.9). As mentioned above, 60% of the emission at 840 nm came from the RCC complex, thus the contribution of the RCC complex will be calculated by the height of the band for the FMO-RCC complex at 602 nm in the excitation spectrum multiplied by 0.6. A_C and A_{FC} are the amplitudes

of the absorption bands at 602 nm in the (1-T) spectra for the RCC complex and the FMO-RCC complex, respectively (Figure 3.8). All the spectra were normalized at 670 nm to carry out the calculation. The energy transfer efficiency from the FMO protein to the RCC complex is calculated to be ~40%. Figure 3.6B shows a 2D-contour plot of time-resolved fluorescence of the FMO-RCC taken at 77 K upon excitation at 602 nm. It is noticeable that the RCC emission is not as well resolved in the TRF profile compared with that in the steady-state.

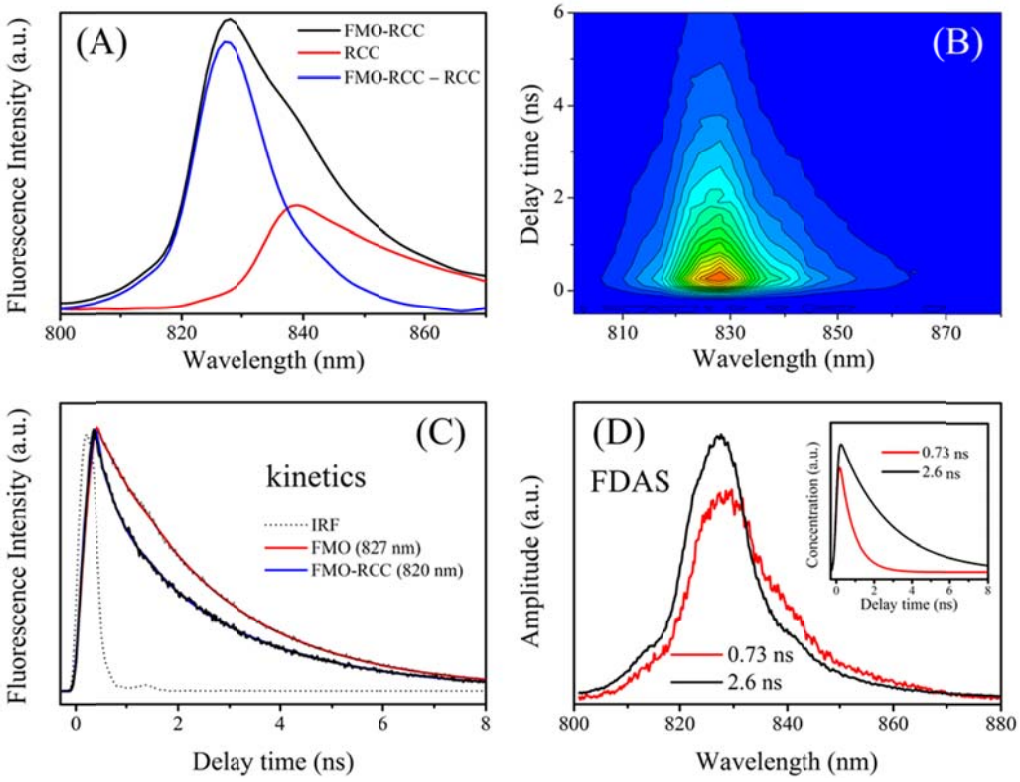

Figure 3.6 (A) Steady-state fluorescence emission spectra of the FMO-RCC (black) and RCC (red) complexes. The blue trace represents a hypothetical spectrum of FMO only obtained by subtracting the RCC profile from the FMO-RCC spectrum; (B) 2D-contour of time-resolved fluorescence of FMO-RCC taken at 77 K upon excitation at 602 nm; (C) Representative kinetic of BChl *a* fluorescence decay in the FMO-RCC and FMO only taken at 77 K accompanied by fits, IRF – instrument response function; (D) Global fitting results of TRF dataset shown in panel B. The inset shows concentrations of the individual FDAS components. FDAS – fluorescence decay associated spectra.

Two representative fluorescence decay kinetics of the FMO are given in Figure 3.6C. The red trace was recorded for separate FMO while the blue trace, extracted from the data presented in panel B, corresponds to fluorescence from FMO in the FMO-RCC complex. The choice of the 820 nm emission wavelength guarantees that the contribution from fluorescence of the RCC complex is negligible (see Figure 3.6A). In order to mimic scattering (bump seen at ~1.6 ns time delay) and improve fitting quality, a fraction of the instrument response function (IRF) was added to the convoluted decay. Fluorescence decay of the FMO-only sample can be successfully fitted with a single exponential decay with lifetime of 2.3 ns. Fluorescence decay of the FMO-RCC required two kinetic components with lifetimes (amplitudes) of: 0.6 ns (34%) and 2.5 ns (66%). Upon the assumption that FMO transfers excitation energy into RCC, as shown in steady-state fluorescence spectrum, the appearance of two time components suggests that the FMO-RCC sample is not homogeneous. Actually, a major part of the FMO complexes (66%), regardless of the fact that they are physically attached to the RCC, is not able to transfer excitation energy due to other unforeseen reasons (wrong orientation, etc.), which can be caused either by an intrinsic property in the native system or by the purification process. This issue could be a reason for the differences between the time-resolved and steady-state fluorescence spectra. Since the excitation laser beam in the TRF experiment was focused on the sample in a circular spot of ~1 mm diameter, there is no guarantee that the sample in such a localized area was frozen in the optimal protein configuration to ensure the maximum FMO-RCC energy transfer.

The remaining 34% of the FMO pool has an effective fluorescence decay lifetime of 0.6 ns. This is the fraction of FMO that participates in the energy transfer and its efficiency (Φ_{EET}) can be calculated according to equation 1:

$$\Phi_{\mathrm{EET}}(\%) = (1 - \frac{\tau_{ef}}{\tau_{int}}) \times 100 \qquad (1)$$

where τ_{eff} = 0.6 ns – fluorescence decay lifetime of BChl *a* in the FMO if excitation energy transfer occurs, τ_{int} = 2.5 ns – intrinsic fluorescence decay lifetime of BChl *a* in the FMO only. The Φ_{EET} of the interacting FMO fraction calculated according to Eq. 1 is 76%.

Similar results (lifetimes) were also obtained if the entire TRF dataset was fitted globally. The fitting results called as FDAS – fluorescence decay associated spectra, are given in Figure 3.6D. This model assumes that spectral components are simultaneously populated by laser excitation and independently decay with calculated lifetimes. The model and fitting results (FDAS) are physically correct only if laser flash-induced species (FMO and RCC) are truly independent from each other (no energy transfer between them, etc.). However, because some fraction of the FMO population energetically interacts with the RCC, both species do not really decay independently and different kinetic model of excitation decay applies. Thus, the "FDASs" have no simple physical meaning and could be some blend of spectra of the individual components (FMO and RCC). The 2.6 ns FDAS seen in Figure 3.6D corresponds well in spectral shape and lifetime to the separate FMO protein. The faster FDAS, 0.73 ns component spectrally fits to the steady-state spectrum of FMO-RCC and can be interpreted as a collective time-resolved spectrum of the FMO-RCC complex. The lack of additional spectral/kinetic components in the data suggests that energy-transferring FMO and RCC show similar fluorescence decay lifetime. To further elucidate FMO-RCC energetic interactions femtosecond time-resolved absorption spectroscopy was performed on individual RCC as well as FMO-RCC complexes.

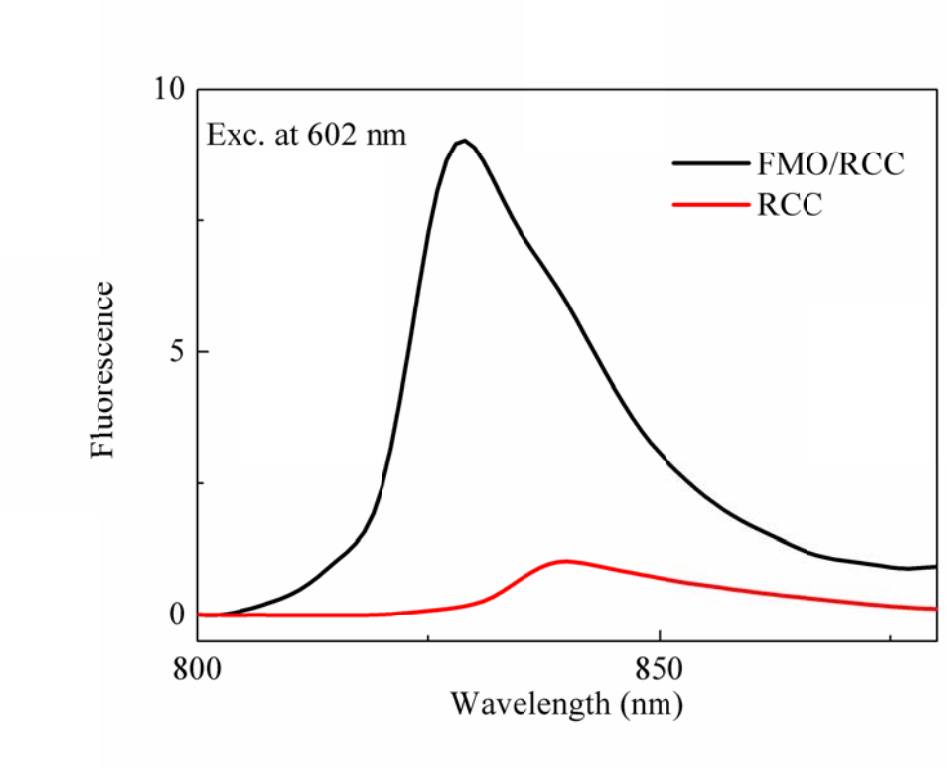

Figure 3.7 Static fluorescence emission spectra of the FMO-RCC (black) and RCC (red) complexes with the same absorption (1-T) at 670 nm

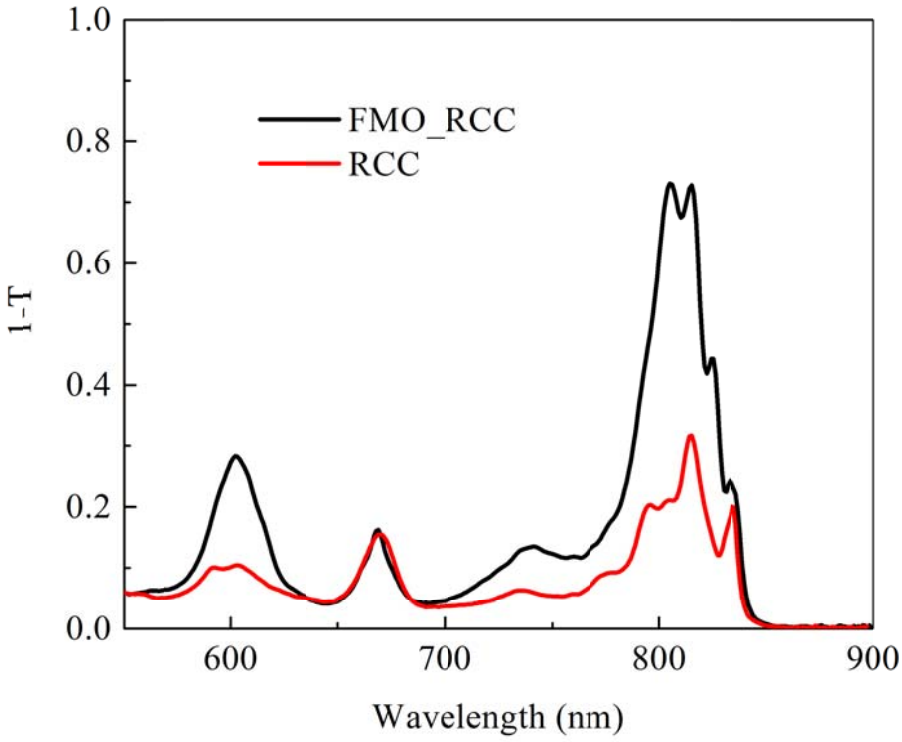

Figure 3.8 The 1-T spectra of the FMO-RCC (black) and RCC (red) complexes, the spectra are normalized at 670 nm

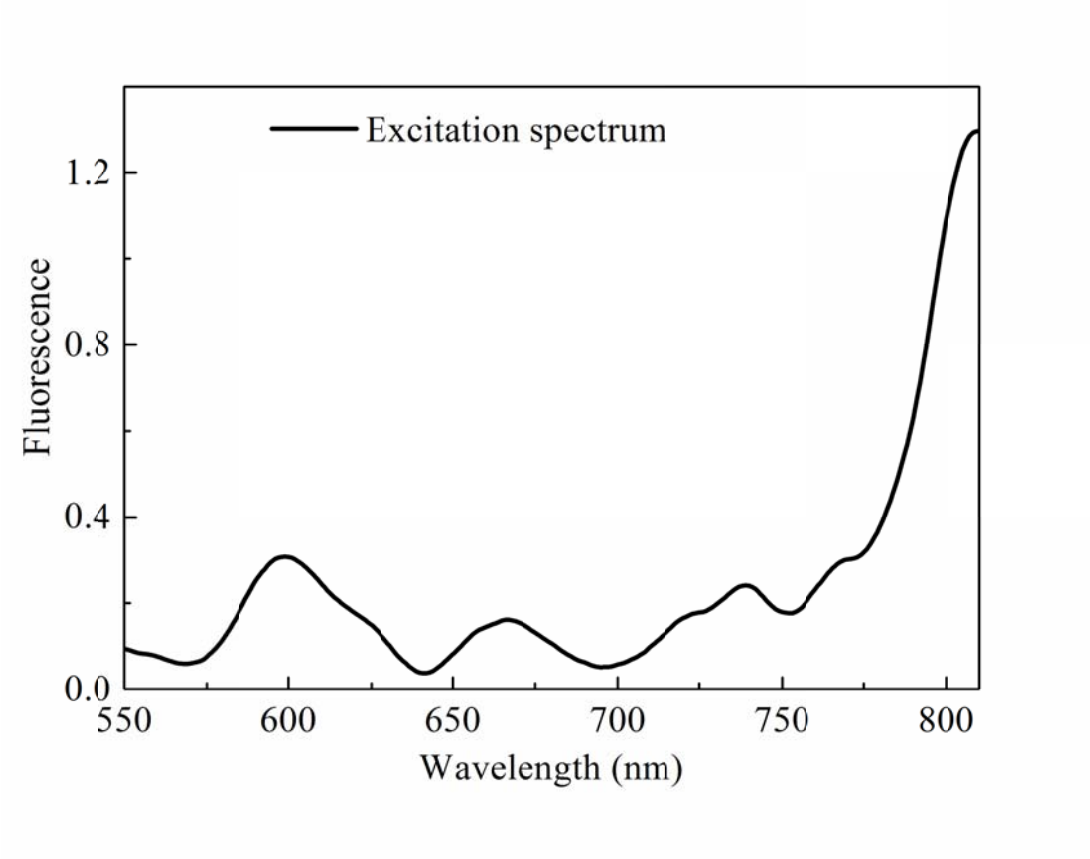

Figure 3.9 Fluorescence excitation spectrum of the FMO-RCC complex for emission at 840 nm.

3.3.3 Transient Absorption Spectroscopy of the RCC complex

Classically, TA experiments of RCC and FMO-RCC complexes from green sulfur bacteria are performed in a way that avoids permanent bleach of the sample. That could be done if accumulation of RCCs in their oxidized state $P840^+$ is limited. It is known that at cryogenic temperatures the $P840^+$ decay ($P840^+ \rightarrow P840$) shows a biphasic character with lifetimes (depending from the bacterial species and temperature) spanning ranges of 100-350 μs and 30-120 ms.[10, 27, 41] . The fast component is associated with cytochrome donation while the slow phase is presumably due to back reaction (charge recombination) with the reduced iron sulfur cluster F_x^-.[20, 41] The $P840^+$ A_0^- charge recombination rate was reported to be 19 ns in the presence

of sodium dithionite.[42] In the laser-TA spectrometer setup that was used for our studies samples are excited every 2 ms (one of two laser flashes is blocked for baseline recording), a time that is quite adequate for completeness of cytochrome-to-$P840^+$ electron transfer as well as for $P840^+$ A_0^- charge recombination. In addition, the energy of the pump beam we were using was as low as 100 nJ, corresponding to photon intensity of $4 - 5 \times 10^{13}$ photons cm^{-2} per pulse, to avoid permanent bleach. Thus, we were able to use a high frequency excitation laser (1 kHz) without permanent bleach of the sample.

Transient absorption spectra of the RCC excited into three representative absorption bands (590, 670 and 840 nm) recorded in the near-infrared spectral range (NIR) and their global analysis results are shown in Figure 3.10.

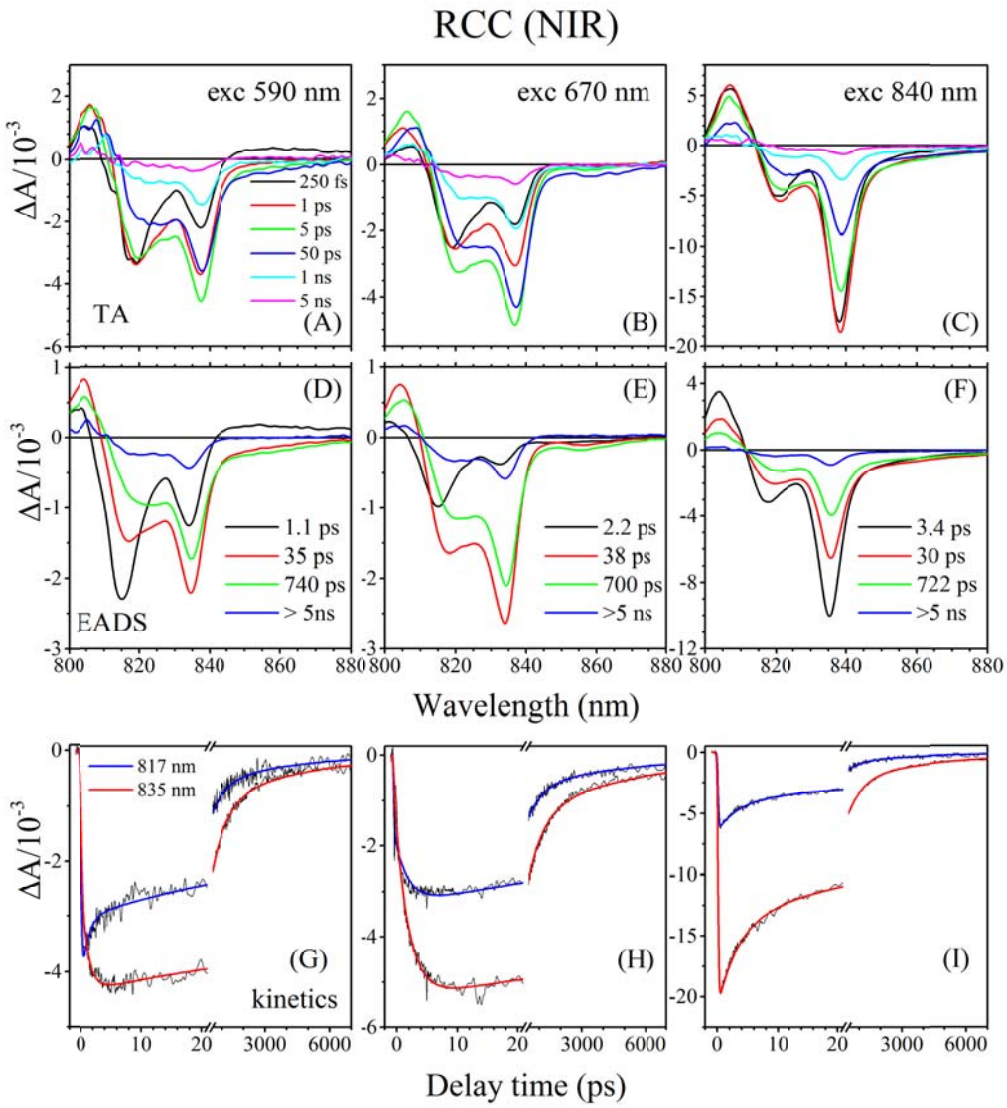

Figure 3.10 Representative TA spectra taken at various delay times after excitation into (A) Q_x band of BChl *a* (590 nm), (B) Q_y band of primary electron acceptor, Chl *a* (670 nm) and (C) energetically lowest BChl *a* exciton in the collective Q_y band (840 nm); (D-F) EADS – evolution associated difference spectra, global analysis results obtained based on sequential path decay of excitation of TA datasets from panels A-C, (G-I) Exemplary kinetic traces recorded at 817 and 835 nm accompanied with fits from global analysis.

Immediately after excitation at 590 nm, two bleaching bands are formed at 819 and 837 nm that initially show similar amplitudes. The positive band at 805 nm is attributed to the collective

excited state absorption (ESA) of all BChls in the RCC complex. Within 5 ps after excitation, a rapid spectral equilibration of the BChl *a* exciton manifold is observed. Bleaching of the higher energy excitonic band shifts from 819 to 821 nm and its amplitude partially diminishes. Simultaneously, bleaching of the low energy exciton develops until it reaches a minimum at ~5 ps. The position of this band remains constant and after spectral equilibration, the $\Delta A_{821}/\Delta A_{837}$ ratio remains essentially constant at ~0.55. Upon excitation into the Q_y band of Chl *a* (Figure 3.10B), an instantaneous development of bleaching of both abovementioned bands is observed. Initially bleaching of the higher energy excitonic band dominates in the TA spectra. As time evolves, and excitonic equilibration is completed, the TA spectra are essentially identical with those from excitation at 590 nm. Excitation at 840 nm (Figure 3.10C) directly populates the low energy exciton and equilibration within the excitonic BChl *a* manifold is not observed. The TA spectra do not reveal changes over time in their spectral envelope in the entire time delay window of the spectrometer.

Global analysis gives more insight about energetic equilibration within the excitonic manifold as well provides some information about the initial steps of the charge separation process. In all cases, four kinetic components were required for satisfactory fits of the TA datasets (Figure 3.10D-F). Better understanding of the individual EADS components can be achieved if those are discussed together with representative kinetic traces (Figure 3.10D-I). The first 1.1 ps – 3.4 ps EADS is associated with different processes in each of the TA datasets. Upon 590 nm excitation, the 817 and 835 nm kinetic traces (bleaching of excitonic bands) suggest that fast process is associated with rapid energy redistribution from higher energy exciton (817 nm) into the lower one (835 nm). It is clearly indicated in the 817 nm kinetics as a fast decay within the first 5 ps coupled with a simultaneous rise of the bleaching at 835 nm. Upon excitation at 670 nm, the 2.2

ps EADS is associated with a simultaneous rise of bleaching of both excitonic bands, suggesting that it is related to energy transfer from Chl *a*. Identical kinetic performances show that there is no specificity in how excitation energy is transferred from the Chl *a*. For 840 nm excitation, the 3.4 ps EADS is spectrally identical with the following components and kinetic traces that have practically equal characteristics at both wavelengths indicate that it is likely associated with excitation annihilation. Lifetimes of the following EADS are essentially (with only small variations) the same for all three TA datasets. The 30-38 ps EADS component was previously assigned to the charge separation process when the oxidized primary electron donor $P840^{+}$ is formed.[19, 27, 28, 30, 43] The origin of the 700-740 ps EADS component is not clear, as such a kinetic component has not been previously observed in similar systems. However, the TRF results demonstrate that in the FMO-RCC complex, both FMO and RCC show a similar fluorescence decay lifetime of ~750 ps, matching very well to 700-740 ps component observed in the TA datasets. Thus, it can be proposed that the 700-740 ps component is associated with long-lived excitons that do not contribute to charge separation but are responsible for fluorescence emission. The steady-state fluorescence spectrum of the RCC (Figure 3.6A) is substantially extended toward longer wavelengths with respect to the absorption spectrum (Figure 3.2). It should also be noticed in the TA spectra that aside from differences in absorption, they also contain stimulated emission induced by the probe beam. Indeed, a closer look at the second and third EADS reveals that both profiles show NIR-extended "bleaching" that does not coincide with the long-wavelength tail of the steady-state absorption (Figure 3.2) and likely corresponds to the stimulated emission. However, this spectral feature is absent in the long-lived (last) EADS (noted as >5 ns). It is another indication that the 700-740 ps EAD is associated with long-lived BChl *a* excitons. Absence of stimulated emission in the spectral profile of the last EADS (noted

as >5 ns) points out that this long-lived component may result from the sub-millisecond $P840^+$ → P840 reduction process occurring through cytochrome electron donation very likely combined with charge recombination between the $P840^+$ and initial electron acceptors.[10, 27, 41] Due to time window limitation of the TA spectrometer, these processes cannot be correctly temporally resolved.

The primary step in the charge separation process in the RCC can be also monitored in the spectral range of the Q_y absorption band of the primary electron acceptor A_0, Chl *a*-670. It is shown in Figure 3.11.

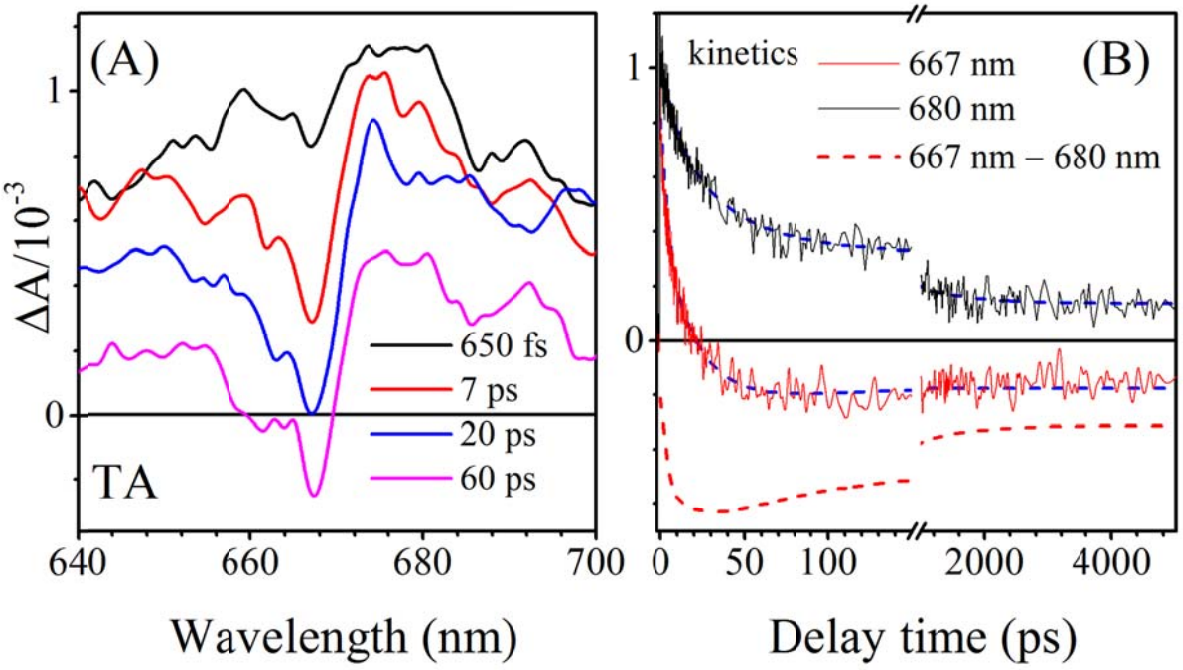

Figure 3.11 Onset of bleaching of the Q_y absorption band of the primary electron acceptor A_0, Chl *a*-670, upon excitation at 840 nm; (A) representative TA spectra taken at various delay times; (B) kinetic traces recorded at Q_y band of Chl *a* (667 nm) and at ESA band of BChl *a* (680 nm).

Figure 3.11A shows representative TA spectra in 640-700 nm spectral range. Initially, there is barely any bleaching of the Q_y band of Chl *a* present, however, it develops promptly within 20 ps after excitation. Figure 3.11B demonstates two kinetic traces, associated with ESA of BChl *a* (680 nm) and at 667 nm that combines two transient signals, ESA of BChl *a* and bleaching of the Q_y band of Chl *a*. The true temporal characteristics of bleaching of the Chl *a* Q_y band can be reconstructed by subtracting the 680 nm kinetic trace with a scaling factor. The scaling assumed that promtly after time of excitation bleaching at 670 nm should be equal to zero (charge separation has not started yet). The resulting trace reveals the initial onset of bleaching of the Q_y band of Chl *a* and is plotted as a dashed red line. The maximum of the Q_y bleaching is reached at ~35 ps and roughly 15% further reduction in the signal is observed between 35 and 150 ps. A modest reduction in the bleaching level of the Chl *a* Q_y band observed in the abovementioned time range most probably represents energetic equlibration of the Chl a^- anion. The decay of the Q_y band of Chl *a* can be fitted to two time components: 55 ps and 750 ps. The ratio of the amplitute of 55 ps to that of 750 ps is 1:3. The 750 ps time component may represent the recovery of the Chl a^- anion by transferreing the electron to F_x.

3.3.4 Transient Absorption Spectroscopy of the FMO-RCC complex

The FMO-to-RCC energy transfer in the FMO-RCC complex was also addressed with application of time-resolved absorption. These studies are difficult to perform due to a few disadvantages. First and the most influential is that it impossible to find a wavelength that will selectively excite FMO but not RCC. Second, even at low intensities there is a chance of excitonic annihilation in the FMO exciton manifold, before an energy transfer occurs. In addition, the studied sample could be also inhomogeneous and contains a mixture of FMOs that are energetically coupled and uncoupled with RCC regardless of the fact that all are physically

attached, as it was demonstrated in the TRF studies. All of it makes kinetic analysis of the TA datasets of the FMO-RCC quite difficult and uncertain. However, some general conclusions can be drawn. Figure 3.12 shows results of TA of FMO-RCC complex upon excitation at 590 nm. A set of demonstrative TA spectra is given in Figure 3.12A. The spectra consist of multiple features and significantly differ in the overall shape from TA spectra of individual RCC (Figure 3.10). The spectra significantly evolve over time and it is apparent that spectral species that dominate at early delay times decay within 1 ns time range after excitation. The TA spectra recorded at later delay times show substantial similarities with TA of separate RCC.

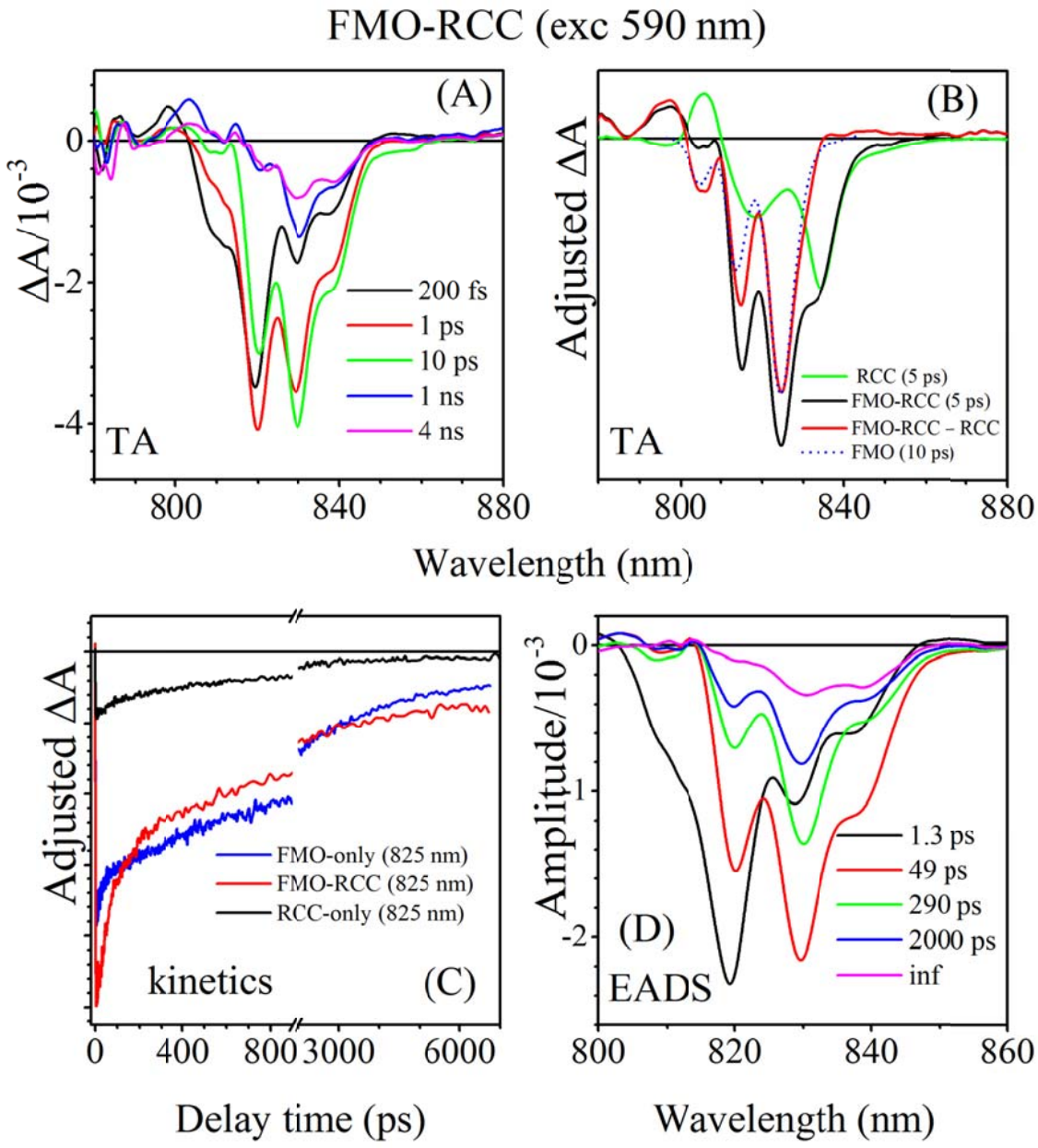

Figure 3.12 Transient absorption of the FMO-RCC complex; (A) Representative TA spectra taken at various delay times after excitation into the Q_x band of BChl *a* (590 nm), (B) Comparison of TA spectra of the FMO-RCC complex and individual FMO and RCC complexes taken at either 5 or 10 ps after excitation at 590 nm. The red trace represents the FMO-RCC minus RCC difference; (C) Kinetic traces recorded at 825 nm from TA datasets of the FMO, RCC and FMO-RCC, recorded upon the same measurement conditions. The amplitudes are adjusted to match ratios of the TA spectra as shown in Figure 3.6B; (D) global analysis results of TA datasets obtained based on sequential path decay of excitation.

It is not surprising that at early delay times after excitation, TA spectra are simply a combination of individual TA spectra of FMO and RCC complexes, as it can be seen in Figure 3.12B. This figure shows FMO-RCC and RCC TA spectra recorded at 5 ps after excitation. The TA spectrum of RCC (green) was adjusted to match its contribution in the overall TA spectrum of the FMO-RCC complex. The red trace is a result of subtraction of the adjusted RCC spectrum from TA spectrum of FMO-RCC. This profile is almost identical with the TA spectrum of separate FMO complexes taken at 10 ps after excitation (dotted blue) and differs only in minor details. It is evident that 590 nm excitation is not selective. It simultaneously excites FMO and RCC, which makes detailed kinetic analysis of FMO-to-RCC energy transfer practically impossible. Some information can be obtained from comparative examination of a few characteristic kinetic traces of FMO-RCC and separated FMO and RCC and global analysis. Kinetic traces extracted at 825 nm, wavelength, which primarily contains signal associated with FMO extracted from the TA of the FMO-RCC, FMO and RCC are given in Figure 3.12C. The amplitudes are adjusted to match ratios of ΔA_{825} at 5 ps as in the FMO-RCC TA spectrum (Figure 3.12B). All kinetic traces were recorded with the same excitation conditions (0.1 μJ). There is apparently a substantial difference between FMO and FMO-RCC that cannot be explained just by taking account of the fraction of the signal related with the RCC and originating from a direct excitation of the core complex (black line). Therefore, the additional fast kinetic component (compare blue and red traces) in the recovery of the 825 nm excitonic band of the FMO in the FMO-RCC complex should be linked to FMO-to-RCC energy transfer. Previous studies of TA of separate FMO performed under identical condidtions demonstrated that the TA dataset can be fitted with four kinetic components with lifetimes of ~1 ps, 60 ps, 2 ns and infinite (triplet).[34] As demonstrated in Figure 3.10 the TA in the RCC sample will multiexponentially decay with lifetime of ~1 ps, 35

ps, 740 ps and infinite (reduction). Therefore, it is possible that in the FMO-RCC sample some components will blend together due to similar temporal characteristics and will be indistinguishable from each other. Global analysis (Figure 3.12D) shows that it is indeed true. Five EADS were suitable for a satisfactory fit of the TA data. The EADSs with lifetimes of 1.3 ps, 49 ps and "infinity" most likely comprise mixed kinetic components from RCC and FMO. The EADS with lifetime of 2 ns is clearly associated with the fraction of the FMO that is not energetically coupled to the RCC and intrinsically decays to the electronic ground state. The 740 ps EADS (RCC) was not necessary, maybe due to the fact that it has very low amplitude and can be masked by the 2 ns-component. However, apparently another 290 ps EADS kinetic component shown for the FMO-RCC sample, which is absent in the isolated FMO, has spectral shape overwhelmingly dominated by FMO absorption bleaching. Ostensibly, this component may be linked to the FMO fraction that is energetically coupled with RCC and efficiently transfer energy.

Figure 3.13 shows the TA spectra and EADS obtained for the FMO-RCC complex upon excitation of BChl Q_x band at 610 nm, where the absorption of the RCC complex is also significantly less than the FMO complex as shown in Figure 3.2. Bleaching bands formed immediately at 805, 819, 829 and 838 nm. As is mentioned before, 829 nm band is the lowest exciton state for FMO, while the 838 nm band is ascribed to the RCC. 819 nm band reached the maximum bleaching around 1 ps, when 829 and 838 nm bands were still increasing. At 5 ps, 829 nm became the dominant bleaching band, indicating most of the energy now was localized to the lowest exciton state of the FMO protein. The bleaching band at 838 nm keeps increasing until 5 ps, indicating that some of the energy is transferred from the FMO protein to the BChl *a*-837 in the RCC complex. The band at 829 nm decays relatively slowly than the bands at 819 nm and

838 nm. The EADS profiles are showed in Figure 3.13D. Five lifetime components, i.e., 2 ps, 40 ps, 300 ps, 2 ns and "infinite lifetime", were obtained. The results are similar to those obtained from exciting the FMO-RCC complex at 590 nm.

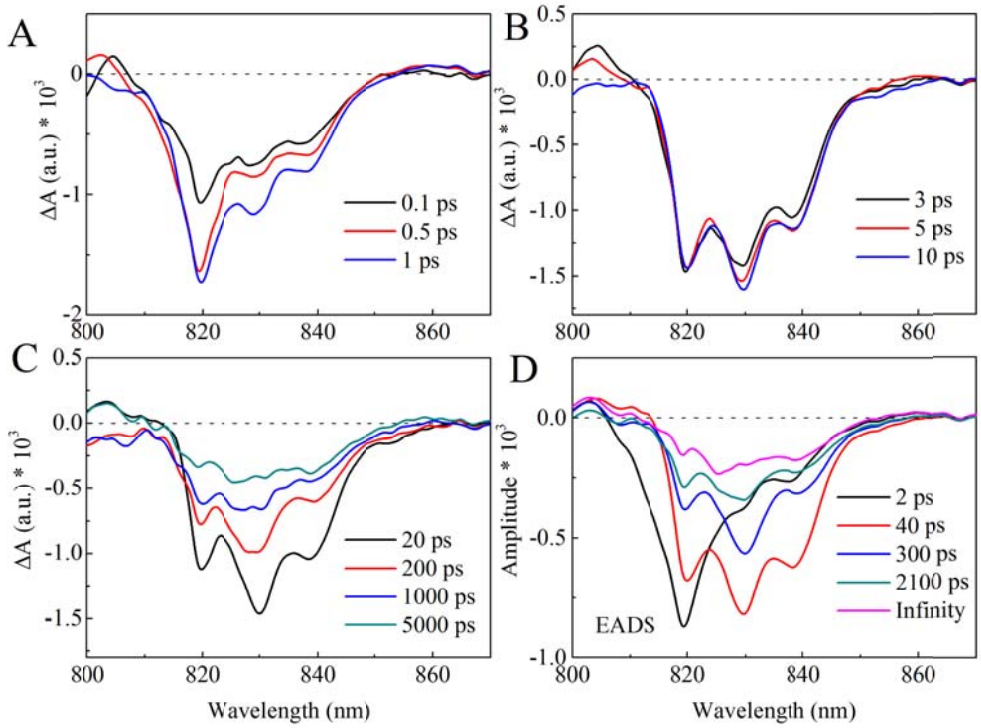

Figure 3.13 (a, b, c) The TA spectra taken at different delay times and (d) Global analysis of the TA datasets using EADS for the FMO-RCC complex after excitation at 610 nm

Figure 3.14 shows TA spectra of FMO-RCC complexes taken at different delay after excitation at 670 nm. The TA spectra for the first 20 ps are very similar to the RCC complex excited at the same wavelength, except for an additional small band at 826 nm owing to excitation of the FMO protein. But compared with the excitation at 590 nm and 610 nm, excitation at 670 nm more selectively excited the RCC complex.

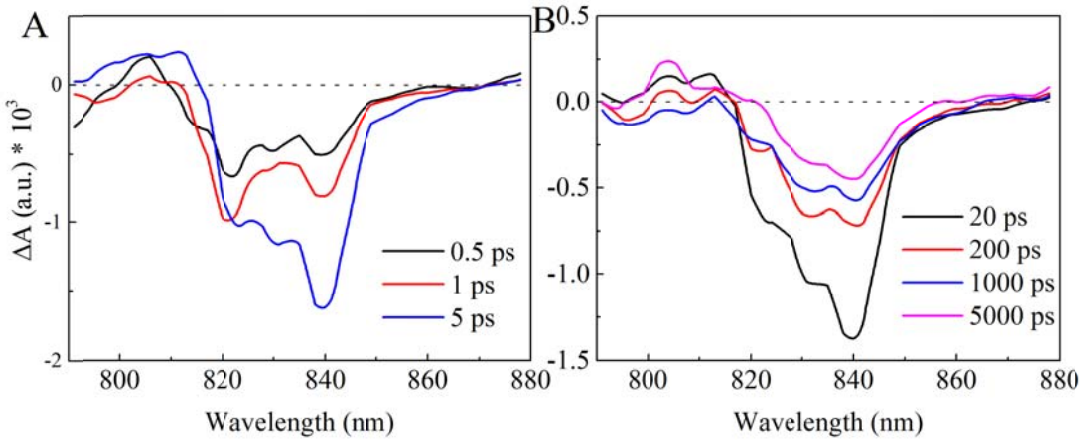

Figure 3.14 The TA spectra taken at different delay times performed on the FMO-RCC complex after excitation at 670 nm

Figure 3.15 shows the TA spectra and EADS obtained from FMO-RCC complex upon excitation at 840 nm. A broad band at 808 nm excited state absorption band is seen and 838 nm formed the main bleaching band right after excitation. 829 nm band indicated that some of the FMO are excited. It is seen that after 1 ps, the 838 nm band decays very quickly indicating very efficient energy transfer from 838 nm to P840. After 20 ps 829 nm became the main bleaching band. Figure 3.15C shows the TA spectra taken at 5 ps and 200 ps, normalized at 829 nm. It shows that the band at 829 nm decays more slowly than the band at 838 nm. EADS profiles in Figure 3.15D shows similar lifetime components as that for RCC, indicating that mostly RCC is excited at 840 nm.

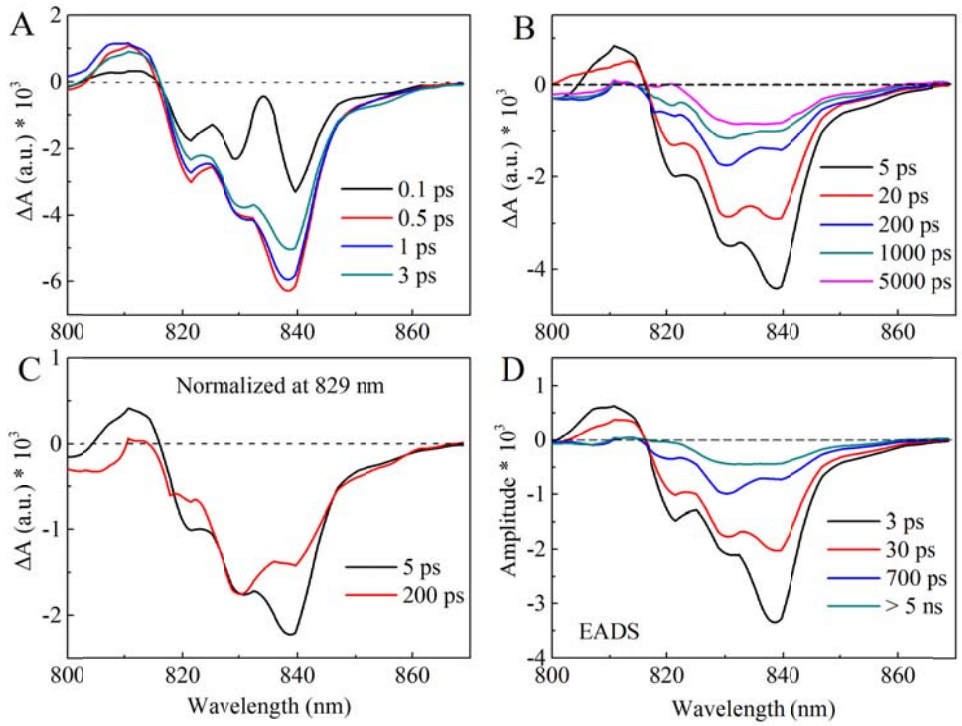

Figure 3.15 (A, B, C) The TA spectra taken at different delay times and (D) Global analysis of the TA datasets using EADS for the FMO-RCC complex after excitation at 840 nm

Figure 3.16 shows the TA spectra of the FMO-RCC complex after excitation at 840 nm with the energy of 0.4 μJ. The spectra and the EADS are very similar compared with that of the 0.1 μJ except the amplitude of the peaks. It indicates that there is no permanent bleaching and that the intrinsic decay processes are maintained even at 0.4 μJ. Excitation with the energy of 0.7 μJ led to permanent bleaching of the FMO-RCC sample, noted by the permanent loss of the 838 nm band (data no shown). It confirmed that the energy of the pump beam we were using was as low enough to avoid permanent bleach of the RCC.

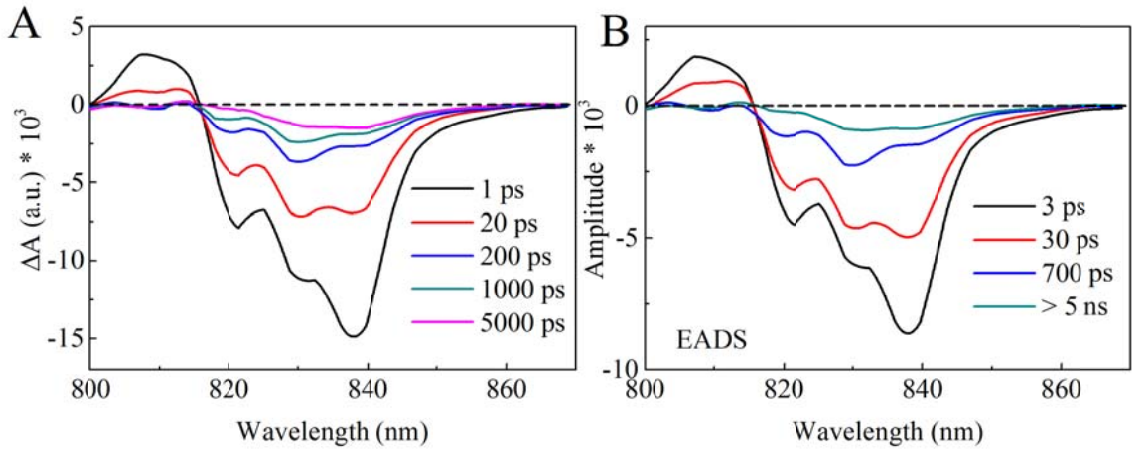

Figure 3.16 The TA spectra taken at different delay times (A) and (B) Global analysis of the TA datasets using EADS for the FMO-RCC complex after excitation at 840 nm with the energy of 0.4 μJ

The energy and electron transfer mechanisms following excitation of the FMO are summarized in Figure 3.17. Photons are absorbed by two fractions of FMO complexes, energetically uncoupled and coupled to the RCC. The first pool of the FMO (uncoupled) releases energy in fluorescence process with lifetime of 2.6 ns that is typical for free FMO. The second pool of FMO transfers absorbed energy to the RCC complex with approximately 76% efficiency resulting in shortening of observed fluorescence lifetime to ~700 ps. The excitation that is passed to RCC initially populates BChl *a* exciton that undergoes fast equilibration (1-3 ps) within excitonic manifold. Finally the excitation is transferred eventually to the special pair P840 or trapped in long-lived exciton that releases it as fluorescence with lifetime of ~700 ps. Upon accepting excitation by P840 an initial $P840^{+}A_0^{-}$ charge separation step occurs with time constant of ~35 ps. Very long recovery of bleaching of absorption of the RCC (marked as > 5 ns) may result from the sub-millisecond $P840^{+} \rightarrow P840$ reduction process occurring through cytochrome electron donation and charge recombination between the $P840^{+}$ and initial electron acceptors.

The following steps of the electron transfer that are showed in the scheme were beyond time domains of the spectroscopic measurements.

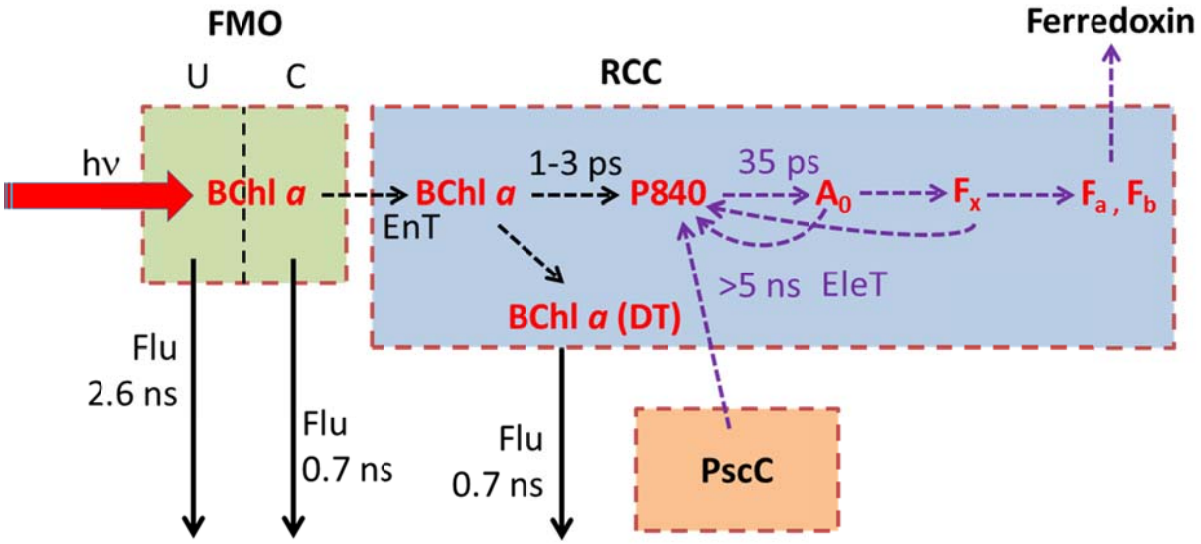

Figure 3.17: Schematic kinetic model of energy and electron transfers within the FMO-RCC complex consolidating results from time-resolved fluorescence and absorption; U – energetically uncoupled from RCC, C – energetically coupled to RCC, EnT – energy transfer, BChl *a* (DT) – deep traps, trapped BChl *a* excitons that are not capable to transfer energy to the special pair and must release it as fluorescence, P840 – BChl *a* special pair, EleT – electron transfer, A_0 – primary electron acceptor (Chl *a* derivative), PscC – cytochrome c_{551}.

3.4 Conclusions

The FMO-RCC complex and RCC (PscA-PscC only) complex were studied comparatively by steady-state fluorescence, TRF and TA spectroscopies. The energy transfer efficiency from the FMO to the RCC complex was calculated to be ~40% based on the steady-state fluorescence. TRF showed that most of the FMO complexes (66%) were not able to transfer excitation energy to the RCC complex, resulting in the heterogeneity of the FMO-RCC sample. In the TA spectra, the RCC complex showed charge separation process regardless of the excitation wavelength and

rapid excitonic equilibrium was seen when excited into the BChl *a* Q_x band at 590 nm and the Chl *a* Q_y band at 670 nm. Excitation into BChl *a* Q_x band showed different kinetics between the FMO-RCC and RCC complex. The TA spectra for the FMO-RCC complex could be interpreted by a combination of the excited FMO protein and RCC complex. But additional fast kinetic component was seen for the FMO-RCC complex, which may be linked to the FMO fraction that is energetically coupled with RCC.

References

(1) Li, Y. F.; Zhou, W. L.; Blankenship, R. E.; Allen, J. P. Crystal structure of the bacteriochlorophyll *a* protein from Chlorobium tepidum. *Journal of Molecular Biology* **1997**, *271*, 456-471.
(2) Freiberg, A.; Lin, S.; Timpmann, K.; Blankenship, R. E. Exciton dynamics in FMO bacteriochlorophyll protein at low temperatures. *Journal of Physical Chemistry B* **1997**, *101*, 7211-7220.
(3) Fidler, A. F.; Caram, J. R.; Hayes, D.; Engel, G. S. Towards a coherent picture of excitonic coherence in the Fenna-Matthews-Olson complex. *Journal of Physics B-Atomic Molecular and Optical Physics* **2012**, *45*.
(4) Busch, M. S. A.; Mueh, F.; Madjet, M. E.-A.; Renger, T. The eighth bacteriochlorophyll completes the excitation energy funnel in the FMO protein. *Journal of Physical Chemistry Letters* **2011**, *2*, 93-98.
(5) Wen, J.; Zhang, H.; Gross, M. L.; Blankenship, R. E. Native electrospray mass spectrometry reveals the nature and stoichiometry of pigments in the FMO photosynthetic antenna protein. *Biochemistry* **2011**, *50*, 3502-3511.
(6) Tronrud, D. E.; Wen, J.; Gay, L.; Blankenship, R. E. The structural basis for the difference in absorbance spectra for the FMO antenna protein from various green sulfur bacteria. *Photosynthesis Research* **2009**, *100*, 79-87.
(7) Engel, G. S.; Calhoun, T. R.; Read, E. L.; Ahn, T. K.; Mancal, T.; Cheng, Y. C.; Blankenship, R. E.; Fleming, G. R. Evidence for wavelike energy transfer through quantum coherence in photosynthetic systems. *Nature* **2007**, *446*, 782-786.
(8) Panitchayangkoon, G.; Hayes, D.; Fransted, K. A.; Caram, J. R.; Harel, E.; Wen, J.; Blankenship, R. E.; Engel, G. S. Long-lived quantum coherence in photosynthetic complexes at physiological temperature. *Proceedings of the National Academy of Sciences* **2010**, *107*, 12766-12770.
(9) Hauska, G.; Schoedl, T.; Remigy, H.; Tsiotis, G. The reaction center of green sulfur bacteria. *Biochimica Et Biophysica Acta-Bioenergetics* **2001**, *1507*, 260-277.
(10) Francke, C.; Permentier, H. P.; Franken, E. M.; Neerken, S.; Amesz, J. Isolation and properties of photochemically active reaction center complexes from the green sulfur bacterium *Prosthecochloris aestuarii*. *Biochemistry* **1997**, *36*, 14167-14172.
(11) Remigy, H. W.; Hauska, G.; Muller, S. A.; Tsiotis, G. The reaction centre from green sulphur bacteria: progress towards structural elucidation. *Photosynthesis Research* **2002**, *71*, 91-98.
(12) Griesbeck, C.; Hager-Braun, C.; Rogl, H.; Hauska, G. Quantitation of P840 reaction center preparations from *Chlorobium tepidum*: chlorophylls and FMO-protein. *Biochimica Et Biophysica Acta-Bioenergetics* **1998**, *1365*, 285-293.
(13) Kobayashi, M.; Oh-oka, H.; Akutsu, S.; Akiyama, M.; Tominaga, K.; Kise, H.; Nishida, F.; Watanabe, T.; Amesz, J.; Koizumi, M.; Ishida, N.; Kano, H. The primary electron acceptor of green sulfur bacteria, bacteriochlorophyll 663, is chlorophyll *a* esterified with Delta 2,6-phytadienol. *Photosynthesis Research* **2000**, *63*, 269-280.

(14) Kjaer, B.; Frigaard, N. U.; Yang, F.; Zybailov, B.; Miller, M.; Golbeck, J. H.; Scheller, H. V. Menaquinone-7 in the reaction center complex of the green sulfur bacterium *Chlorobium vibrioforme* functions as the electron acceptor A_1. *Biochemistry* **1998**, *37*, 3237-3242.
(15) Figueras, J. B.; Cox, R. P.; Hojrup, P.; Permentier, H. P.; Miller, M. Phylogeny of the PscB reaction center protein from green sulfur bacteria. *Photosynthesis Research* **2002**, *71*, 155-164.
(16) Tsukatani, Y.; Miyamoto, R.; Itoh, S.; Oh-oka, H. Function of a PscD subunit in a homodimeric reaction center complex of the photosynthetic green sulfur bacterium *Chlorobium tepidum* studied by insertional gene inactivation - Regulation of energy transfer and ferredoxin-mediated $NADP^+$ reduction on the cytoplasmic side. *Journal of Biological Chemistry* **2004**, *279*, 51122-51130.
(17) Azai, C.; Kim, K.; Kondo, T.; Harada, J.; Itoh, S.; Oh-oka, H. A heterogeneous tag-attachment to the homodimeric type 1 photosynthetic reaction center core protein in the green sulfur bacterium *Chlorobaculum tepidum*. *Biochimica Et Biophysica Acta-Bioenergetics* **2011**, *1807*, 803-812.
(18) Schmidt, K. A.; Neerken, S.; Permentier, H. P.; Hager-Braun, C.; Amesz, J. Electron transfer in reaction center core complexes from the green sulfur bacteria *Prosthecochloris aestuarii* and *Chlorobium tepidum*. *Biochemistry* **2000**, *39*, 7212-7220.
(19) Neerken, S.; Schmidt, K. A.; Aartsma, T. J.; Amesz, J. Dynamics of energy conversion in reaction center core complexes of the green sulfur bacterium *Prosthecochloris aestuarii* at low temperature. *Biochemistry* **1999**, *38*, 13216-13222.
(20) Miller, M.; Liu, X. M.; Snyder, S. W.; Thurnauer, M. C.; Biggins, J. Photosynthetic electron transfer reactions in the green sulfur bacterium *Chlorobium vibrioforme* - evidence for the functional involvement of iron-sulfur redox centers on the acceptor side of the reaction center. *Biochemistry* **1992**, *31*, 4354-4363.
(21) He, G.; Zhang, H.; King, J. D.; Blankenship, R. E. Structural analysis of the homodimeric reaction center complex from the photosynthetic green sulfur bacterium *Chlorobaculum tepidum*. *Biochemistry* **2014**, *53*, 4924-4930.
(22) Hagerbraun, C.; Xie, D. L.; Jarosch, U.; Herold, E.; Buttner, M.; Zimmermann, R.; Deutzmann, R.; Hauska, G.; Nelson, N. Stable photobleaching of P840 in chlorobium reaction-center preparations - Presence of the 42-kDa bacteriochlorophyll *a*-protein and a 17-kDa polypeptide. *Biochemistry* **1995**, *34*, 9617-9624.
(23) Remigy, H. W.; Stahlberg, H.; Fotiadis, D.; Muller, S. A.; Wolpensinger, B.; Engel, A.; Hauska, G.; Tsiotis, G. The reaction center complex from the green sulfur bacterium *Chlorobium tepidum*: A structural analysis by scanning transmission electron microscopy. *Journal of Molecular Biology* **1999**, *290*, 851-858.
(24) Oh-oka, H.; Kakutani, S.; Kamei, S.; Matsubara, H.; Iwaki, M.; Itoh, S. Highly purified photosynthetic reaction-center (Psca/cytochrome $c_{551})_2$ complex of the green sulfur bacterium *Chlorobium Limicola*. *Biochemistry* **1995**, *34*, 13091-13097.
(25) Permentier, H. P.; Schmidt, K. A.; Kobayashi, M.; Akiyama, M.; Hager-Braun, C.; Neerken, S.; Miller, M.; Amesz, J. Composition and optical properties of reaction centre core complexes from the green sulfur bacteria *Prosthecochloris aestuarii* and *Chlorobium tepidum*. *Photosynthesis Research* **2000**, *64*, 27-39.
(26) Tsiotis, G.; Hager-Braun, C.; Wolpensinger, B.; Engel, A.; Hauska, G. Structural analysis of the photosynthetic reaction center from the green sulfur bacterium *Chlorobium tepidum*. *Biochimica Et Biophysica Acta-Bioenergetics* **1997**, *1322*, 163-172.

(27) Oh-Oka, H.; Kamei, S.; Matsubara, H.; Lin, S.; van Noort, P. I.; Blankenship, R. E. Transient absorption spectroscopy of energy-transfer and trapping processes in the reaction center complex of *Chlorobium tepidum*. *Journal of Physical Chemistry B* **1998**, *102*, 8190-8195.
(28) Neerken, S.; Ma, Y. Z.; Aschenbrucker, J.; Schmidt, K. A.; Nowak, F. R.; Permentier, H. P.; Aartsma, T. J.; Gillbro, T.; Amesz, J. Kinetics of absorbance and anisotropy upon excited state relaxation in the reaction center core complex of a green sulfur bacterium. *Photosynthesis Research* **2000**, *65*, 261-268.
(29) Vassiliev, I. R.; Kjaer, B.; Schorner, G. L.; Scheller, H. V.; Golbeck, J. H. Photoinduced transient absorbance spectra of P840/P840^{+} and the FMO protein in reaction centers of *Chlorobium vibrioforme*. *Biophysical Journal* **2001**, *81*, 382-393.
(30) Neerken, S.; Permentier, H. P.; Francke, C.; Aartsma, T. J.; Amesz, J. Excited states and trapping in reaction center complexes of the green sulfur bacterium *Prosthecochloris aestuarii*. *Biochemistry* **1998**, *37*, 10792-10797.
(31) Francke, C.; Otte, S. C. M.; Miller, M.; Amesz, J.; Olson, J. M. Energy transfer from carotenoid and FMO-protein in subcellular preparations from green sulfur bacteria. Spectroscopic characterization of an FMO-reaction center core complex at low temperature. *Photosynthesis Research* **1996**, *50*, 71-77.
(32) Orf, G. S.; Tank, M.; Vogl, K.; Niedzwiedzki, D. M.; Bryant, D. A.; Blankenship, R. E. Spectroscopic insights into the decreased efficiency of chlorosomes containing bacteriochlorophyll *f*. *Biochimica et Biophysica Acta-Bioenergetics* **2013**, *1827*, 493-501.
(33) Niedzwiedzki, D. M.; Bina, D.; Picken, N.; Honkanen, S.; Blankenship, R. E.; Holten, D.; Cogdell, R. J. Spectroscopic studies of two spectral variants of light-harvesting complex 2 (LH2) from the photosynthetic purple sulfur bacterium *Allochromatium vinosum*. *Biochimica et Biophysica Acta-Bioenergetics* **2012**, *1817*, 1576-1587.
(34) Orf, G. S.; Niedzwiedzki, D. M.; Blankenship, R. E. Intensity dependence of the excited state lifetimes and triplet conversion yield in the Fenna-Matthews-Olson antenna protein. *Journal of Physical Chemistry B* **2014**, *118*, 2058-2069.
(35) Niedzwiedzki, D. M.; Orf, G. S.; Tank, M.; Vogl, K.; Bryant, D. A.; Blankenship, R. E. Photophysical properties of the excited states of bacteriochlorophyll f in solvents and in chlorosomes. *Journal of Physical Chemistry B* **2014**, *118*, 2295-2305.
(36) van Stokkum, I. H.; Larsen, D. S.; van Grondelle, R. Global and target analysis of time-resolved spectra. *Biochimica et Biophysica Acta-Bioenergetics* **2004**, *1657*, 82-104.
(37) Shevchenko, A.; Tomas, H.; Havlis, J.; Olsen, J. V.; Mann, M. In-gel digestion for mass spectrometric characterization of proteins and proteomes. *Nature Protocols* **2006**, *1*, 2856-2860.
(38) Jiang, J.; Zhang, H.; Kang, Y. S.; Bina, D.; Lo, C. S.; Blankenship, R. E. Characterization of the Peridinin-chlorophyll *a*-protein complex in the *dinoflagellate Symbiodinium*. *Biochimica Et Biophysica Acta-Bioenergetics* **2012**, *1817*, 983-989.
(39) Zhang, H.; Huang, R. Y. C.; Jalili, P. R.; Irungu, J. W.; Nicol, G. R.; Ray, K. B.; Rohrs, H. W.; Gross, M. L. Improved mass spectrometric characterization of protein glycosylation reveals unusual glycosylation of maize-derived bovine trypsin. *Analytical Chemistry* **2010**, *82*, 10095-10101.
(40) Xu, H.; Freitas, M. A. MassMatrix: A database search program for rapid characterization of proteins and peptides from tandem mass spectrometry data. *Proteomics* **2009**, *9*, 1548-1555.
(41) Oh-oka, H.; Kamei, S.; Matsubara, H.; Iwaki, M.; Itoh, S. 2 molecules of cytochrome-c function as the electron-donors to P840 in the reaction-center complex isolated from a green sulfur bacterium, *Chlorobium tepidum*. *FEBS Letter* **1995**, *365*, 30-34.

(42) Kusumoto, N.; Setif, P.; Brettel, K.; Seo, D.; Sakurai, H. Electron transfer kinetics in purified reaction centers from the green sulfur bacterium *Chlorobium tepidum* studied by multiple-flash excitation. *Biochemistry* **1999**, *38*, 12124-12137.
(43) Vulto, S. I. E.; Neerken, S.; Louwe, R. J. W.; de Baat, M. A.; Amesz, J.; Aartsma, T. J. Excited-state structure and dynamics in FMO antenna complexes from photosynthetic green sulfur bacteria. *Journal of Physical Chemistry B* **1998**, *102*, 10630-10635.

Chapter 4: Dynamics of Energy and Electron Transfer in the Reaction Center Core Complex from the Green Sulfur Bacterium *Prosthecochloris aestuarii*

Abstract

The PscA-PscB complex was purified from the green sulfur bacterium *Prosthecochloris aestuarii*. The complex is studied by femtosecond time-resolved transient absorption (TA) spectroscopy. The TA spectra of the PscA-PscB complex showed a 30 ps lifetime component regardless of the excitation wavelengths, which is attributed to charge separation. Excitonic equilibration was shown in TA spectra of the PscA-PscB complex when excited into the BChl *a* Q_x band at 590 nm and the Chl *a* Q_y band at 670 nm, while excitation at 840 nm directly populated the low energy excited state and equilibration within the excitonic BChl *a* manifold was not observed. Comparing with the PscA-PscC complex in the previous chapter, 700 ps time component made relatively less contribution.

4.1 Introduction

The reaction center complex in the green sulfur bacteria is a type I reaction center, composed of the bacteriochlorophyll *a* (BChl *a*)-containing Fenna-Matthews-Olson (FMO) protein and the reaction center core complex (RCC). [1, 2] The RCC complex is composed of an 82 kDa homodimer PscA protein, a 24 kDa PscB, a 23 kDa cytochrome c_{551} (PscC) protein and a 17 kDa PscD protein.[3, 4] 16 BChls *a* revealing Q_y bands between 780 and 840 nm, four Chl *a* molecules

including the primary electron acceptor A_0, two carotenoid molecules, a possible secondary electron acceptor A_1 (menaquinone) and an iron-sulfur cluster F_x, are all associated with the PscA homodimer. [3, 5-8] The PscB is a terminal electron acceptor, containing the iron-sulfur clusters F_A and F_B. [9] The function of the PscD subunit is unknown. Figure 4.1 shows the energy/electron transfer scheme in the reaction center complex. The energy is transferred from the FMO complex to the RCC complex. Energy transfer between individual pigments/excitons in the FMO protein reveals wave-like quantum coherence.[1, 2] The excitation populates the low energy exciton BChl *a* 837 through fast equilibration within the excitonic BChl *a* manifold. The excitation is transferred eventually from BChl *a* 837 to the special pair P840, followed by charge separation when $P840^+A_0^-$ is formed. The electron is then transferred to the F_x in the PscA subunit and eventually to the terminal electron acceptor F_A and F_B in the PscB subunit, which directs the electron to the ferredoxin protein.[3, 10-12]

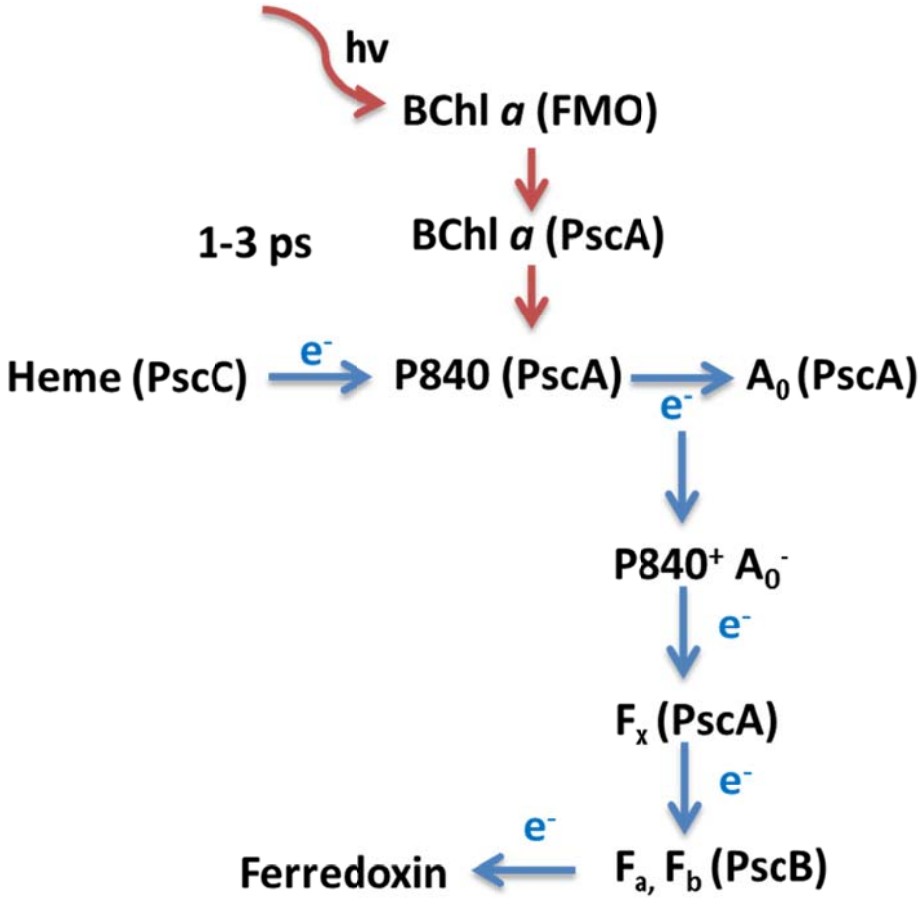

Figure 4.1 The energy and electron transfer mechanism in the reaction center complex. The red arrow indicates energy transfer; the blue arrow indicates electron transfer

Both the intact reaction center complex and the subunits of the RCC complex can be purified from the green sulfur bacteria.[8, 11, 13-16] The composition of the purified RCC complex depends on the species origin. The PscA-PscB complex was purified previously from the green sulfur bacterium *Prosthecochloris aestuarii* by using a hydroxyapatite column after detergent treatment.[4, 12, 16] The PscA-PscC complex was purified from *Chlorobaculum tepidum* and *Chlorobium limicola*.[8, 12, 15, 17] It was shown previously that the dynamics of the excitation energy and electron transfer in the PscA-PscB complex is similar to those of the intact reaction center

complex when excited to the RCC. [10-12, 18-21] Transient absorption (TA) studies performed in the sub-nanosecond time scale on the intact reaction center complex and the PscA-PscB complex excited at 840 nm both revealed a ~30 ps lifetime component, which may be attributed to charge separation in the RCC complex.[10, 11, 16, 19]

In this chaper, we describe the purification of the PscA-PscB complex from the green sulfur bacterium *Prosthecochloris aestuarii*. We also address the energy and electron transfer of the PscA-PscB complex by using the femtosecond time-resolved transient absorption spectroscopy.

4.2 Materials and methods

4.2.1 Protein purification and basic spectroscopic characterization

The PscA-PscB complex was purified from the green sulfur bacterium *Prosthecochloris aestuarii* as previously reported with some modifications.[22] The dark green band obtained from the centrifugation in the sucrose gradient was loaded onto a hydroxyapatite column of approximately 10 mL bed volume (Figure 4.2). The column was equilibrated with 5 mM potassium phosphate buffer (pH = 7.0) and 0.05% n-dodecyl β-D-maltoside (DDM). The sample was eluted with a linear gradient from 5 mM to 1 M potassium phosphate buffer (pH = 7.0) with 0.05% (w/v) DDM. Fractions containing the RCC were collected. Before conducting spectroscopic experiments sodium dithionite was added to 5 mM final concentration to keep the complex in a "reduced" state during measurements. Experiments at cryogenic temperature (77 K) were performed on samples diluted in 60% (v/v) glycerol/buffer mixture in either VNF-100, a liquid nitrogen cryostat from Janis (Janis Research Corp., Woburn, MA, USA. The concentrations of the sample were adjusted to an absorbance of approximately 0.2 at 814 nm in a square 1 cm cuvette. Steady-state absorption spectra were taken by using a UV-1800 UV/Vis

spectrophotometer from Shimadzu (Shimadzu North America, Columbia, MD, USA). SDS-PAGE and Blue-native (BN) gel were performed as described before.[23, 24]

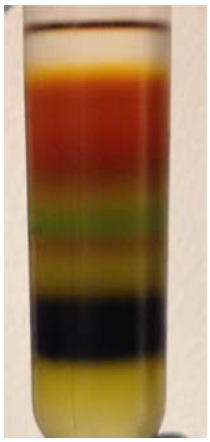

Figure 4.2 Sucrose gradient ultracentrifugation for the PscA-PscB purification. The dark green band in the middle of the gradient contains the PscA-PscB complex

4.2.2 LC-MS/MS and Data Analysis

The stained bands of SDS-PAGE were excised and digested with trypsin. The samples were analyzed by LC-MS/MS using both a Waters Synapt G2 Q-IM-TOF and a Thermo LTQ Orbitrap (Thermo-Scientific, San Jose, CA) as described in a published protocol. [25] The data from Waters Synapt G2 Q-IM-TOF were submitted to the ProteinLynx Global Server (V2.5, Waters Inc., Milford, MA) to identify the peptide sequence. The data for cross-linked peptide identification obtained from a Thermo LTQ Orbitrap were analyzed by using MassMatrix.[26]

4.2.3 Time-resolved absorption spectroscopy

Transient absorption measurements were taken at 77 K by using Helios, a TA spectrometer (UltrafastSystems LCC, Sarasota, FL, USA) coupled to a femtosecond laser system from Spectra-Physics, as previously described in detail.[27] The energy of the pump beam was unified

for all excitation wavelengths and samples to 100 nJ in a circular spot size of 1 mm diameter corresponding to photon intensity of $4 - 5 \times 10^{13}$ photons cm^{-2} per pulse.

4.2.4 Spectroscopic dataset correction and analysis

The TA datasets ware corrected for temporal dispersion by using Surface Xplorer Pro 2.0 software from UltrafastSystems by building a dispersion correction curve from a set of initial times of transient signals obtained from single wavelength fits of representative kinetics. Global analysis of the TA datasets was performed by using a modified version of ASUfit 3.0, program kindly provided by Dr. Evaldas Katilius at Arizona State University. Global analysis of TA datasets were done assuming an irreversible sequential decay path of the excitation decay or electron transfer, procedure that gives so-called evolution-associated difference spectra (EADS).[28]

4.3 Results and discussion

4.3.1 Purification and identification of the PscA-PscB complexes

The steady-state absorption spectra of the PscA-PscB complex recorded at room temperature is shown in Figure 4.3. The purified PscA-PscB complex exhibits a BChl *a* absorption band at 814 nm with a shoulder at 835 nm, which is consistent with previous work, as shown in Figure 4.3A.[4, 10, 16, 19] The Q_x band of the BChl *a* at 600 nm and Q_y band of Chl *a* at 670 nm are also observed. The steady-state absorption spectra of the PscA-PscB complex recorded at 77 K is shown in Figure 4.4. Comparing with the absorption spectra at room temperature, the Q_x band of BChl *a* at 600 nm splits into two peaks at 594 nm and 608 nm, and the shoulder at 836 nm becomes more obvious. Two bands on the SDS-PAGE at 60 kDa and 30 kDa were identified to

be PscA and PscB, respectively, by in-gel digestion and subsequent LC-MS/MS analysis (Figure 4.5A). The complex was further evaluated by BN gels (Figure 4.5B). It showed a band approximately 200 kDa, corresponding to the mass of the PscA-PscB complex.

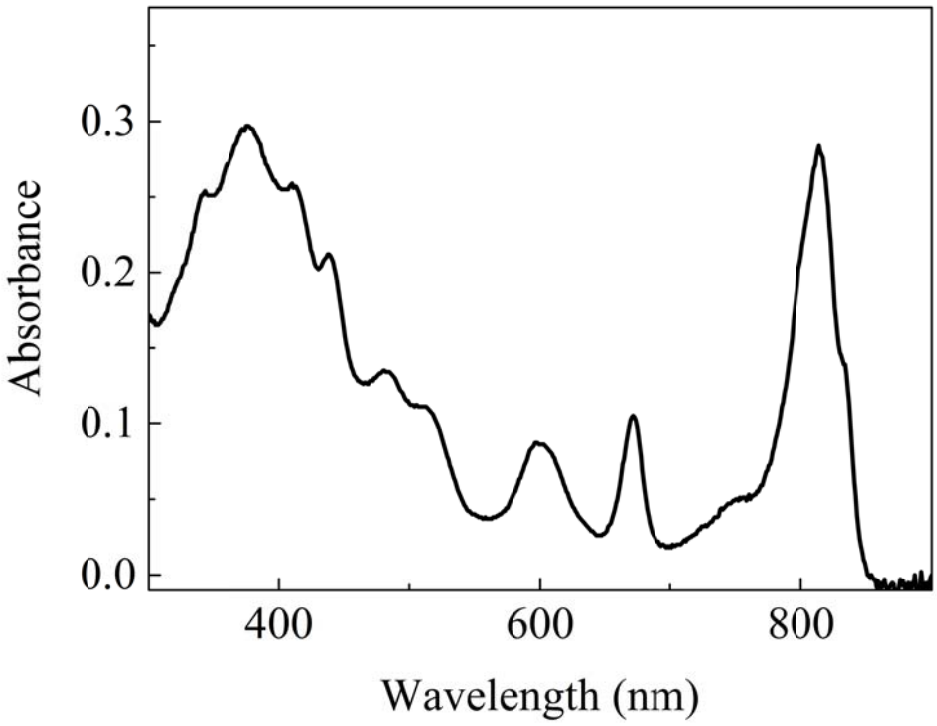

Figure 4.3 Absorption spectrum of the PscA-PscB complex at room temperature

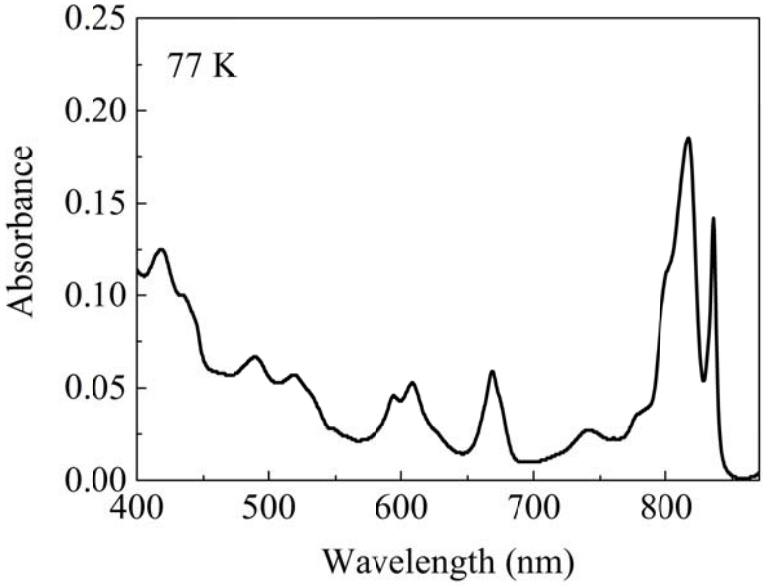

Figure 4.4 Absorption spectrum of the PscA-PscB complex at 77 K

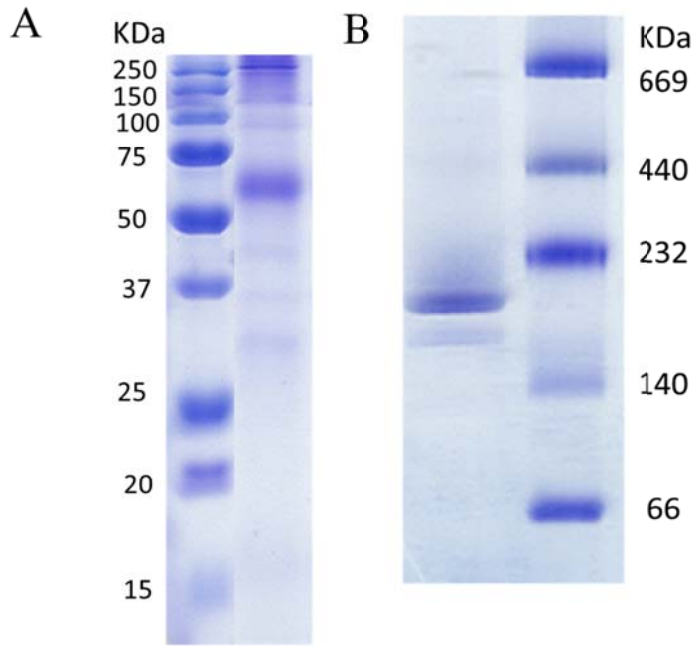

Figure 4.5 SDS-PAGE (A) and BN gel (B) analysis of the PscA-PscB complex

4.3.2 Transient absorption spectroscopy

The TA spectra of the PscA-PscB complex taken at different delay times after excitation at the Q_x show a band for BChl *a* at 590 nm (Figure 4.6). A positive band at 810 nm, associated with excited-state absorption of BChl *a*, is formed immediately after excitation. The main bleaching band localized at 840 nm immediately after excitation. Later, a rapid spectral evolution is seen, exhibiting fast energy transfer to the BChl *a*-837. The amplitude of the bleaching band at 840 nm increased, whereas that of the band at 824 nm kept decreasing. At 5 ps, the band at 840 nm reached its maximum bleaching, and the signal started decaying. The position of this band remains constant and after spectral equilibration, the $\Delta A_{824}/\Delta A_{840}$ ratio remains essentially constant at ~0.55.

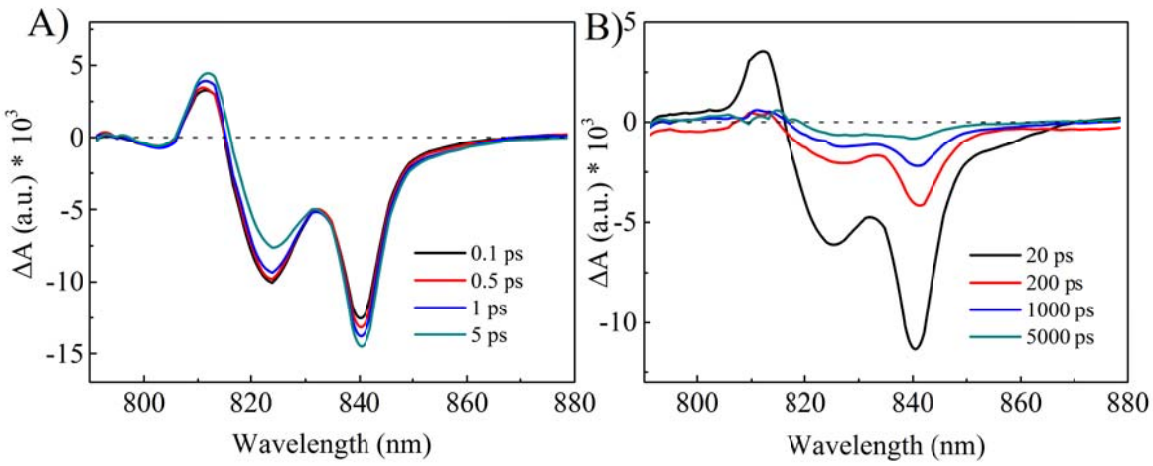

Figure 4.6 The TA spectra of the PscA-PscB complex taken at different delay times after excitation at 590 nm

Upon excitation at Q_y band of BChl *a* at 840 nm, the main bleaching band formed at 840 nm immediately after excitation (Figure 4.7). Two other bands (i.e., the positive band at 813 nm and the bleaching band at 824 nm), are seen. All three bands decayed with time, and the TA spectra do not reveal changes over time in their spectral envelope over the entire time delay window of the spectrometer.

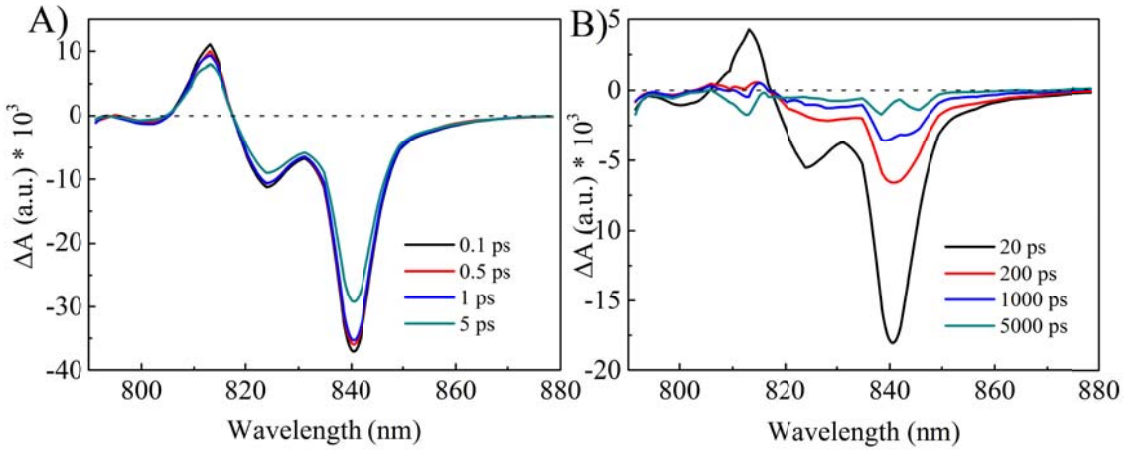

Figure 4.7 The TA spectra of the PscA-PscB complex taken at different delay times after excitation at 840 nm

The global analysis (EADS) profiles showed components of four lifetimes, which are 1-3 ps fast lifetime component, 30 ps, 700 ps and "infinite lifetime" (> 5 ns) (Figure 4.8). The fast lifetime components indicated energy equilibrium.[11, 29] The 30 ps lifetime component is attributed to the charge-separated state of P840 when the oxidized primary electron donor $P840^+$ is formed. [18, 30] The 700 ps lifetime component is not definitely assigned. It may be associated with long-lived excitons that do not contribute to charge separation as discussed in chapter three. The long-lived component (> 5 ns) may result from the sub-millisecond $P840^+ \rightarrow$ P840 reduction process occurring by charge recombination between the $P840^+$ and the initial electron acceptors.[4, 18, 31]

Figure 4.8A shows a dominant bleaching band at 823 nm for 1 ps lifetime component. For the other time components, the main bleaching band locates at 840 nm. It indicates that the fast energy transfer occurs from the intermediate BChl *a* to the BChl *a*-837 when the PscA-PscB complex is excited at the BChl *a* Q_x band. Figure 4.8B shows that the main bleaching band locates at 840 nm for all the time components when the PscA-PscB complex is excited at 840 nm. In conclusion, when PscA-PscB complex was excited at BChl *a* Q_x band, energy would localize to the lowest energy state very quickly through intermediate energy levels of BChl *a* excitons, while most of the energy would localize to the lowest energy state of BChl *a* excitons immediately after excitation at 840 nm. The EADS of the PscA-PscB complex excited at 840 nm, when compared with that of the PscA-PscC sample discussed in the chapter three, shows less contribution from the 700 ps time component. One possible reason is that the existence of the terminal acceptor PscB subunit can reduce the amount of long-lived excitons by accepting the electrons from the F_x cluster.

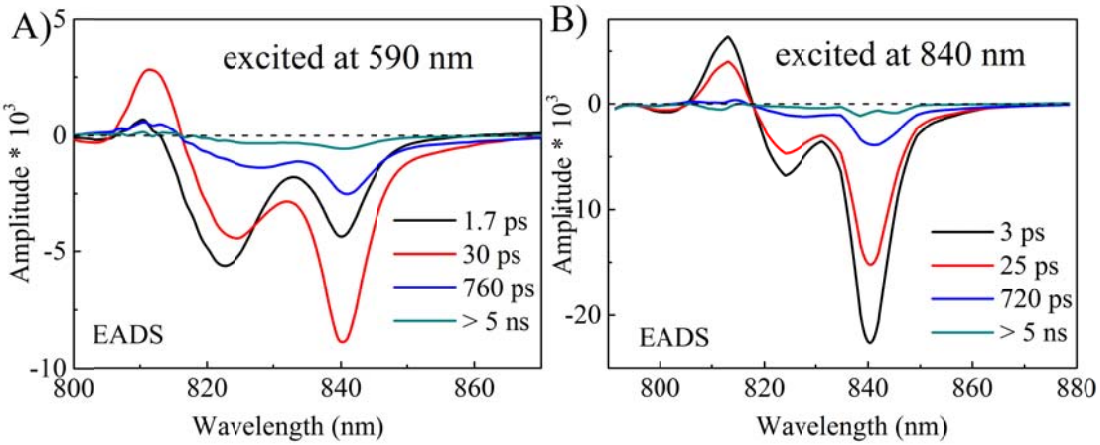

Figure 4.8 Global analysis results (EADS) of the TA datasets of the PscA-PscB complex excited at (A) 590 nm and (B) 840 nm.

The PscA-PscB complex was also excited at Chl *a* 670 as shown in Figure 4.9. The excited-state absorption band at 811 nm immediately formed after excitation. The bleaching band at 840 nm increases dramatically within 5 ps, indicating the energy is transferred from the Chl *a* to the BChl *a*-837. The 840 nm band became the main bleaching band at 0.5 ps and started to decay after 5 ps. As time evolves, and excitonic equilibration is completed, the TA spectra are essentially identical with those from excitation at 590 nm. EADS in Figure 4.10 shows similar lifetime components as excitation at 590 nm and 840 nm.

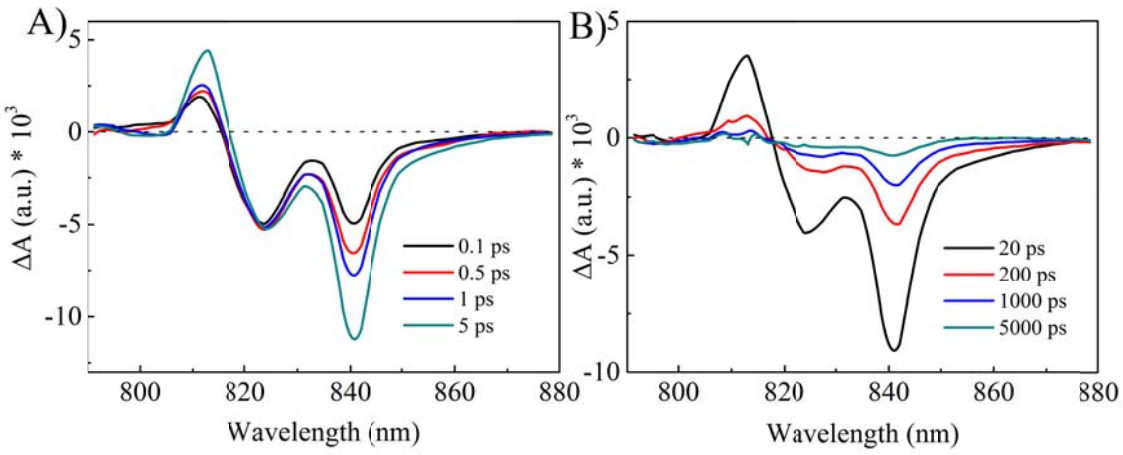

Figure 4.9 The TA spectra of the PscA-PscC complex taken at different delay times after excitation at 670 nm

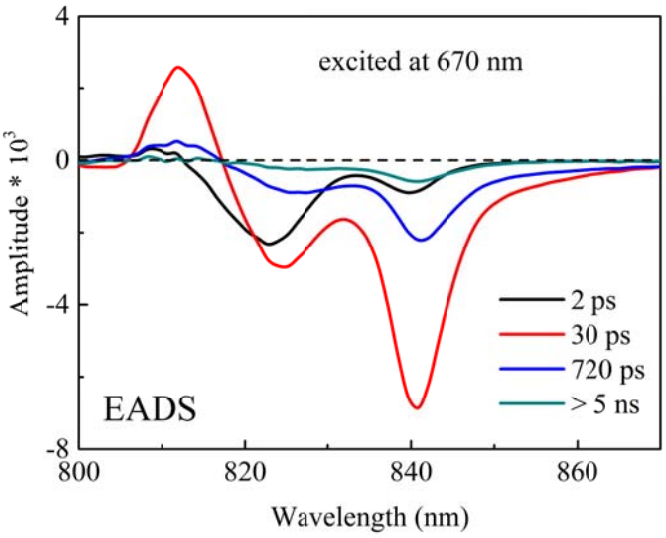

Figure 4.10 Global analysis results (EADS) of the TA datasets of the PscA-PscB complex excited at 670 nm.

In conclusion, the PscA-PscB complex showed a charge separation rate of ~30 ps no matter what the excitation wavelength. When excited at BChl *a* Q_x band at 590 nm and the Chl *a* Q_y band at 670 nm, the energy equilibrium within the excitonic BChl *a* manifold is seen, whereas energy equilibration is not seen when excited directly into the lowest energy exciton at 840 nm. The EADS showed four time components: a 1-3 ps fast lifetime component, a 30 ps, a 700 ps and an "infinite lifetime", just as does the PscA-PscC complex described in chapter three. The 700 ps time component made relatively less contribution compared with the PscA-PscC complex. It may be caused by a more complete electron transport chain in the PscA-PscB complex, which has all the iron-sulfur clusters in the electron transport chain.

4.4 Conclusion

We purified the PscA-PscB complex from the green sulfur bacterium *Prosthecochloris aestuarii* and studied by TA spectroscopy. In the TA spectra, the PscA-PscB complex showed charge separation regardless of the excitation wavelengths and rapid excitonic equilibrium was seen when excited into the BChl *a* Q_x band at 590 nm and the Chl *a* Q_y band at 670 nm. The EADS showed four time components, which are 1-3 ps fast lifetime component, 30 ps, 700 ps and "infinite lifetime". Comparing with the EADS of the PscA-PscC complex in the previous chapter, 700 ps time component made relatively less contribution for the PscA-PscB complex.

References

(1) Engel, G. S.; Calhoun, T. R.; Read, E. L.; Ahn, T. K.; Mancal, T.; Cheng, Y. C.; Blankenship, R. E.; Fleming, G. R. Evidence for wavelike energy transfer through quantum coherence in photosynthetic systems. *Nature* **2007**, *446*, 782-786.
(2) Panitchayangkoon, G.; Hayes, D.; Fransted, K. A.; Caram, J. R.; Harel, E.; Wen, J.; Blankenship, R. E.; Engel, G. S. Long-lived quantum coherence in photosynthetic complexes at physiological temperature. *Proceedings of the National Academy of Sciences* **2010**, *107*, 12766-12770.
(3) Hauska, G.; Schoedl, T.; Remigy, H.; Tsiotis, G. The reaction center of green sulfur bacteria. *Biochimica Et Biophysica Acta-Bioenergetics* **2001**, *1507*, 260-277.
(4) Francke, C.; Permentier, H. P.; Franken, E. M.; Neerken, S.; Amesz, J. Isolation and properties of photochemically active reaction center complexes from the green sulfur bacterium *Prosthecochloris aestuarii*. *Biochemistry* **1997**, *36*, 14167-14172.
(5) Kobayashi, M.; Oh-oka, H.; Akutsu, S.; Akiyama, M.; Tominaga, K.; Kise, H.; Nishida, F.; Watanabe, T.; Amesz, J.; Koizumi, M.; Ishida, N.; Kano, H. The primary electron acceptor of green sulfur bacteria, bacteriochlorophyll 663, is chlorophyll *a* esterified with Delta 2,6-phytadienol. *Photosynthesis Research* **2000**, *63*, 269-280.
(6) Kjaer, B.; Frigaard, N. U.; Yang, F.; Zybailov, B.; Miller, M.; Golbeck, J. H.; Scheller, H. V. Menaquinone-7 in the reaction center complex of the green sulfur bacterium *Chlorobium vibrioforme* functions as the electron acceptor A_1. *Biochemistry* **1998**, *37*, 3237-3242.
(7) Remigy, H. W.; Hauska, G.; Muller, S. A.; Tsiotis, G. The reaction centre from green sulphur bacteria: progress towards structural elucidation. *Photosynthesis Research* **2002**, *71*, 91-98.
(8) Griesbeck, C.; Hager-Braun, C.; Rogl, H.; Hauska, G. Quantitation of P840 reaction center preparations from *Chlorobium tepidum*: chlorophylls and FMO-protein. *Biochimica Et Biophysica Acta-Bioenergetics* **1998**, *1365*, 285-293.
(9) Figueras, J. B.; Cox, R. P.; Hojrup, P.; Permentier, H. P.; Miller, M. Phylogeny of the PscB reaction center protein from green sulfur bacteria. *Photosynthesis Research* **2002**, *71*, 155-164.
(10) Neerken, S.; Permentier, H. P.; Francke, C.; Aartsma, T. J.; Amesz, J. Excited states and trapping in reaction center complexes of the green sulfur bacterium *Prosthecochloris aestuarii*. *Biochemistry* **1998**, *37*, 10792-10797.
(11) Neerken, S.; Schmidt, K. A.; Aartsma, T. J.; Amesz, J. Dynamics of energy conversion in reaction center core complexes of the green sulfur bacterium *Prosthecochloris aestuarii* at low temperature. *Biochemistry* **1999**, *38*, 13216-13222.
(12) Schmidt, K. A.; Neerken, S.; Permentier, H. P.; Hager-Braun, C.; Amesz, J. Electron transfer in reaction center core complexes from the green sulfur bacteria *Prosthecochloris aestuarii* and *Chlorobium tepidum*. *Biochemistry* **2000**, *39*, 7212-7220.
(13) Hagerbraun, C.; Xie, D. L.; Jarosch, U.; Herold, E.; Buttner, M.; Zimmermann, R.; Deutzmann, R.; Hauska, G.; Nelson, N. Stable photobleaching of P840 in Chlorobium reaction-center preparations - Presence of the 42-kDa bacteriochlorophyll *a*-protein and a 17-kDa polypeptide. *Biochemistry* **1995**, *34*, 9617-9624.
(14) Remigy, H. W.; Stahlberg, H.; Fotiadis, D.; Muller, S. A.; Wolpensinger, B.; Engel, A.; Hauska, G.; Tsiotis, G. The reaction center complex from the green sulfur bacterium *Chlorobium*

tepidum: A structural analysis by scanning transmission electron microscopy. *Journal of Molecular Biology* **1999**, *290*, 851-858.
(15) Oh-oka, H.; Kakutani, S.; Kamei, S.; Matsubara, H.; Iwaki, M.; Itoh, S. Highly purified photosynthetic reaction center (Psca/cytochrome $c_{551})_2$ complex of the green sulfur bacterium *Chlorobium limicola*. *Biochemistry* **1995**, *34*, 13091-13097.
(16) Permentier, H. P.; Schmidt, K. A.; Kobayashi, M.; Akiyama, M.; Hager-Braun, C.; Neerken, S.; Miller, M.; Amesz, J. Composition and optical properties of reaction centre core complexes from the green sulfur bacteria *Prosthecochloris aestuarii* and *Chlorobium tepidum*. *Photosynthesis Research* **2000**, *64*, 27-39.
(17) Tsiotis, G.; Hager-Braun, C.; Wolpensinger, B.; Engel, A.; Hauska, G. Structural analysis of the photosynthetic reaction center from the green sulfur bacterium *Chlorobium tepidum*. *Biochimica Et Biophysica Acta-Bioenergetics* **1997**, *1322*, 163-172.
(18) Oh-Oka, H.; Kamei, S.; Matsubara, H.; Lin, S.; van Noort, P. I.; Blankenship, R. E. Transient absorption spectroscopy of energy transfer and trapping processes in the reaction center complex of *Chlorobium tepidum*. *Journal of Physical Chemistry B* **1998**, *102*, 8190-8195.
(19) Neerken, S.; Ma, Y. Z.; Aschenbrucker, J.; Schmidt, K. A.; Nowak, F. R.; Permentier, H. P.; Aartsma, T. J.; Gillbro, T.; Amesz, J. Kinetics of absorbance and anisotropy upon excited state relaxation in the reaction center core complex of a green sulfur bacterium. *Photosynthesis Research* **2000**, *65*, 261-268.
(20) Vassiliev, I. R.; Kjaer, B.; Schorner, G. L.; Scheller, H. V.; Golbeck, J. H. Photoinduced transient absorbance spectra of P840/$P840^+$ and the FMO protein in reaction centers of *Chlorobium vibrioforme*. *Biophysical Journal* **2001**, *81*, 382-393.
(21) Francke, C.; Otte, S. C. M.; Miller, M.; Amesz, J.; Olson, J. M. Energy transfer from carotenoid and FMO-protein in subcellular preparations from green sulfur bacteria. Spectroscopic characterization of an FMO-reaction center core complex at low temperature. *Photosynthesis Research* **1996**, *50*, 71-77.
(22) He, G.; Zhang, H.; King, J. D.; Blankenship, R. E. Structural analysis of the homodimeric reaction center complex from the photosynthetic green sulfur bacterium *Chlorobaculum tepidum*. *Biochemistry* **2014**, *53*, 4924-4930.
(23) Schagger, H.; Vonjagow, G. Blue native electrophoresis for isolation of membrane-protein complexes in enzymatically active form. *Analytical Biochemistry* **1991**, *199*, 223-231.
(24) Schaegger, H. Tricine-SDS-PAGE. *Nature Protocols* **2006**, *1*, 16-22.
(25) Liu, H.; Zhang, H.; Niedzwiedzki, D. M.; Prado, M.; He, G.; Gross, M. L.; Blankenship, R. E. Phycobilisomes supply excitations to both photosystems in a megacomplex in cyanobacteria. *Science* **2013**, *342*, 1104-1107.
(26) Xu, H.; Hsu, P.-H.; Zhang, L.; Tsai, M.-D.; Freitas, M. A. Database search algorithm for identification of intact cross-links in proteins and peptides using tandem mass spectrometry. *Journal of Proteome Research* **2010**, *9*, 3384-3393.
(27) Niedzwiedzki, D. M.; Bina, D.; Picken, N.; Honkanen, S.; Blankenship, R. E.; Holten, D.; Cogdell, R. J. Spectroscopic studies of two spectral variants of light-harvesting complex 2 (LH2) from the photosynthetic purple sulfur bacterium *Allochromatium vinosum*. *Biochimica et Biophysica Acta-Bioenergetics* **2012**, *1817*, 1576-1587.
(28) van Stokkum, I. H.; Larsen, D. S.; van Grondelle, R. Global and target analysis of time-resolved spectra. *Biochimica et Biophysica Acta-Bioenergetics* **2004**, *1657*, 82-104.
(29) Vanburgel, M.; Wiersma, D. A.; Duppen, K. The dynamics of one-dimensional excitons in liquids. *Journal of Chemical Physics* **1995**, *102*, 20-33.

(30) Vulto, S. I. E.; Neerken, S.; Louwe, R. J. W.; de Baat, M. A.; Amesz, J.; Aartsma, T. J. Excited-state structure and dynamics in FMO antenna complexes from photosynthetic green sulfur bacteria. *Journal of Physical Chemistry B* **1998**, *102*, 10630-10635.
(31) Oh-oka, H.; Kamei, S.; Matsubara, H.; Iwaki, M.; Itoh, S. 2 molecules of cytochrome-c function as the electron-donors to P840 in the reaction center complex isolated from a green sulfur bacterium, *Chlorobium tepidum*. *FEBS Letter* **1995**, *365*, 30-34.

Chapter 5: Conclusions and Future Directions

The intact reaction center complex of the green sulfur bacterium *Chlorobaculum tepidum* was purified. This complex is composed of the FMO antenna protein and the RCC complex. The spatial interaction between FMO and RCC was studied by chemically cross-linking the purified FMO-RCC sample followed by LC-MS/MS analysis. All the subunits of RC can be linked together by BS^3, DSS and DTSSP. The results showed that the FMO and RCC complexes are closely associated. FMO, PscB, PscD and part of PscA are exposed on the cytoplasmic side of the membrane. The soluble domain of the heme-containing cytochrome subunit PscC and part of the core subunit PscA are located on the periplasmic side of the membrane. The PscD subunit is thought to stabilize FMO to RCC complex and facilitate the electron transfer from RCC to ferredoxin. The close distance of soluble domain of PscC and PscA explains the efficient electron transfer between PscC and P840. A structural model that is consistent with these results is proposed for the FMO-RCC complex. The question that remains is how many copies of FMO are associated with each RCC in the native state. Our result showed that there is 1-2 FMO associated with each RCC but it is uncertain whether the loss of one FMO is due to the detergent treatment. The in-vivo cross linking with hydrophobic chemical linkers in the whole cell might be an effective protocol to answer that question. Besides, it is also possible to crystallize the FMO-RCC complex and obtain the structure of the intact complex with our proposed orientation and location of each subunit.

The RCC complex and the FMO-RCC complex from the green sulfur bacterium *Chlorobaculum tepidum* were purified and studied comparatively by steady-state fluorescence, TRF, and TA

spectroscopies. The energy transfer efficiency from the FMO to the RCC complex was calculated to be ~40% based on the steady-state fluorescence. TRF showed that photons were absorbed by two fractions of FMO complexes, energetically uncoupled and coupled to the RCC. The first pool of the FMO (uncoupled) releases energy in fluorescence process with lifetime of 2.6 ns that is typical for free FMO. The second pool of FMO transfers absorbed energy to the RCC complex with approximately 76% efficiency resulting in shortening of observed fluorescence lifetime to ~700 ps. The TA spectra show that the excitation that is passed to the RCC initially populates BChl *a* excited state that undergoes fast equilibration (1-3 ps) within the excitonic manifold. The excitation is transferred eventually to the special pair P840 or trapped in a long-lived exciton that decays with a lifetime of ~700 ps. Upon accepting excitation by P840 an initial $P840^{+}A_0^{-}$ charge separation step occurs with a time constant of ~35 ps. The TA spectra for the FMO-RCC complex could be interpreted by a combination of the excited FMO protein and RCC complex. But additional fast kinetic component was seen for the FMO-RCC complex that may be linked to the FMO fraction that is energetically coupled with RCC.

In addition, the PscA-PscB complex was purified from the green sulfur bacteria *Prosthecochloris aestuarii* and studied by the TA spectroscopy. It showed a charge separation rate of ~30 ps independent of the excitation wavelengths. The EADS showed four time components; they are a 1-3 ps fast lifetime component, a 30 ps, a 700 ps and an "infinite lifetime", as similar to the PscA-PscC complex from *Chlorobaculum tepidum*. The 700 ps time component made relatively less contribution compared with the PscA-PscC complex.

It is not clear why a fraction of the FMO is unable to transfer energy to RCC and releases energy in fluorescence process with lifetime of 2.6 ns, a time that is similar to that of free FMO, even though they are physically attached to the RCC. The energetically uncoupled FMO could be

caused either by an intrinsic property in the native system or by the purification process. One possible approach to answer this question is to study the energy transfer efficiency of the FMO-RCC in either the whole cell or the membrane pellet without detergent treatment process. The use of detergent could be the major reason causing BChl *a* disorientation if there is any due to purification process. Because both the whole cell and the membrane pellet contain a significant amount of chlorosomes that will interfere with the signal from FMO-RCC complex, a BChl *c*-less mutant of *Chlorobaculum tepidum* would be ideal for this study.